TÉCNICO
LISBOA

Special foundations solutions using ductile iron driven piles

Hélène Vandekerkhove

Thesis to obtain the Master of Science Degree in

Civil Engineering

Supervisor

Prof. Alexandre da Luz Pinto

Jury

Chairperson:
Prof. Teresa Maria Bodas de Araùjo Freitas

Supervisor:
Prof. Alexandre da Luz Pinto

Member of the Committee:
Prof. Peter John Bourne-Webb

June 2023

Declaration

I declare that this document is an original work of my own authorship and that it fulfills all the requirements of the Code of Conduct and Good Practices of the Universidade de Lisboa.

Acknowledgements

First, I would like to thank my supervisor professor Alexandre Luz Pinto since he made this master thesis possible. I am grateful for the time he took to answer my questions and the needed documents he provided.

Through this way I would also like to thank Carlos Caxias, geotechnical supplier at ANP, for taking me to a site where I could see the installation of the ductile piles. This helped me to visualize everything I had read about installing ductile driven piles. I would also like to thank Ines Braz, geotechnical designer at JETsj, for providing me with documents I needed. I am thankful for the clear explanations she gave where needed.

A very special thank you goes out to my friends Tibo Blauwaert, Ella Vanooteghem, Julie Anthone and Sander Descheemaecker. Their support throughout this thesis meant the world to me. Lastly, I would like to thank my dad, stepmom and grandparents for making it possible for me to go on Erasmus exchange in Lisbon and always believing in me.

In general, I am thankful this thesis gave me a lot of insight in the use of ductile iron piles as a foundation solution. I had no prior knowledge about ductile piles or the calculations of them as a foundation solution. This thesis brought me a lot of new know-how I can carry with me to Belgium.

Abstract

The use of ductile iron driven piles as a foundation solution was analyzed. First the ductile piles are looked at in general. Second the use of them for the foundation of the stage and roof for the World Youth Day event was investigated. The general analysis of the piles discusses the main components such as the pile pipe, pile shoe and pile head plate. Next, the manufacturing and installation process as an end-bearing or friction pile is explained. The environmental impact of the piles during their life is examined by studying the EPD report. This report concludes that the production process has the biggest environmental impact. For the analysis of the project, the site and foundations solutions together with the performed full scale load tests and design calculations where explained. The load tests exist of a compression and tension test. For each test the results show a graph that gives the deformations with accompanying loads and a load distribution graph that shows how much load is transferred to the ground at which depth. The design calculations confirm that the design loads of the compression piles are smaller than the design cross-section resistances of these piles. Lastly the possibility of optimization was investigated. This showed that for the compression piles of the roof a ductile pile with a smaller diameter could be used. This results in 158 kg ductile iron saved per pile. The tension self-drilling bar for the roof and the compression piles for the stage could not be optimized.

Keywords: Ductile driven piles, TRM piles, end-bearing piles, skin-friction piles, design loads, cross-section design resistance.

Resumo

A utilização de estacas cravadas de ferro dúctil como solução de fundação foi analisada. Primeiro, as estacas dúcteis são analisadas em geral. Em segundo lugar, foi investigada a sua utilização para a fundação do palco e da cobertura do evento da Jornada Mundial da Juventude. A análise geral das estacas aborda os principais componentes, tais como o tubo da estaca, a sapata da estaca e a placa da cabeça da estaca. Em seguida, explica-se o processo de fabrico, durabilidade e instalação como estaca de suporte ou de fricção. O impacto ambiental das estacas durante a sua vida útil é examinado através do estudo do relatório EPD. Este relatório conclui que o processo de produção tem o maior impacto ambiental. Para a análise do projecto, são explicadas as soluções para o local e para as fundações, bem como os ensaios de carga realizados à escala real e os cálculos de concepção. Os ensaios de carga consistem num ensaio de compressão e num ensaio de tracção. Para cada ensaio, os resultados mostram um gráfico que apresenta as deformações com as cargas de acompanhamento e um gráfico de extensómetros que mostra quanta carga é transferida para o solo e a que profundidade. Os cálculos de projecto confirmam que as cargas de projecto das estacas de compressão são inferiores às resistências da secção transversal de projecto destas estacas. Finalmente, foi investigada a possibilidade de optimização. Isto mostrou que, para as estacas de compressão da cobertura, poderia ser utilizada uma estaca dúctil com um diâmetro mais pequeno. Isto resulta em 158 kg de ferro dúctil poupado por estaca. As estacas de tracção para a cobertura e as estacas de compressão para o palco não puderam ser optimizadas.

Palavras-chave: Estacas dúcteis cravadas, estacas TRM, estacas de apoio, estacas de atrito superficial, cargas de projecto, resistência de projecto da secção transversal.

Contents

List of tables

List of figures

List of symbols

A	Cross-section
A_c	Cross-section of the inner pile concrete
A_{DP}	Cross-section of the ductile iron pile
A_s	Shaft surface
A_t	Pile toe area
C_u	Shear strength of the undrainded soil
d	Inner diameter
D	Outer diameter
D_B	Pile embedment depth into the bearing layer
d_i	Nominal inner diameter of the ductile iron pipe
E_c	Modulus of elasticity of the internal concrete
E_d	Design value of a load effect (on a single pile)
E_{DP}	Modulus of elasticity of the ductile iron pipe
EI	Flexural rigidity
EI_c	Flexural rigidity of the internal concrete
EI_{DP}	Flexural rigidity of the ductile pile
E_p	Modulus of elasticity of the pile
$E_{v,d}$	Design action effects to be transmitted via skin friction
f_{ck}	Characteristic cylinder compressive strength of the cement mortar or concrete after 28 days
$f_{ck}(t)$	Characteristic compressive strength of the cement mortar/concrete as a function of time (age) t

f_y Yield strength of the material

G_k Permanent characteristic load

I_c Moment of inertia of the internal concrete

I_{DP} Moment of inertia of the ductile pile

I_p Second order moment of inertia of the cross-section of the pile

k_l Stiffness of the bedding

K_p Passive lateral pressure coefficient

L Length of the pile

L_{eff} Effective length of the pile not taking into account the coupling areas

$M_{c,Rd}$ Design bending moment resistance of the cross-section for bending about one principal axis

M_{Ed} Design value of the bending moment

M_{Rk} Characteristic value of the bending moment resistance

n Integer buckling number, factor accounting for the end conditions

$N_{c,Rd}$ Design resistance of the cross-section for uniform compression

N_{Ed} Design value of the compressive/tensile axial force

N_{Rk} Characteristic value of the resistance to an axial force

$N_{t,Rd}$ Design resistance of the cross-section for uniform tension

$\overline{N}'$ Corrected SPT value

$\overline{N_B'}$ Corrected SPT value for the bearing layer

$\overline{N_o'}$ Corrected SPT value for the weaker layer (overbearing the bearing layer)

N_{10} Blow count (DPH)

P_c Critical load at which buckling will occur

P_p	Test load
$q_{b,bb,k}$	Pile base resistance per unit area in cohesive soil
$q_{b,nb,k}$	Pile base resistance per unit area in non-cohesive soil
q_c	Mean cone resistance (CPT)
q_s	Shaft resistance unit
$q_{s,bb,k}$	Pile shaft resistance per unit area in cohesive soil
$q_{s,nb,k}$	Pile shaft resistance per unit area in non-cohesive soil
q_t	Toe resistance unit
Q_k	Variable characteristic load
Q_u	Ultimate geotechnical load bearing capacity
r	Radius
R_{ck}	Characteristic value of the resistance of the concrete
R_{DPk}	Characteristic value of the resistance of the ductile pile
$R_{i,d}$	Design value of the resistance
$R_{i,k}$	Characteristic value of the particular resistance
$R_{s,d}$	Component of the design value $R_{i,d}$ that is transferred via skin friction
$R_{v,d}$	Design longitudinal shear strength of the interface between the ductile iron pipe and the shaft grouting
$R_{vi,d}$	Design longitudinal shear strength of between the internal cement mortar / concrete and the ductile iron pipe interface
t	Wall thickness
W	Section modulus of the cross-section
W_{el}	Elastic section modulus of the cross-section

$W_{k,\mathrm{h}}$ Horizontal characteristic load caused by the wind

$W_{k,\mathrm{v}}$ Vertical characteristic load caused by the wind

W_{pl} Plastic section modulus of the cross-section

Φ Diameter

φ' Angle of friction of the drained soil (effective angle of friction)

ε Strain

γ_c Partial safety factor for the cement mortar/concrete

γ_G Partial safety factor for permanent action loads

γ_M Partial safety factor for the ductile iron pipe

$\gamma_{M,v}$ Partial safety factor for the bond strength of the interface between the ductile cast iron pipe and the shaft-grouting

$\gamma_{Mi,v}$ Partial safety factor for the bond strength of the internal cement mortar/concrete with the ductile iron pipe interface

γ_Q Partial safety factor for variable action loads

$\gamma_{s;t}$ Partial safety factor for the total pile resistance (compression), or skin resistance (tension) from load or based on empirical values

τ_M Skin friction in the grout with the floor interface in the serviceability limit state

$\tau_{M,k}$ The characteristic value of the pile skin friction determined from the load tests or the empirical values, according to their inclination out of the vertical

$\tau_{R,d}$ Design value of the bond strength of the interface between the ductile cast iron pipe and the shaft-grouting

$\tau_{R,k}$ Characteristic value of the bond strength of the interface between the ductile cast iron pipe and the shaft-grouting

$\tau_{Ri,d}$ Design value of the bond strength of the internal cement mortar/concrete with the ductile iron pipe interface

$\tau_{Ri,\mathrm{k}}$ Characteristic value of the bond strength of the internal cement mortar/concrete with the ductile iron pipe interface

μ_k Coefficient of friction between cast iron pipe and shaft-grouting

σ_N Lower characteristic value for the contact pressure from earth pressure and bracing effect acting horizontally along the circumference of the pile

ρ_{soil} Mass density of the soil

η_c Concrete scaling factor

1. Introduction

In August 2023 the World Youth Day takes place in Lisbon. This is a gathering of Catholic young people from all over the world with the Pope. For this event, a large stage with a roof is being built in Lisbon. The special foundations solution for this construction implements ductile driven piles. The goal of this thesis is to look deeper into the use of ductile piles for foundations in general, to explain the foundations of the WYD site and to check for optimization.

Pile foundations are widely used in various construction projects due to their effectiveness in transferring loads and providing stability. They are commonly employed in buildings and structures that encounter challenging soil conditions, such as soft or weak soils, expansive clay, or high-water tables. They are typically cylindrical in shape and made of materials such as concrete, steel, or timber. Pile foundations are driven or drilled into the ground to reach a firm stratum capable of supporting the loads imposed by the structure. Their versatility, strength, and adaptability make them a vital solution for constructing safe and durable structures in diverse environments.

Chapter 2 of the thesis will go more in depth about ductile micropiles in general. The main components like the pile pipe, shoe and head plate are discussed. Next, the manufacturing process and quality management are explained. How the piles can be installed as end-bearing or skin friction piles is also clarified. Some general calculations that can be done to structurally design the piles was listed as well. Lastly, the life cycle of the ductile piles was analyzed to discuss the environmental impact.

Next in this thesis, the project of the World Youth Day site is analyzed. This site is located above a sanitary landfill which involves challenges for the foundations design. Taking the challenges into consideration, the geotechnical company JETsj designed the foundations solutions with ductile iron piles. The roof will be fully founded on ductile piles with the implementation of a self-drilling steel bar so the piles can absorb both the compressive and tensile forces. The foundation of the stage itself exists of concrete slabs in combination with some ductile piles loaded on compression.

In chapter 3 of this thesis, the WYD site is presented and the local geological conditions are explained. The implemented foundations and the preparatory work are clarified. Next, the results of the performed full scale load tests are analyzed. Conclusions about the deformations and load distribution in the ground are drawn. The foundations design is an essential part of this thesis. Here the design loads were calculated and the structural and geological load bearing capacities of the piles were verified.

Chapter 4 investigates whether the pile foundations at the site can be optimized. Lastly, in the fifth and final chapter, the final remarks are discussed.

2. Ductile iron driven piles

2.1 Main components

The ductile driven piles discussed in this thesis are prefabricated ductile cast iron piles from the Austrian company TRM. These piles, used as a solution for foundations, are usually made up of one or more pile pipes, a pile shoe and a pile head plate. Figure 1 shows these main components. (*TRM Piling Systems Fast. Simple. Safe*, n.d.)

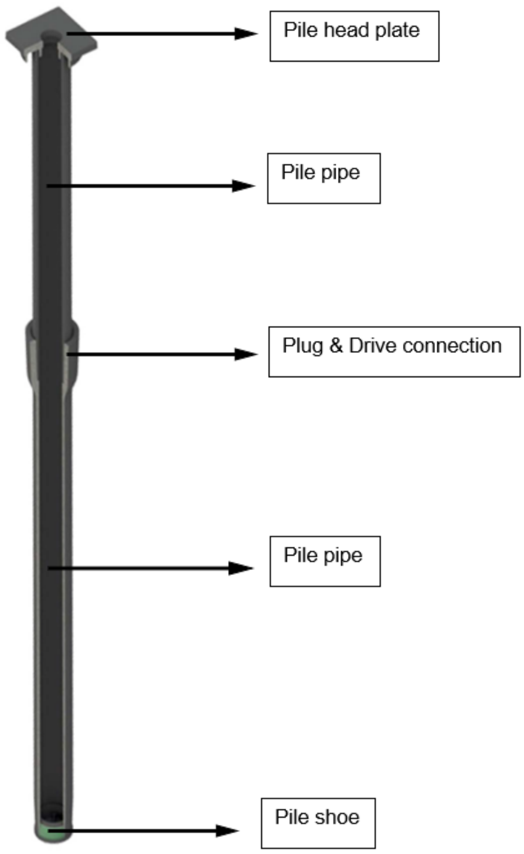

*Figure 1: Main components of a ductile iron driven pile (*TRM Piling Systems Fast. Simple. Safe*, n.d.)*

2.1.1 Pile pipe

According to the outside diameter of the pile pipes there are three different types available, namely Φ 98mm, Φ 118mm and Φ 170mm. The length of the ordered pipes is always 5 m but the desired foundation depth can be reached by joining the piles with the Plug&Drive® connection and cutting of the excess length. To have no waste, the cut off part of the pile can be used as the first element for the new pile. (*TRM Piling Systems Fast. Simple. Safe*, n.d.)

Some characteristics by pile type are shown in the Table 1.

Table 1: Main characteristics of the ductile driven piles (Steinlechner, n.d.)

Type - outside diameter	Wall thickness	Mass	Cross-section	Resistance moment	Bending moment M_{Rd}
mm	mm	kg/m	cm²	cm³	kNm
98	6,0	14,4		38	-
98	7,5	17,2		45	-
118	7,5	21,0	26,04	68	21,7
118	9,0	24,4	30,82	78	25,0
118	10,6	28,0	35,77	88	28,2
170	7,5	33,8		149	47,7
170	9,0	37,1	45,52	174	55,7
170	10,6	42,5	53,08	199	63,7
170	13,0	50,4		234	74,9

The piles of type 118 and 170 are provided by a tapered spigot at the bottom and a conical socket at top. This allows the piles to be connected through the Plug&Drive® jointing system, shown in Figure 4, which does not require the use of any special tools. The high vertical driving forces, used to install the piles, create high stresses in the conical socket and connect the two pile shafts by friction. The connection is rigid and torsionally stiff without the need of special tools or welding. The plug-in coupling system, where the spigot end is “crushed” against the socket, allows for total transmission of compression, shear and bending moment effort. Testing revealed that the joint system develops a strength greater than the pile shaft. If the spigot was shortened by 2.0 cm, the joint still retained a higher axial strength than the base shaft. The connection ensures a traction capacity of 250 kN in the joint. For stronger tensile forces, reinforcement should be applied. (*ANP-Systems GmbH FPG Piles Full Displacement Pressurized Grouted Piles*, n.d.; Steinlechner, n.d.)

In tests carried out by the supplier at the request of a customer, the connection between two pipes was subjected to a load test, with the objective of verifying the behavior of the connection. A force was applied at the jointing system of two piles. The schematic representation of the test is shown in Figure 2 and the setup is shown in Figure 3. During the test the connection was subjected to a load of 7800 kN, with a transverse displacement of 16,5 cm and a corresponding moment of 39,0 kNm. The connection did not suffer any breakage and there was no plastic deformation of the connection or tube after the relief. (Geosol, 2023)

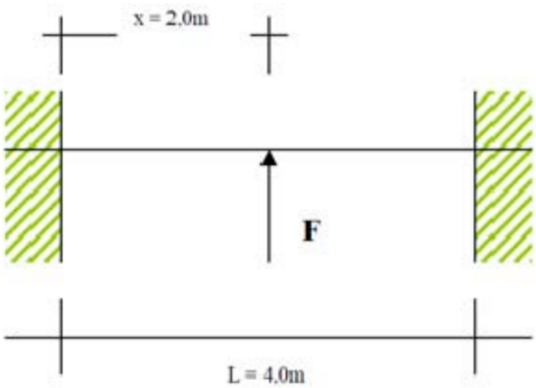

Figure 2: Schematic representation of the test on the connection of the ductile piles (Geosol, 2023)

Figure 3: Setup of the test on the connection of the ductile piles (Geosol, 2023)

The ductile driven piles can also be used at sites with restricted headroom. In these conditions the 5m long pile shaft is presumably too long. In this case, the pile is cut into shorter lengths and coupler hardware is used to connect the pile pipes again. Glued couplers are not permitted to use and the couplers should be spaced apart at least 1,00 m from each other in the longitudinal direction of the pile. The friction connection of the coupler provides the full bending resistance of the shaft. (*TRM Piling Systems Fast. Simple. Safe*, n.d.)

*Figure 4: Plug&Drive® jointing system of the ductile driven piles (*TRM Piling Systems Fast. Simple. Safe, *n.d.)*

*Figure 5: Coupler hardware of ductile driven piles (*TRM Piling Systems Fast. Simple. Safe*, n.d.)*

The dimensions and tolerances of the pile pipe for the different types are given in Table 2 with corresponding Figure 6. (*TRM Piling Systems*, n.d.)

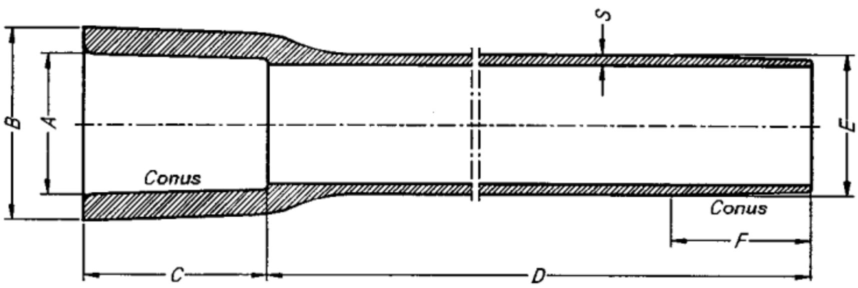

*Figure 6: Drawing of a pile pipe (*TRM Piling Systems*, n.d.)*

*Table 2: Dimensions and tolerances for the pile pipe (*TRM Piling Systems*, n.d.)*

			Type 89	Type 118	Type 170
	SOCKET				
A	Internal diameter	mm	104 +2,0/-1,0	118,5 +2,0/-1,0	171,5 +2,0/-1,0
B	External diameter	mm	132 ±1,6	≥162	≥220
	Conus		-	1:10 – 1:18	1:12 – 1:18
C	Conus length	mm	-	155 ±1,0	215 ±1,0
	PILE PIPE SHAFT				
E	External diameter	mm	98 +1,5/-1,0	118 +1,5/-1,0	170 +2,5/-1,0
S	Wall thickness	mm	6,0 -0,8	7,5 -0,8	7,5 -0,8
			7,5 -0,8	9,0 -0,8	9,0 -0,8
				10,6 -0,8	10,6 -0,8
					13,0 -0,8
D	Pile pipe length	mm	5020 ± 100	5000 ± 100	5000 ± 100
	SPIGOT END				
	Conus		-	1:10 – 1:18	1:12 – 1:18
E	External diameter	mm	98 +1,5/-1,0	118 +1,5/-1,0	170 +2,5/-1,0
F	Conus length	mm	-	110 -20,0	150 -20,0

2.1.2 Pile shoe

The first pile pipe is fitted with a pile driving shoe. This prevents water and soil from entering the pile shaft. When driven with an open end, about 1,5m of the leading section will be filled with soil.

The type of pile shoe that is used depends on if the pile is externally grouted or not and the type of soil. As seen in Figure 7, the pile shoes can be categorized by type A, B, C and D. Externally grouted piles, also called friction piles, are fitted with a conical grout shoe that has a larger diameter than the pile shaft. Consequently, an annulus between the pile shaft and the soil surrounding it is created while driving. This annulus is simultaneously filled with grout. Inside the conical grout shoe are a series of keeper plates to keep the pile in place. The oversized grout shoe is available with an outside diameter of 180, 220, 270 , 320 and 370 mm. Table 3 shows the pile types with their compatible shoe sizes. (*TRM Piling Systems*, n.d.)

*Table 3: Compatible oversized grout shoe type for each pile type (*TRM Piling Systems*, n.d.)*

Pile type	Pile shoe type C		Pile shoe type D				
	Φ220	Φ270	Φ180	Φ220	Φ270	Φ320	Φ370
Type 98			X				
Type 118	X			X	X	X	X
Type 170		X			X	X	X

In soil that contains no obstacles a flat shoe can be used as the end plug. For soils with obstructions that need to be penetrated, a steel plug with a rock point is opted. The pile types 118 and 170 can be fitted with any of the four types of pile shoes, while the pile type 98 can only be used with a type B or type D pile shoe. (*TRM Piling Systems*, n.d.)

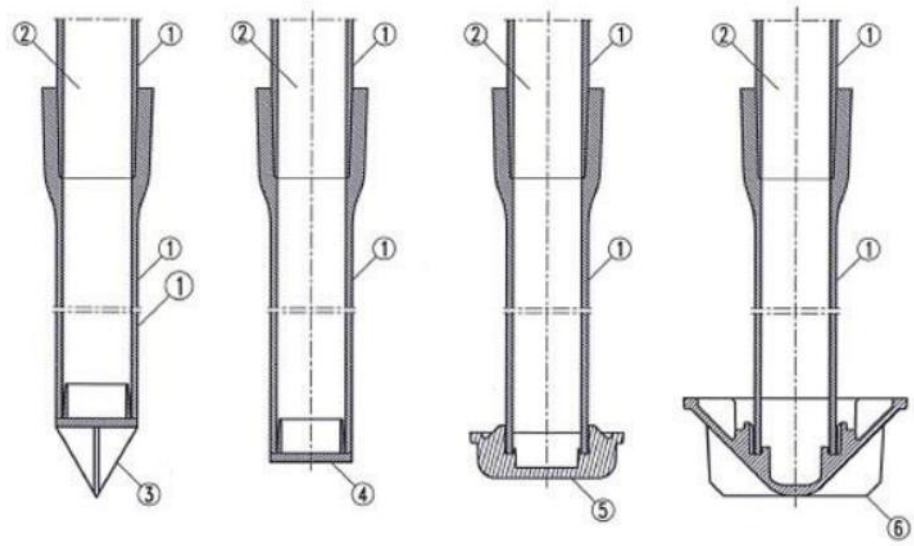

*Figure 7: The four types of pile shoes (*TRM Piling Systems*, n.d.)*

2.1.3 Pile plate

Once the pile has reached its desired depth, the top of the pile gets cut-off if needed and the pile is fitted with a pile cap plate. This self-centering head plate receives the load from the superstructure and transfers it into the pile. There are three categories of pile plates, namely A, B and C. They can be seen in Figure 8. Type B cannot be used for tensile or alternating load (tension-compression) piles. The dimensions of the plates, as seen in annex 1, are designed to transfer the maximum allowable forces. If a larger contact area is needed, shown mathematical proof, a pile head plate with larger dimensions can be used. An aperture is left in the plate for the insertion of steel reinforcement bars if necessary. This is always the case for tension piles. For type 118 piles the reinforcement is often two rebars of 25 mm S500/550 and for type 170 it is often 2 rebars of 32 mm S500/550. (Rohre GmbH, n.d.)

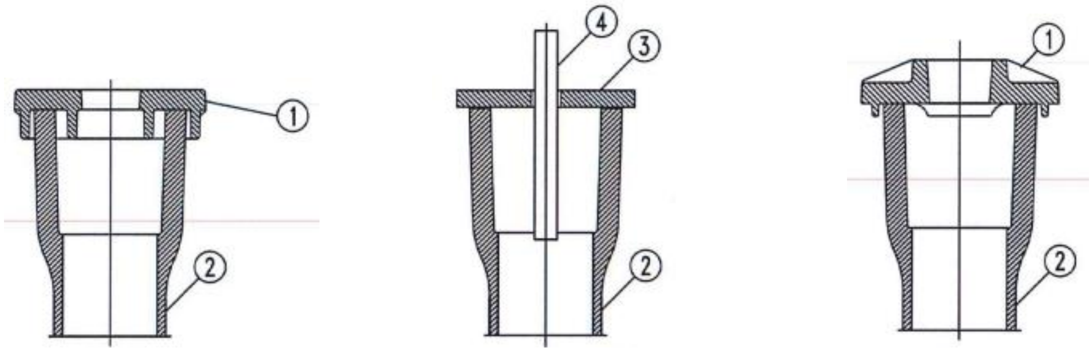

Figure 8: The three types of head plates (Rohre GmbH, n.d.)

2.2 Areas of application

The ductile iron piles have a wide application range. Figure 9 visualizes some of them. The standard use of the ductile piles is the foundation of buildings. Using the iron piles here can save a lot of concrete. Extra advantages are the relatively small and mobile equipment and the low vibration installation which offers the opportunity to install the piles close to existing buildings such as inner-city districts. The piles also provide an excellent solution for foundations of prefabricated structures. Steel or concrete prefabricated columns can transfer their load directly onto the piles. They are well suited for light weighted structures sensitive to differential subsidence. (*TRM Piling Systems Fast. Simple. Safe*, n.d.)

The ductile iron driven piles are also used as a foundation for bridge constructions since they have the advantage of having an overall short construction time. Horizontal forces are absorbed using inclined piles. Since the piles can easily be installed at an angle, they can also be used as reinforcement to support slopes with a high risk of failure. This way the unstable layers can be stitched together with competent ground. (*TRM Piling Systems Fast. Simple. Safe*, n.d.)

Ductile iron piles are easily executed as tension piles with the use of reinforcement and shaft-grouting. As a tension pile they can be used for the foundation of structures that easily uplift, like tanks, subways and construction pits in the groundwater fluctuation range. Thanks to their capacity to transfer tensile loads, the piles are also great for founding tall structures such as silos, rotating tower cranes, wind turbines, electricity pylons and transmission towers. The foundations of these structures require the capacity to transfer high compression and tensile loads. (*TRM Piling Systems Fast. Simple. Safe*, n.d.)

Lastly, the ductile iron piles also opt for a great solution to underpin existing foundations. When an old building gets a new function with additional loads, the existing foundation needs to be reinforced. Since this execution takes place with restricted headroom, the piles are a great solution since short piles can be connected with couplers during the installation. (*TRM Piling Systems Fast. Simple. Safe*, n.d.)

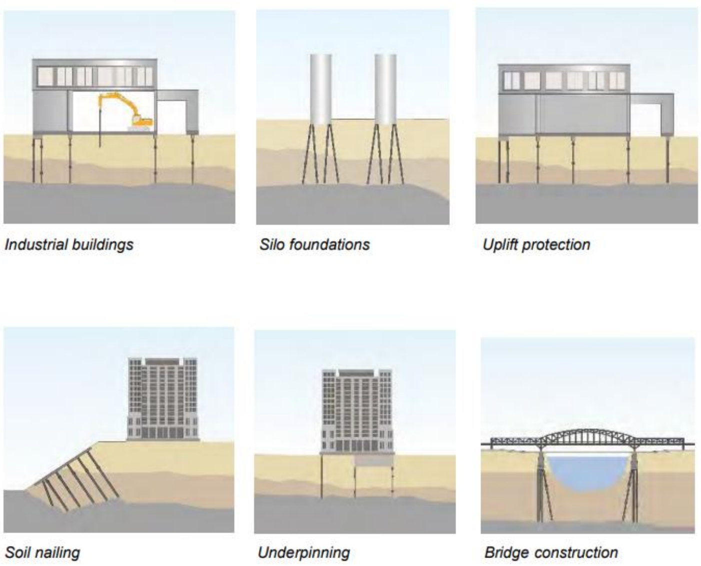

*Figure 9: Areas of application of the ductile driven piles (*TRM Piling Systems Fast. Simple. Safe*, n.d.)*

2.3 Manufacturing process and durability

The ductile driven piles are prefabricated out of ductile cast iron. The used piles at the site discussed in this thesis originate from the company TRM (Tiroler Rohre GmbH) in Hall in Tirol, Austria. They have been offering the ductile driven piles as a complete solution for foundations since 1986. (*About Us*, n.d.)

2.3.1 Ductile cast iron

Cast iron in the form of gray iron is seen as a relatively old construction material. In Europe it has been used for commercial pipeline construction since the 1800’s. Nowadays it’s rarely used because of its low tensile strength and ductility. Having barely any impact and shock resistance as a brittle material is a huge disadvantage. (*About Us*, n.d.)

To avoid this downside of gray cast iron, ductile cast iron is being used to pre-fabricate the ductile driven piles. The shape of the graphite of the two types of cast irons are different. Traditional cast iron contains small lamellar flakes of graphite while ductile iron has spherical graphite nodules. The stress lines in the graphite of gray cast iron become highly concentrated at the tip of the graphite lamellae. The spherical graphite nodules are obtained by adding magnesium into the grey cast iron melt. Thanks to this spheroidal shape, the stress lines flow around the separated graphite without concentrating. Due to this microstructure and the appropriate heat treatment, the tensile strength, flexibility, durability, and elasticity are highly improved. This spheroidal iron withstands bending and shock loading far better than traditional gray cast iron. (*About Us*, n.d.) (David, 2023) (Dey A. K., 2023)

The chemical composition of ductile cast iron can be found in Table 4. The remaining percentage, around 94%, consists of iron (Fe). (*About Us*, n.d.)

Table 4: Chemical composition of ductile cast iron

Carbon	C	3,3 – 3,8 %
Silicon	Si	2,1 – 2,6 %
Manganese	Mn	< 0,5 %
Phosphorus	P	< 0,1 %
Sulphur	S	< 0,01 %
Magnesium	Mg	0,03 – 0,05 %

The material properties of ductile cast iron can be found in Table 5. Due to these resilient properties the piles are resistant to temperatures of at least -20°C.

*Table 5: Material properties of ductile cast iron (*TRM Piling Systems*, n.d.)*

Tensile strength	450 MPa
Yield strength	320 MPa
Compressive strength	900 MPa
Modulus of elasticity	170 000 MPa
Density	7050 kg/m^3

2.3.2 Manufacturing and quality management

Figure 10 shows the visualization of the manufacturing process of the ductile piles.

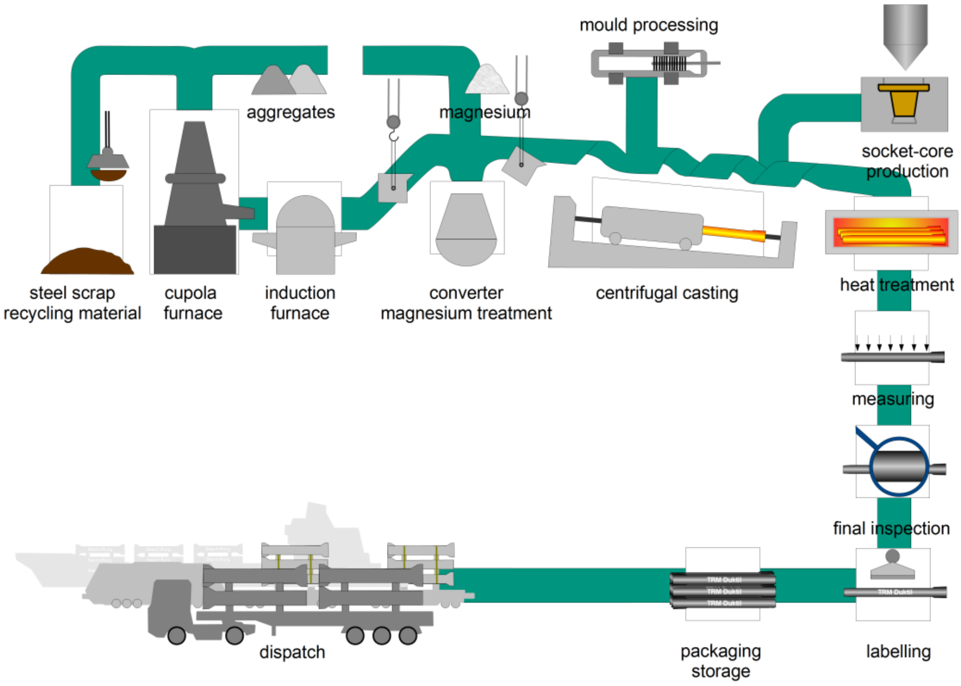

*Figure 10: Production process ductile iron piles (*TRM PILING SYSTEMS Tiroler Rohre GmbH*, 2022)*

The production process starts with the use of all steel scrap and recycled materials. To this mixture, aggregates are added. These aggregates are hard stone, coke, limestone and silicon carbide. Hard stone is a slag former and coke is used as an energy source while increasing the carbon content. Limestone is added for a better slag composition and desulphurization. The purpose of adding the silicon carbide is to increase the silicon content in the iron. The mixture of approximately 10 ton is melted in a melting pot in a cupola furnace. Thereafter the mixture goes into the George Fisher converter. In here the mixture is further processed at around 1500 degrees Celsius and the magnesium is added. The melted iron is immediately being checked for its chemical composition since the graphite should form spherical nodules to create the desired ductile iron. For this check a sample of the mixture is taken out with a big and long spatula (see Figure 11) and send directly to the laboratory in the factory trough a vacuum pipe system. With the use of x-rays a spectral analysis is performed in the lab to confirm the chemical composition of the iron mixture. Figure 12 shows the lab where the analysis is performed. It takes only around 15 minutes between the sample taking and getting the results of the analysis. If the chemical composition is within the right values, the casting process will start. (*About Us*, n.d.)

Figure 11: Taking a sample of the ductile iron mixture

Figure 12: Analysis of the chemical composition

The ductile piles are manufactured by a centrifugal spun-cast process using the De Lavaud process. The pile shaft of nearly uniform thickness is formed by placing the molten iron in a rotating mold. The production process is created so that the outside of the poles is not completely smooth. This is visible in Figure 16. This allows the pole to apply a tiny amount of skin friction. With the use of quartz sand cores, the spigot end is created. While the pipe shaft is still hot, it is taken out from the mold by an automatic transport system and placed in an annealing furnace. This is essential to dissolve the brittle carbides during the rapid solidification in the manufacturing process of the piles. The annealing furnace gets heated to 920-950 °C and cooled following a certain temperature curve to 200-250 °C. The cooling process must be slow and steady to ascertain the right tensile and elongation properties. During the process a high corrosion protection oxide-layer is created. (*About Us*, n.d.) (*DeLavaud process*, n.d.)

After the cooling process, the quality of the piles is tested. A tensile test is carried out on the test bar in accordance with EN ISO 6892-1. The results must comply with Table 5. The ultimate tensile strength R_m shall be at least 450 MPa, the yield stress minimum 320 MPa and the elongation at rupture at least 10%. Additionally, a Brinell hardness test according to EN ISO 6506-1 is being performed on the pipe or on a sample cut of the pipe. The tested surface has to be prepared by local grinding and the used ball must have a diameter of 2,5 mm, 5 mm or 10 mm. The hardness shall not exceed 230 HBW. If the ductile iron does not achieve the required material properties, the reason must be investigated and the castings must be reheated and retested or rejected. (*TRM Piling Systems*, n.d.)

Figure 13 shows the ductile iron test bars that are taken out of a sample that was cut from the ductile pile. Figure 14 shows the tensile test carried out on the test bar.

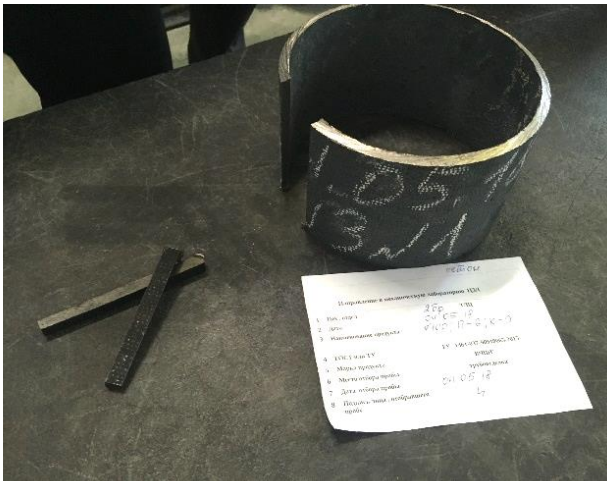

Figure 13: Taking test bar out of the pile

Figure 14: Tensile test on the test bar

The outside diameter, the connection dimensions, the wall thickness, the length and the straightness of the piles are also being checked. The used methods follow ÖNORM EN 545:2011, Clause 6.1 and 6.2. The outside diameter of all the manufactured piles is being measured and checked, while the other characteristics are only being tested on 1% of the produced piles. All the measured dimensions must comply with Table 2. The external diameter at the spigot end of the pipes is measured with circumferential tape or checked by pass/fail gauges. The manufacturer is obliged to be able to demonstrate that the wall thickness of the shaft meets the predetermined value. The allowed error limit of the measuring equipment is ± 0,1 mm. The wall thickness of TRM ductile piles is measured at 32 different locations using ultrasonic waves. (*TRM Piling Systems*, n.d.)

When pipes are cast from a new mold, the length of one pipe from the first pipe always must be checked. To ensure the straightness of the pipes, the pipe is rolled on two gantries or rotated around its axis on rollers. The gantries or rollers should be at least two thirds of the standardized pipe length apart. The maximum deviation from the straight axis is being measured and should not be more than 0,125% of the pile pipe length. (*TRM Piling Systems*, n.d.)

After the ductile pipes are being approved by the tests, a quality certificate can be issued. Certificate type 2.2 conform to EN 10204 confirm the mechanical properties such as the yield and ultimate stress, the elongation and hardness. This is a common certificate to issue the client. Certificate type 3.1 conform to EN 10204 confirms the chemical and mechanical properties. (*TRM Piling Systems*, n.d.)

Lastly, the piles are labeled with the outer diameter, the wall thickness if required and the date and time of manufacture. Then the piles are bundled with the help of squared lumber and PET binding tapes and stored for shipment. The bundled and labeled piles can be seen in Figure 15. The most common transportation methods are by ship for overseas destinations and via truck within Europe. (*TRM PILING SYSTEMS Tiroler Rohre GmbH*, 2022)

Figure 15: Bundled and labeled piles

Figure 16: Texture of the piles

2.3.3 Piles corrosion and fire resistance

As with any steel product, corrosion resistance must be examined. As mentioned above, the annealing process creates a corrosion protection layer over the piles. In conjunction with the high carbon and silicon content, the ductile cast iron has in general a higher corrosion resistance than steel. (*TRM Piling Systems*, n.d.)

Corrosion of the ductile piles will lead to material loss which will shrink the thickness of the pile. This influences the load-bearing capacity of the pile requiring it to be considered in the structural design. More about this can be found in '*2.5.3 Corrosion'* of this thesis. (*TRM Piling Systems*, n.d.)

Besides having a relative high corrosion resistance, the piles also have a good resistance to fire. The ductile iron pipes meet the requirements for an A1 fire rating in accordance with the EC Decision and Commission Delegated Regulation (EU). Performance class A1 is the highest fire resistance rating a material can get. This means that ductile iron is non-combustible and will not contribute at any stage of the fire. Despite the piles having good fire resistance, this is irrelevant when used for deep foundations. (*TRM Piling Systems*, n.d.)

2.4 Installation process

2.4.1 End-bearing or friction solutions

There are two main ways to install the ductile piles, as an end-bearing or as a friction pile. The difference in the two types is based on the way they transfer the load to the ground. Like the name suggests, end-bearing piles transmit the load to strong soil or rock which the end of the pile is driven into. This way the piles resist loads through the bearing capacity of their cross-section. By contrast, friction piles resist load through shear stresses along the side of the pile. These piles develop skin friction along their length, so they don't have to be driven into strong strata. Figure 17 show an illustration of both pile solutions. (Iqbal S., 2017)

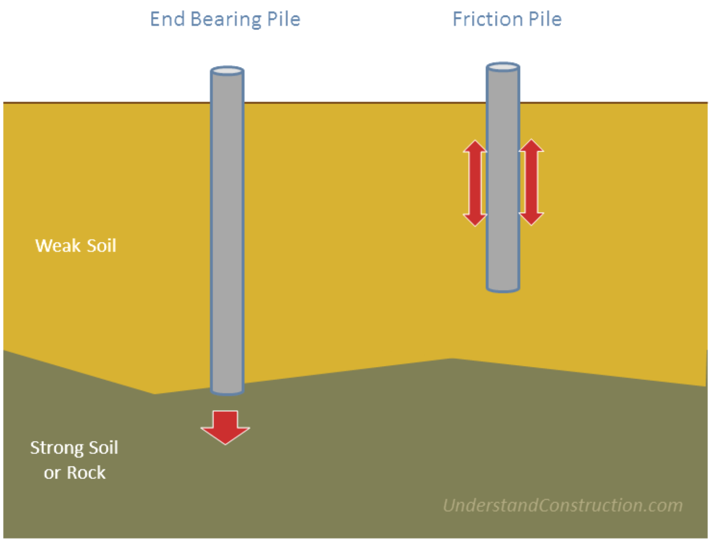

Figure 17: Visualization of an end-bearing and friction pile

The use of end-bearing ductile piles can be chosen when the very dense and hard soil or rock layers can support the required loads through end-bearing pressure. In general, an embedment length in the load-bearing subsoil of 2,5 m is recommended. The installation of these piles is executed without the use of external grout. For this reason, these piles are also called the non-grouted piles and are installed using the dry method. The pile shoe fitted on the lead section is a standard tight fitted driving shoe or end plug, type A or B. (Steinlechner, n.d.; *TRM Piling Systems Fast. Simple. Safe*, n.d.)

Friction piles can be used when the dense and hard soil or rock layers are at an unreachable depth. While part of the load can still be carried by end-bearing pressure, the other part is now carried by the skin friction of the grouted mortar. The piles can be driven into cohesive and non-cohesive soils. (Steinlechner, n.d.; *TRM Piling Systems Fast. Simple. Safe*, n.d.)

The installation of these piles is executed with the use of grout around the pile shaft; hence they are also called externally grouted piles and are installed using the wet method. The pile shoe used is oversized to create an annulus between the pile surface and the soil. While driving the pile, this annulus is simultaneously filled with a sand grout. The thickness of the grout coat shall be at least 20 mm along the whole pile. The high frictional capacity is created through the grout-to-ground bonding with the compacted soil. The grout must have a high flowability. This can be achieved by using 500 kg cement per cubic meter and having a slump in the range of 180 mm. The shape of the sand aggregate should also be taken into consideration. Table 6 gives an idea of the required amount of grout for two combinations of pile type and grout shoe. (Machinery S., 2021) (Steinlechner, n.d.; *TRM Piling Systems Fast. Simple. Safe*, n.d.)

Table 6: Estimation of the amount of grout required for two pile types (Bauer, 2019)

Pile type	Pile shoe	Quantity of grout
Type 118 x 7,5 mm	200 mm	35 L/m
Type 170 x 9,0 mm	250 mm	55 L/m

The skin-friction pile is initially driven in the ground to a depth of 20 – 30 cm. After that the driving continues while pumping grout at a pressure of approximately 30-40 bar along the pile shaft. Sufficient pumping capacity must ensure that the required amount of grout is delivered in proportion to the pile drop per second. At no time should the driving speed exceed the speed of the grout pump. The level of grout in the annulus should not be lower than 0,5 m below ground level. (Bauer, 2019; *TRM Piling Systems Fast. Simple. Safe*, n.d.; Steinlechner, n.d.)

The grout from the grout pump goes through the hammer driving tool and through the inside of the pile to the pile shoe. The grout escapes by a wedge opening, around 5 – 8 cm wide and 10 cm long, that is cut at the end of the leading section. If it is desired to reduce the risk of damage to the pile shoe, instead of the wedge a triangle shape can be cut 30 – 50 cm above the bottom of the leading section. This is illustrated in Figure 18. Figure 19 shows the result of the external grout around the pile. (Bauer, 2019)

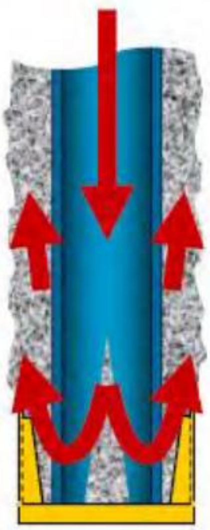

Figure 18: Skin-grouting during installation (Bauer, 2019.)

Figure 19: Internally and externally grouted ductile iron pile with two rebars (Bauer, 2019)

The choice of installing the piles as end-bearing or fiction piles is mostly based on the total cost. Which method has the lower cost is dependent on several factors. For example, a friction pile requires less iron due to the shorter pile length but the cost of cement and water for grout is added. The total working hours of the workmen and the transportation of the piles and possible grout must also be taken into account. The total cost of both methods is very dependent on the location and possible resources of the site.

2.4.2 Ductile iron piles installation

The spigot end of the first pipe is cut off, so the pile shoe is fit perfectly to the shaft. The minimum spacing between the two centers of a pile is 0,7 m for ductile piles of type 98 and type 118. For type 170 this minimum distance is 1,0 m. The minimum distance to existing structures is always 50 cm due to the geometry and dimensions of the hydraulic hammer. Using a lifting sling the first pile section is picked up and positioned at the desired place. When starting to install a pile, a levelling instrument is used to check the verticality of the pipe. (Bauer, 2019)

Whether a friction or end-bearing pile is installed, the ductile piles are always driven. The driving process takes absolutely no soil out of ground and compacts the ground around the pile. According to Broms (1966), the zone of densification caused by pile driving in non-cohesive soils is 3 to 5,5 times the pile diameter. Figure 20 shows the zone of densification. When driven at allowed close spacing, the driving process densifies the soil. This can have the advantage of reducing the risk of liquefaction of the soil. The process of liquefaction is the loss of shear strength between the grains of the soil. (Bauer, 2019)

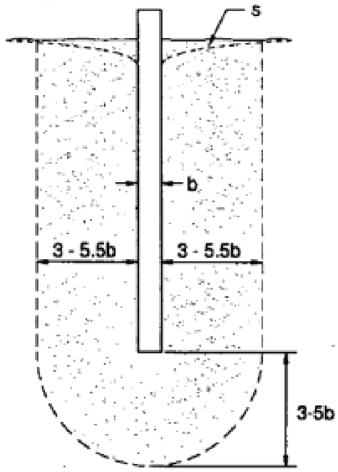

Figure 20: Zone of densification caused by pile driving (Bauer, 2019)

It is important that not more than 90% of the piles 0,2% proof stress limit is reached during the driving. Angled piles can be implemented up to a slope of 45° for non-externally grouted piles and 30° for shaft-grouted piles. (*TRM Piling Systems Fast. Simple. Safe*, n.d.)

The piles are driven in the ground using a high impact and high frequency hydraulic hammer. This hammer is typically mounted on an excavator with an adapter plate or frame that is mounted on the tapered socket of the pile. The excavator and adapter plate and frame can be seen in Figures 21, 22 and 23. The drive adapter or 'drive shank' is necessary and has a different design for grouted and not grouted piles. Each adapter can be used for 118 mm or 170 mm pile type. The use of an excavator is more mobile and cost-effective than using a traditional pile driving rig. The two generally used hydraulic hammers are the following: the MB1700 for the type 118 piles and the HB2200 for type 170. (Bauer. (2019).

Figure 21: Excavator to drive piles

Figure 22: Adapter plate (Bauer, 2019)

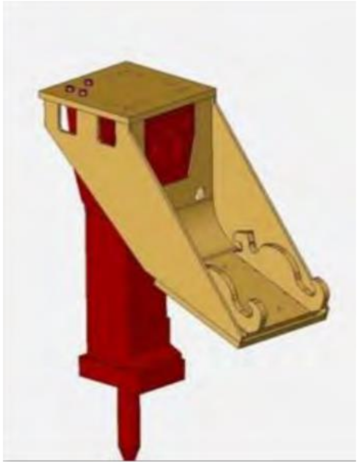

Figure 23: Adapter frame (Bauer, 2019))

After the first pipe is driven, the spigot ends of the next pipes are repeatedly inserted into the sockets of the previous driven pipes. With continuing the driving process, a stable connection with full load capacity is created between the two pile sections. In some cases, for example when the available working height is limited, the pipes are being cut into smaller pieces and connected again using coupling devices. (Bauer, 2019.; Steinlechner, n.d.)

Pipes keep being driven until the desired depth and/or resistance is reached. During the driving, the lowering of the pile and time are measured. Therefore, the penetration of the pile per second is registered. The desired resistance is expressed by a criterion for the load-bearing capacity of the ground. A typical refusal criterion for end-bearing piles is a penetration rate of maximum 10 mm in 20 seconds. practically, this is carried out by drawing a line on the pole at ground level and a second line 30 mm above it. This can be seen in Figure 24. After 1 minute of drilling, a check is made to see if the second line is still visible. If it is, refusal is achieved and the driving is stopped; if not, they continue. (Bauer, 2019)

As seen in Figure 25, an angle grinder is used to cut the pile to the designed length. This cut off section has no longer a spigot end which ensures that a driving shoe can be mounted on it immediately, thus becoming the new lead section for the next pile. This continuous system results in no wastage during the installation of the piles. (Bauer, 2019)

Figure 24: Drawn lines to check refusal

Figure 25: Cutting off the pile

When the piles are designed as internally grouted, a grout or concrete is used to fill up the inside of the piles. With shaft-grouted piles this happens during the driving and with not externally grouted piles this takes place after the insertion without any pressure. ÖNORM EN 206 sets some requirements for the grout used for the inner filling of the piles and the external grouting. Both should have a compressive strength of at least C20/25 and an aggregate with a size up to 4mm. (Steinlechner, n.d.; *TRM Piling Systems Fast. Simple. Safe*, n.d.)

In most cases, a head plate is placed at the upper end piece for an even load distribution from the upper structure to the piles. Any cavity under the head plate is also filled with concrete or grout to correct a possible deviation and ensure the best force transmission.

While the cement-based filling is still wet, reinforcement for the piles can be installed. The reinforcement bars must cross al sockets of the pile pipes. They go through the hole of the head plate and are anchored in the upper foundation structure. At least three bush spacers are used to guarantee that the reinforcement is installed along the center of the pile. The spacers need to be placed at maximum 1,50 m from the pile head or foot and should be placed not further than 3 m from each other. This last distance can be reduced according to the inclination of the pile. When dealing with tension or alternating load piles, the shaft should always be externally grouted. Annex 2 gives a full illustration of a tensile or alternating load pile with the accompanying dimensions. (Rohre GmbH, n.d.)

The installation process is repeated until all the piles are installed. Figures 26 and 27 show the two ways of installing the ductile driven piles.

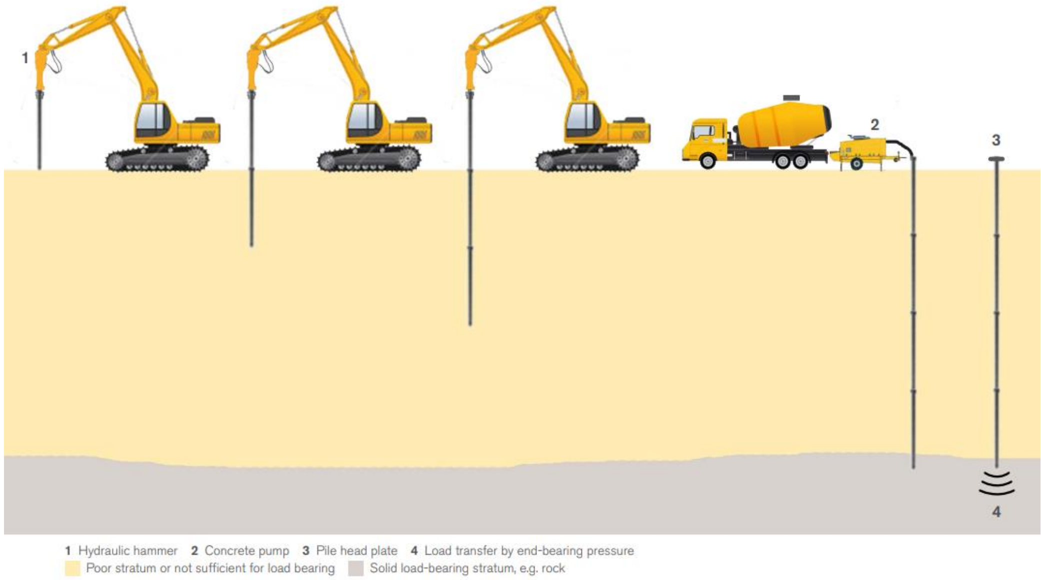

*Figure 26: Visualization of the installation of end-bearing ductile iron driven piles – dry method (*TRM Piling Systems Fast. Simple. Safe*, n.d.)*

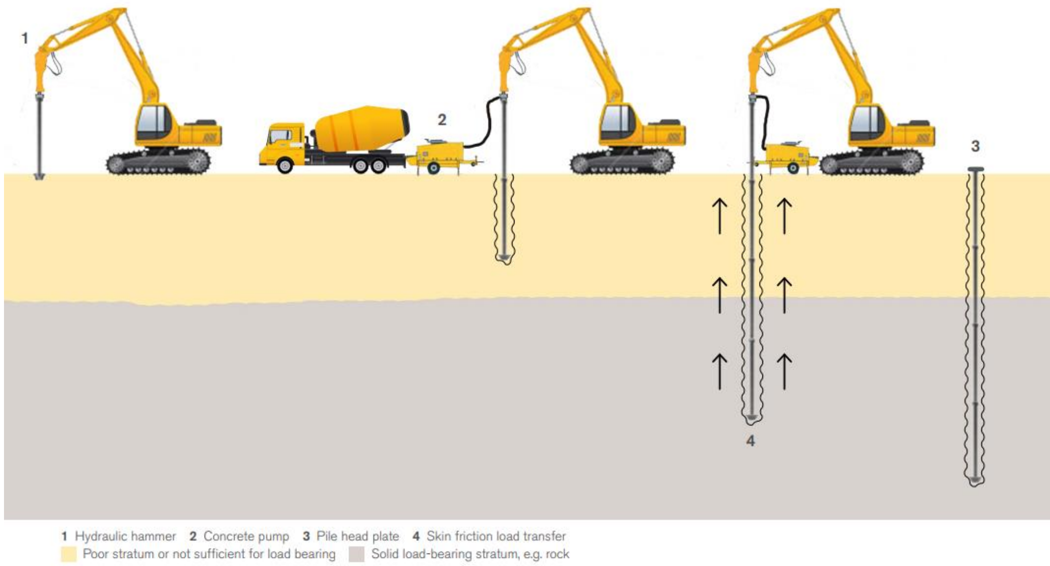

*Figure 27: Visualization of the installation of skin friction ductile iron driven piles – wet method (*TRM Piling Systems Fast. Simple. Safe*, n.d.)*

2.4.3 Vibrations and sound level

Although the hammer has a high impact and high frequency, the piles are being driven into the ground with a low vibration. The high frequency of the hydraulic hammer ensures that the stroke has no time for a recoil, keeping the amplitude of the vibrations low. Furthermore, the high frequency waves quickly dissipate with distance from their energy source. Also, the displacement of soil due to the driving of the pile is not much due to the small cross-sectional area. This all contrasts with the hammers used to install concrete piles and other traditional driven piles. These hammers are a lot heavier and create waves with a much higher amplitude and low frequency. These waves can travel longer distances and more soil is displaced due to the larger cross-sectional area of the pile. (Nagel I Pfahl ZERTIFIZIERT, n.d.)

Driving the piles with a low vibration has the advantage that the piles can be installed close to existing structures. As a rule of thumb, a pile can be driven as close as 50 m to an existent construction. The risk that the vibrations damage a building can be examined by looking at the maximum vertical velocity of oscillation. Table 7 shows the maximum permitted vertical velocity oscillation in relation to the quality of the building. This can be seen as a general rule since the risk of damage is also dependent on the soil conditions and has to be evaluated at every site specifically. (*Steel Pipe Piles Finnish National Road Administration (FinnRA) Bridge Engineering*, 2000)

*Table 7: Maximum vertical velocity of oscillation in relation to the quality of the building (*Steel Pipe Piles Finnish National Road Administration (FinnRA) Bridge Engineering*, 2000b)*

Class of the building	Quality of the building	Maximum vertical velocity of oscillation [mm/s]
1	Old historic buildings	2
2	Cracked buildings, Brick buildings	5
3	Buildings in good condition without damage	10
4	Very strong buildings	10 - 40

Generally, a maximum velocity of 1,45 mm/s can be assumed for the installation of ductile driven piles. Looking at Table 7 it can be concluded that the installation of ductile driven piles is harmless for any type of building that can be found in proximity.

Regarding the sound generated when installing the piles, a value of 110 to 112 dB at about 30 feet, which is around 9 m, can be assumed. The loudest noise is created during the initial driving. During the further penetration of the pile in the ground, the sound levels quickly drop below 100 dB. With the installation of grouted piles, the emitted noise is reduced due to the damping effect of the grout. If desired, noise abatement devices can be used to lower the noise level during driving even more. This device usually consists of rubber belts that can be attached to the hammer on three sides and hangs down approximately 1 to 1,5 m. The device can be seen in Figure 28. (Nagel I Pfahl ZERTIFIZIERT, n.d.)

Figure 28: Noise abatement device on a driving hammer

2.5 Design

Ductile driven piles are designed to transfer static axial forces to the ground. Predominantly, the piles are subjected to pressure, but tension or alternating load may also occur. The general calculation for the structural design of the piles is based on Eurocode 3 (NBN EN 1993, 2015) and 4 (NBN EN 1994, 2005). Two components of the design resistance are considered the structural and geotechnical designs of the load-bearing capacity of the pile.

Due to the small diameter of the ductile piles, they have a limited capacity to transfer lateral loads and are sensitive to buckling. Buckling in the ground will be investigated regarding the geotechnical load bearing capacity. To transfer horizontal loads, the piles can be installed at an angle. (Bauer, 2019)

It is necessary to verify that the design value of a load effect on a single pile E_d, such as an internal force, a moment or a combination of one or several forces and/or moments do not exceed the corresponding calculated design value of the resistance $R_{i,d}$, where all structural and geotechnical properties are given. (NBN EN 1993, 2015)

$$E_d \leq R_{i,d} \tag{1}$$

To meet this ultimate limit state criteria, the following three types of possible failure must be investigated: the failure of construction by failure in the soil (geotechnical load bearing capacity), structural failure (structural load bearing capacity) and a combination of failure in the soil and structural failure (structural and geotechnical load bearing capacity)

2.5.1 Structural design

The structural load bearing capacity, also called cross-sectional load-bearing capacity, is expressed in terms of the maximum permissible load bearing capacity of the pile to not have structural failure.

2.5.1.1 Verification of the structural resistance of ductile iron piles

The design resistance of the ductile driven piles can be calculated as follows: (NBN EN 1993, 2015)

$$R_{i,d} = \frac{R_{i,k}}{\gamma_M} \tag{2}$$

Where:

γ_M = the partial factor for the ductile iron pipe = 1,0

R_k = the characteristic value of the particular resistance

With the use of this safety factor, the design resistance for compression, tension and bending moments can be calculated.

The design resistance for compression and tension can be calculated in the same way. The design value of the compressive/tensile axial force N_{Ed} at each cross-section has to be smaller than the design resistance of the cross-section for uniform compression/tension $N_{c,Rd}/N_{t,Rd}$ (NBN EN 1993, 2015)

$$N_{Ed} \leq N_{c,Rd}/N_{t,Rd} \tag{3}$$

$$N_{c,Rd}/N_{t,Rd} = \frac{N_{Rk}}{\gamma_M} \tag{4}$$

The characteristic resistance to an axial force is calculated as follows: (NBN EN 1993, 2015)

$$N_{Rk} = A * f_y \tag{5}$$

With:

A = the cross-section of the pile

f_y = the yield strength of the material

Analogously, the design resistance for a bending moment can also be calculated. The design value of the bending moment M_{Ed} at each cross-section must be smaller than the design bending moment resistance of the cross-section for bending about one principal axis $M_{c,Rd}$. (NBN EN 1993, 2015)

$$M_{Ed} \leq M_{c,Rd} \tag{6}$$

$$M_{c,Rd} = \frac{M_{Rk}}{\gamma_M} \tag{7}$$

The characteristic bending moment resistance is calculated as follows: (NBN EN 1993, 2015)

$$M_{y,Rk} = W_y * f_y \tag{8}$$

$$M_{z,Rk} = W_z * f_y \tag{9}$$

With:

W = the section modulus of the cross-section of the pile

f_y = the yield strength of the material

For general design, the elastic section modulus, applicable up to the yield point, is used. Multiply this value with the yield strength of the material to get the yield resistance moment. The elastic section modulus of a hollow pipe is calculated as follows:

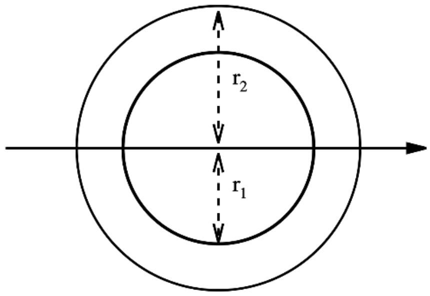

Figure 29: Cross-section of the piles where the arrow represents the neutral axis for the section modulus

$$W_{el} = \frac{\pi * (r_2^4 - r_1^4)}{4 * r_2} = \frac{\pi * (d_2^4 - d_1^4)}{32 * d_2} \quad (10)$$

Besides the elastic, there is also a plastic section modulus. By multiplying the plastic section modulus with the yield strength of the material, the plastic moment is calculated. The formula for finding the plastic section modulus of a hollow pipe is the following:

$$W_{pl} = \frac{8 * \pi * (r_2^3 - r_1^3)}{6} = \frac{\pi * (d_2^3 - d_1^3)}{6} \quad (11)$$

The above calculations solely apply to the ductile iron micropiles and not on the piles when they are filled with concrete and reinforcement is possibly used. In this case, the cross-section becomes a composite cross-section where the iron and concrete work together. To work with the composite cross-section, there are multiple ways to calculate the design resistance. The simplest way is explained down below (2.5.1.2). The method with an equivalent iron cross-section is calculated later for the compression load test (3.5.1) and the method according to Yan-Gang Zhao (2009) is used in the foundations design of the compression piles (3.6.2).

2.5.1.2 Verification of the structural resistance of grouted ductile iron piles in compression

The design cross-sectional load-bearing capacity $R_{i,d}$ can be calculated as the sum of the design load-bearing capacities of the ductile cast iron pipe and of the cement mortar or concrete inside the pipe. For shaft-grouted piles, too, only the cement mortar inside the ductile iron post needs to be considered. (Rohre GmbH, n.d.)

$$R_{i,d} = \frac{R_{DPk}}{\gamma_M} + \frac{R_{ck}}{\gamma_c} \quad (12)$$

$$R_{DPk} = A_{DP} * f_y \quad (13)$$

With:

f_y = the yield strength of the material = stress at 0,2% elongation = 320 N/mm^2

A_{DP} = cross-sectional area of the ductile cast iron pile

γ_M = partial safety factor for the iron pipe = 1,0 for all design situations according to Eurocode

$$R_{ck} = A_c * f_{ck} \tag{14}$$

With:

f_{ck} = characteristic cylinder compressive strength of the cement mortar after 28 days

A_c = cross-section of the inner pile cement mortar or concrete

γ_c = partial safety factor for the cement mortar/concrete = 1,50 according to Eurocode

Since there are many constants in this calculation, the design values of $R_{i,d}$ for can be found in a table according to the pile type and service life. These design values can be found in tables in annex 3.

2.5.1.3 Verification of the inner pile-grout bond of tension ductile iron piles

For tension piles the longitudinal shear strength between the inner cement mortar or concrete and the inner interface of the ductile iron pile should be examined. It should be verified that, in the ultimate state, the design action effects on the individual pile E_d do not exceed the design longitudinal shear strength $R_{vi,d}$. (Rohre GmbH, n.d.)

$$E_d \leq R_{vi,d} \tag{15}$$

$$R_{vi,d} = \tau_{Ri,d} * \pi * d_i * L \tag{16}$$

With:

d_i = nominal inner diameter of the ductile iron pipe

L = length of the pile

$$\tau_{Ri,d} = \frac{\tau_{Ri,\mathrm{k}}}{\gamma_{Mi,v}} \tag{17}$$

With:

$\tau_{Ri,k}$ = Characteristic value of the bond strength of the internal cement mortar/concrete with the ductile iron pipe interface = 0,7 N/mm^2 (Rohre GmbH, n.d.)

$\gamma_{Mi,v}$ = partial safety factor = 2,1 (Rohre GmbH, n.d.)

2.5.1.4 Verification of the outer bond between the grout ductile iro pile-grout bond

It must be verified that in the ultimate limit state, the component of the design action effects $E_{v,d}$ to be transmitted via skin friction are smaller than the design longitudinal shear strength of the interface between the cast iron pipe and the shaft-grouting $R_{v,d}$. (Rohre GmbH, n.d.)

$$E_{v,d} \leq R_{v,d} \tag{18}$$

$$E_{v,d} = \frac{E_d}{R_{i,d}} * R_{s,d} \tag{19}$$

With:

E_d = The design load action effects in the individual pile

$R_{i,d}$ = Design value of the resistance (structural load bearing capacity)

$R_{s,d}$ = the component of the design value R_d that is transferred via skin friction. In case of combined load transfer via end pressure and skin friction, $R_{s,d}$ cannot be specified and $E_{v,d} = E_d$ shall apply. (Rohre GmbH, n.d.)

$$R_{v,d} = \tau_{R,d} * \pi * D * L_{eff} \tag{20}$$

With:

D = nominal outer diameter of the cast iron pipe

L_{eff} = effective length of the pile not taking into account the coupling areas

$\tau_{R,d}$ = the design bond strength of the interface between the ductile cast iron pipe and the shaft-grouting = $\frac{\tau_{R,k}}{\gamma_{M,v}} + \mu_k * \sigma_N$ (21)

With:

$\tau_{R,k}$ = basic value of the bond strength = 0,32 N/mm^2 (Rohre GmbH, n.d.)

$\gamma_{M,v}$ = partial safety factor = 2,1 (Rohre GmbH, n.d.)

μ_k = coefficient of friction between cast iron pipe and shaft-grouting = 0,5 (Rohre GmbH, n.d.)

σ_N = lower characteristic value for the contact pressure from earth pressure and bracing effect acting horizontally along the circumference of the pile in N/mm² = $\frac{\tau_M}{\tan\varphi'}$ (22)

With:

φ' = angle of friction of the drained soil (effective angle of friction)

τ_M = skin friction in the grout with the interface
= $\frac{\tau_{M,k}}{\gamma_{s;t}}$ (23)

With:

$\tau_{M,k}$ = the characteristic value of the pile skin friction determined from the load tests or the empirical values, according to their inclination out of the vertical.

$\gamma_{s;t}$ = partial safety factor for the total pile resistance (compression), or skin resistance (tension) from load or based on empirical values.

2.5.2 Geotechnical load-transfer verification

The geotechnical load bearing capacity of the pile, also called geotechnical load-bearing capacity, takes into consideration the soil conditions at the particular site. The geotechnical design of foundations in general rely mostly on Terzaghi's and Meyerhof's theory of Bearing capacity.

The verification of the external load-bearing capacity shall be provided by performing a load test at the site. The static load test is carried out according to ÖNORM EN 1997-1. The maximum test load should not exceed 90% of the structural load bearing capacity of the ductile iron piles. (*External Load-Bearing Capacity of TRM Ductile Driven Piles*, n.d.)

$$\max P_p = 0{,}9 * f_y * A_{DP} \qquad (24)$$

Where:

f_y = yield strength = stress at 0,2% elongation = 320 N/mm²

A_{DP} = cross-sectional area of the ductile cast iron pile

When working with piles that are internally and externally grouted and have an inclination that does not exceed 5° out of the vertical, the test load may be increased by the proportion contributed by the inner cement mortar or concrete. (*External Load-Bearing Capacity of TRM Ductile Driven Piles*, n.d.)

$$\max P_p = 0{,}9 * f_y * A_{DP} + 0{,}8 * \ f_{ck}(t) * A_c \tag{25}$$

Where:

$f_{ck}(t)$ = characteristic compressive strength of the cement mortar/concrete as a function of time (age) t

A_c = cross-section of the inner pile cement mortar/concrete

The ultimate geotechnical load bearing capacity Q_u can be calculated as the sum of the shaft resistance and the toe resistance. (Design and Construction of Driven Pile, National Highway Institute, n.d.)

$$Q_u = \ R_s + R_t \tag{26}$$

$$Q_u = \ q_s * A_s + q_t * A_t \tag{27}$$

Where:

q_s = the shaft unit resistance [kN/m^2]

A_s = the shaft surface [m^2]

q_t = the toe unit resistance [kN/m^2]

A_t = pile toe area [m^2]

To calculate the shaft and toe unit resistance, it is necessary to get geotechnical information about the site where the piles must be installed. This is possible via dynamic penetrometer test. An example of these is a SPT or standard penetration test. More about these tests can be found in 2.5.2.2. (Design and Construction of Driven Pile, National Highway Institute, n.d.)

An example of a way to calculate the shaft resistance unit, is by doubling the corrected SPT values. (Design and Construction of Driven Pile, National Highway Institute, n.d.)

$$q_s = 2 * \overline{N}' \tag{28}$$

The toe resistance unit can possibly be found through the following formula: (Design and Construction of Driven Pile, National Highway Institute, n.d.)

$$q_t = 400 * \overline{N'_o} + \frac{D_B * (40 * \overline{N'_B} - 40 * \overline{N'_o})}{\phi} \tag{29}$$

Where:

$\overline{N'_o}$ = the corrected SPT value for the weaker layer (overbearing the bearing layer)

$\overline{N'_B}$ = the corrected SPT value for the bearing layer

D_B = pile embedment depth into the bearing layer [m]

ϕ = the pile diameter [m]

2.5.2.1 Geotechnical load-transfer verification for end-bearing piles

Non-grouted end-bearing piles can use the permissible internal load bearing capacity to full extent if the concentrated loads on the pile can be absorbed by the loadbearing soil. For these piles a cohesive loadbearing soil requires to have a firm to stiff consistency (SPT>20 with a driving rate of 15-30 sec/m). A non-cohesive loadbearing soil needs to have a high density (SPT>30 with a driving rate of 20-30 sec/m). (Bauer, 2019)

End-bearing piles are not externally grouted, which means they only have a little bit of skin-friction trough the surface of the pile. This is such a small value in comparison with the toe resistance that the shaft resistance is neglected for end-bearing piles. The permissible internal load bearing capacity that can be used to the full extent for the non-grouted end-bearing piles, can be found in the tables in annex 3.

In rock formations or very dense sand and pebbles, the maximum load bearing capacity is already reached after a shallow penetration depth. When the pile is being fully refused by driving, the external bearing capacity is at least equivalent to the analytical internal bearing capacity of the pile. In practice, the piles are usually not driven to full refusal but a stopping criterion is a penetration rate of 10 mm per 20 seconds or 30 mm per minute. (Bauer, 2019)

2.5.2.2. Geotechnical load-transfer verification for skin-friction piles

When the choice for an externally grouted pile is made, the pile load can be transferred into the surrounding soil trough skin friction. The permissible skin friction values used to evaluate the external load capacity of grouted piles can be found in Table 9. These values already include the safety coefficient η = 2,0. The values are related to dynamic penetrometer tests. Some characteristics of these tests can be found in Table 8. (Bauer, 2019)

Table 8: Characteristics of dynamic penetrometer tests (Bauer, 2019.)

Type of test	Acronym	Cross-sectional area of cone	Weight	Drop height
Medium Dynamic Probe	DMP	10 cm^2	30 kg	500 mm
Heavy Dynamic Probe	DPH	15 cm^2	50 kg	500 mm
Standard Penetration Test	SPT	20 cm^2	63,5	760 mm

Table 9: Permissible skin friction values (Bauer, 2019)

Cohesive (C) or non-cohesive (N) soil	Driving rate [sec/m]	Density	SPT (N30)	DPH (N10)	DPM (N10)	Permissible skin friction values q_{sk} [kN/m^3]
N	Pushed	Very loose	<4	0-2	0-4	0
N	5-10	Loose	4-10	3-5	4-11	(40)
N	10-20	Medium dense	10-30	6-15	11-26	80
N	20-30	Dense	30-50	16-30	26-44	120
N	30-…	Very dense	>50	>30	>44	150
C	Pushed	Very soft				0
C	Pushed	Soft	0-2	0-1	0-3	0
C	5-10	Firm	3-8	2-5	3-8	(20)
C	10-15	Stiff	8-15	5-7	8-14	(40)
C	15-30	Very stiff/hard	16-30	8-15	14-28	70
C	30-…	Very hard	>30	>15	>28	100

In function of the skin friction value for each particular soil type and layer thickness, the varying maximum allowable load bearing capacities are defined. Although externally grouted piles can also be partially end-bearing, the point resistance is usually neglected in the structural design process. (Bauer, 2019)

Through the design process, the depth of the piles are calculated, this way the right amount of piles can be ordered. For this calculation, the shaft unit resistance q_s has to be known. The empirical values for the characteristic skin friction from the research project by the University of Kassel can be used for this. This research project aimed for a better exploring of the interaction of the ductile driven pile with the surrounding soil layers. The used data consisted of documents of 121 construction projects such as comprehensive ground investigations, detailed information on the manufacturing process including the driving times over depth and the static and/or dynamic test loads. Extensive static and dynamic pile test were carried out additionally in cohesive and non-cohesive soils. (*External Load-Bearing Capacity of TRM Ductile Driven Piles*, n.d.)

By investigating the correlation between the pile and penetration resistance, the skin friction q_s and pile base resistance per unit q_b were determined from the CPT and DPH resistances. The results are summarized in graphs that can be found in Figure 30 for cohesive soils and 31 for non-cohesive soils. (*External Load-Bearing Capacity of TRM Ductile Driven Piles*, n.d.)

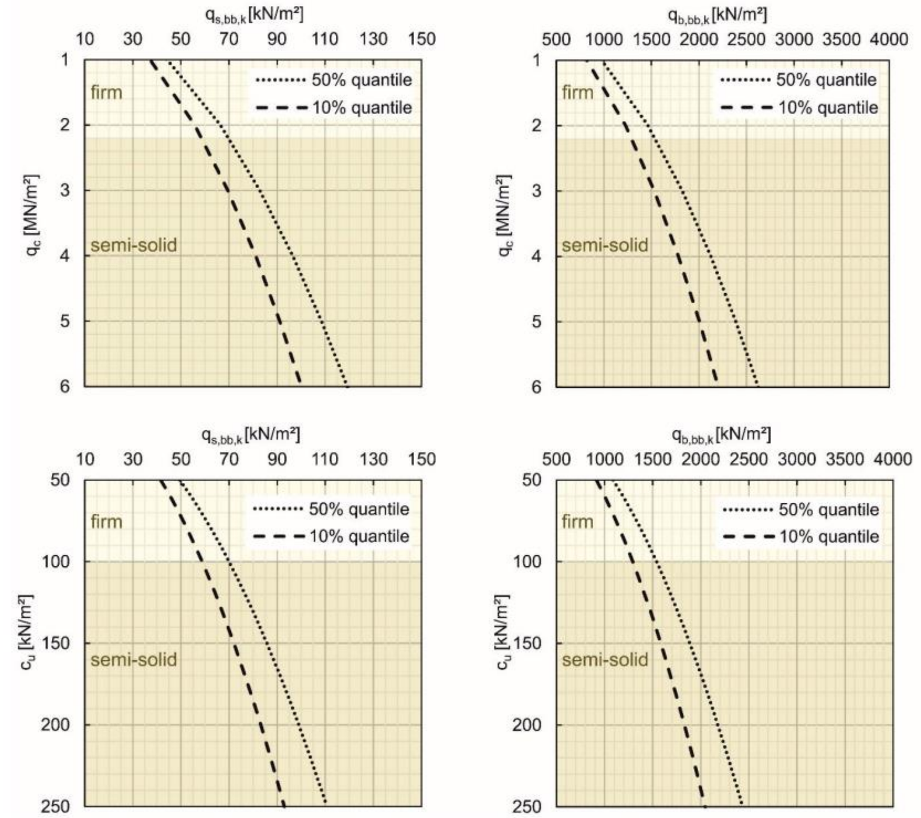

*Figure 30: Correlations between the unit of the pile base resistance or the skin friction resistance in cohesive soils (*External Load-Bearing Capacity of TRM Ductile Driven Piles*, n.d.)*

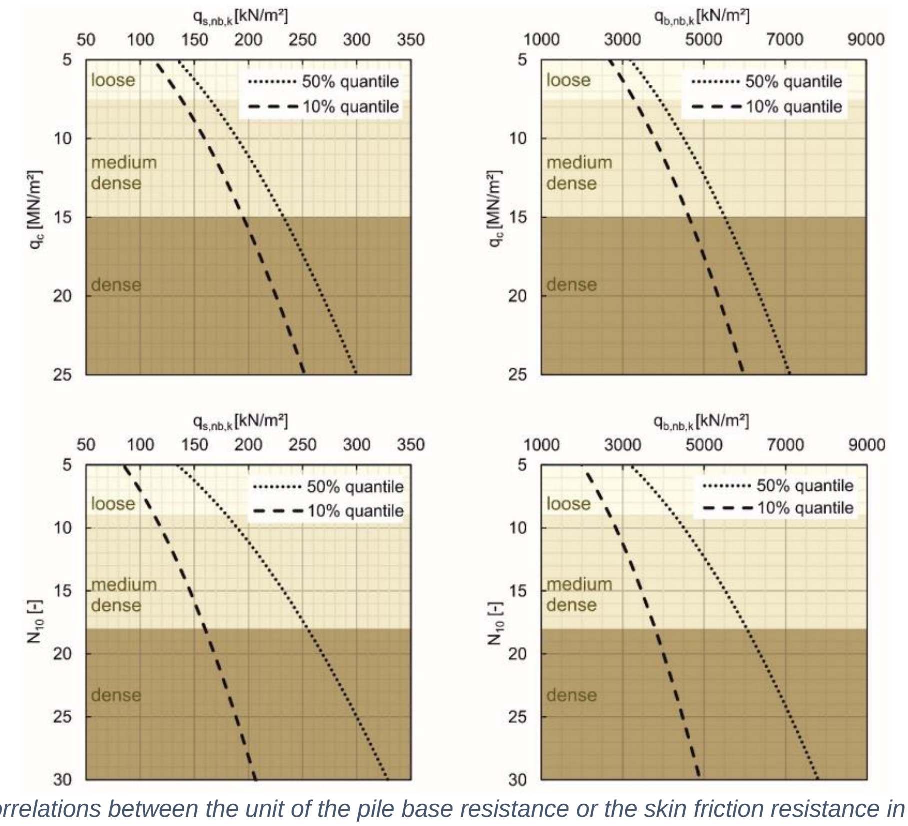

*Figure 31: Correlations between the unit of the pile base resistance or the skin friction resistance in non-cohesive soils (*External Load-Bearing Capacity of TRM Ductile Driven Piles*, n.d.)*

In these graphs:

$q_{s,bb,k}$ = pile skin friction per unit area in cohesive soil [kN/m^2]

$q_{b,bb,k}$ = pile base resistance per unit area in cohesive soil [kN/m^2]

$q_{s,nb,k}$ = pile skin friction per unit area in non-cohesive soil [kN/m^2]

$q_{b,nb,k}$ = pile base resistance per unit area in non-cohesive soil [kN/m^2]

q_c = mean cone resistance (CPT) [MN/m^2]

C_u = shear strength of the undrained soil [kN/m^2]

N_{10} = blow count (DPH) [-]

According to the shear strength of the cohesive soil, the mean cone resistance of the CPT or the blow count of the performed DPH, the pile skin friction unit and pile base resistance unit can be found in the graphs. When the needed geotechnical load bearing capacity is divided by the skin friction unit, the needed amount of pile surface in this soil layer can be found. Starting from this value and the diameter of the external grout, the depth of the skin friction pile is calculated.

$$Q_u = q_s * A_s \Leftrightarrow A_s = \frac{Q_u}{q_s} \tag{30}$$

$$d = \frac{A_s}{\pi * 2 * r} \tag{31}$$

Where:

Q_u = ultimate geotechnical load bearing capacity [kN]

A_s = the shaft surface [m^2]

d = the depth of the pile [m]

r = the radius of the grouted skin of the pile [m]

2.5.2.3 Buckling

Analyzing the safety against buckling is essential for cohesive soils with these small ductile piles. The analysis is unnecessary for non-cohesive soils since it can be assumed that the lateral support by the embedding is sufficient. Eurocode states that in soils with an undrained shear strength (c_u) of lower than 10 kPa, the buckling of piles needs to be investigated. (Vogt et al., 2009)

Euler created a formula to calculate the critical load at which buckling will occur. The Euler equation is the following: (Vogt et al., 2009)

$$P_c = n * \frac{\pi^2 * \ E_p * \ I_p}{L^2} \tag{32}$$

Where:

n = integer buckling number, factor accounting for the end conditions

E_p = modulus of elasticity of the pile

I_p = second order moment of inertia of the cross-section of the pile

L = effective length of the pile

This equation was created for piles that are not surrounded by soil. For pile foundations, this equation leads to oversized cross sections and inefficient designs since the resistance of the soil is not taken into account. To extend the equation, it is necessary to quantify the supporting lateral forces provided by the soil. Therefore, an applicable mechanical model should be used. Linear elastic bedding is the simplest approach to model lateral soil support. Starting from the Euler equation, Engesser found a solution to calculate the buckling load of an elastically bedded beam: (Vogt et al., 2009)

$$P_c = \ n^2 * \left(\frac{\pi}{L}\right)^2 * \ E_p * \ I_p + \frac{1}{n^2} * \left(\frac{L}{\pi}\right)^2 * k_l \tag{33}$$

With k_l = stiffness of the bedding

The critical buckling can also be found with the diagram by Pflüger, given in Figure 32.

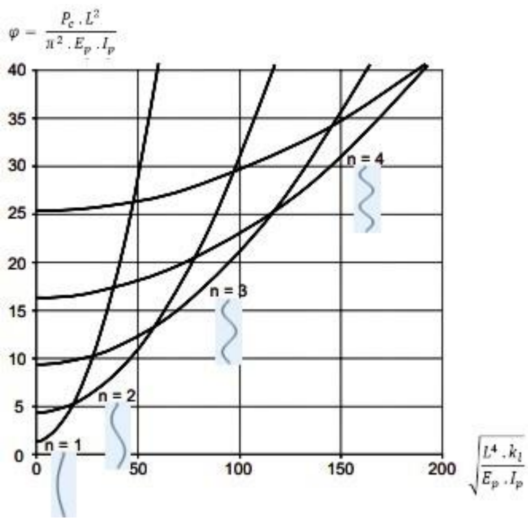

Figure 32: Diagram to find the critical buckling load (Pflüger)

The diagram is used by calculating the value on the x-axis, since the parameters out the formula should be known. Then, looking at the correct curve, the parameter ϕ can be read on the y-axis. Lastly, the formula of ϕ can be transformed to find the critical buckling load. (Vogt et al., 2009)

$$\varphi = \frac{P_c * L^2}{\pi^2 \, . E_p \, . I_p} \Leftrightarrow P_c = \varphi \, . \frac{\pi^2 \, . E_p \, . I_p}{L^2} \tag{34}$$

When checking the buckling for piles in soil, it is important to understand the influence of the soil characteristics on the stiffness of bedding. The stiffness of bedding k_l is typically correlated with undrained shear strength c_u, as described in *Pile foundation analyses and design* (*Poulos*, 1980). It is dedicated to adopted:

$$60 * Cu \leq k_l \leq 100 * Cu \tag{35}$$

When analyzing the behavior of cohesive soil in relation to the lateral soil resistance of piles, it is important to consider that an elastic approach is not applicable. This is because the deformation caused by pressing into clay is not easily reversible, and the soil behaves in an extremely plastic manner. As a result, deformations may occur during buckling and it becomes necessary to describe the behavior of soft clay in a more precise manner.

When the soil is considered to be a perfectly plastic cohesive material, the calculation of the ultimate lateral resistance to horizontal movement reduces to a plane strain problem in plasticity theory. In general, for cohesive soils, the ultimate lateral resistance p_u increases from the surface down to a depth of about three pile diameters. This is because the soil close to the surface is subject to the influence of external loads and may be more compacted or denser, leading to higher shear strengths. As the depth increases, the soil experiences less external influence and the shear strength approaches a constant value. It is common to assume: (*Poulos*, 1980)

$$8 \, . c_u \, . d \leq p_u \leq 12 \, . c_u \, . d \tag{36}$$

The soil resistance of clay is limited to some ultimate strength, and models that assume an elastic bedding will typically overestimate the buckling load of a pile. This is because an elastic model assumes that the soil resistance will increase linearly with increasing deformation, whereas in reality the soil will eventually reach a yield point beyond which it cannot resist any further lateral deformation. Therefore, more sophisticated models that consider the non-linear behavior of the soil are needed to accurately predict the buckling load of a pile. (Vogt et al., 2009)

2.5.3 Corrosion

Corrosion causes loss of the iron material which leads to a smaller cross-section. Since this influences the load bearing capacity of the pile, it must be taken into consideration in the structural design.

Depending on the type of soil and the presence of groundwater, the corrosion rate will vary. For this reason, it is important to consider corrosion when deciding the design life of the project. Corrosion in fact causes a decrease in wall thickness and, therefore, a decrease in structural load bearing capacity. The values for the loss of thickness for piles due to corrosion, according to EN 1993-5, is giving in Table 10. (OIB – Austrian Institute of Construction Engineering, 2017)

Table 10: Loss of thickness for piles due to corrosion (OIB – Austrian Institute of Construction Engineering, 2017)

Type of soil	Corrosion exposure	Required design working life				
		5 years	25 years	50 years	75 years	100years
Undisturbed natural soils (sand, silt, clay, schist, etc.)	Low	0,00 mm	0,30 mm	0,60 mm	0,90 mm	1,20 mm
Polluted natural soils and industrial sites	Medium	0,15 mm	0,75 mm	1,50 mm	2,25 mm	3,00 mm
Aggressive natural soils (swamp, marsh, peat, etc.)	Medium	0,20 mm	1,00 mm	1,75 mm	2,50 mm	3,25 mm
Non-compacted & non-agressive fills (clay, schist, sand, silt, etc.)	Medium	0,18 mm	0,70 mm	1,20 mm	1,70 mm	2,20 mm
Non-compacted & aggressive fills (ashes, slag, etc.)	High	0,50 mm	2,00 mm	3,25 mm	4,50 mm	5,75 mm

It is noted that the thickness losses of the Table above are measured values for the 5 and 25 years while the others are extrapolated. The values correspond to knowledge of the rusting behavior of steel in soils of different corrosivity. The values of Table 10 can be halved for compacted fills since this lowers the corrosion rates. (OIB – Austrian Institute of Construction Engineering, 2017)

For piles that are filled with grout or concrete, the corrosion is reduced to the external surface of the installed pile. For piles that are not externally grouted, a table with the wall thickness losses in 100 years according to the different ductile piles with their load-bearing capacity was composed. This document can be found in annex 4. The maximum allowed wall thickness loss of the pile is 3,25 mm. For pile type 98 with a wall thickness of 6,0 mm, the permitted loss is only up to 1,75 mm. (*TRM Piling Systems*, n.d.)

If the ductile driven piles are skin grouted, the shaft is enclosed by a concrete coating. This cover of mostly at least 40 cm protects the iron against wall thickness loss for soils with low and medium corrosiveness. High corrosive soils are protected for up to 50 years. If the required planned lifespan for piles in this type of soil is more than 50 years, an expert in corrosion protection should be consulted. (*TRM Piling Systems*, n.d.)

2.6 Environmental impact

To draw conclusions about the environmental impact, the 'Environmental Product Declaration' (EPD) of the TRM Piling System is studied. In contrary to eco-labels, EPDs give not only the good but also the bad aspects of the environmental performance of the product. (The EPD | EPD International, n.d.)

The EPD report is based on a life cycle assessment (LCA). The life cycle assesment takes into account the entire value chain, from material sourcing to manufactured product, the utilization phase and end of life. In this way, the environmental impact over the entire life cycle is evaluated. At the end of their use as a foundation, the piles can either be left in the ground if they don't hinder other foundation work or they can be removed and recycled. The piles are very rarely disposed as waste. It is technically and economically feasible to remove and recycle the ductile driven piles. Therefore the EPD takes the 100% removal of the piles in to account. However, this scenario should be examined and adjusted according to the particular case. (*EPD TRM PILING SYSTEMS Tiroler Rohre GmbH*, 2022)

To perform the LCA, a unit of 1 metre of pile is considered. This metre focusses exclusively on the ductile iron pipe. The pile shoe, pile cap, concrete filling and external grouting are not taken into account. (*EPD TRM PILING SYSTEMS Tiroler Rohre GmbH*, 2022)

Figure 33 shows the life cycle report of the ductile iron driven piles.

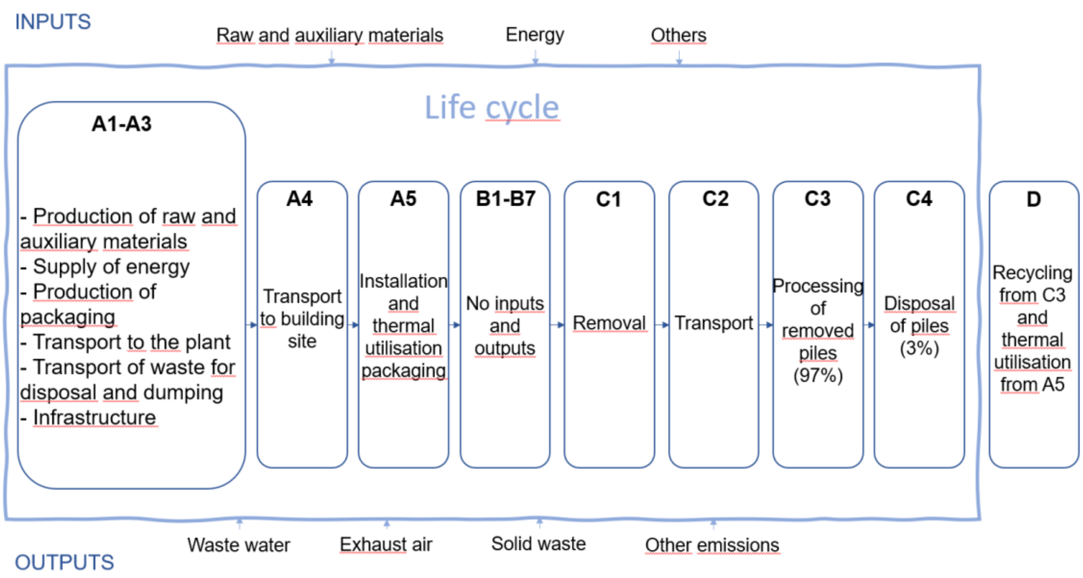

Figure 33: Life cycle flow chart

From the EPD, it can be concluded that the production of piles (A1-A3), with especially the cupola furnace, is the main contributor to the most impact categories. Transport (A4) to the building site and installation (A5)/removal (C1) of piles are identified as the next most influential processes. The full analysis of the EPD report can be found in annex 5.

3. Project analysis

3.1 Site presentation

From August the first till August the sixth 2023, Lisbon will host the World Youth Day.

World Youth Day (WYD) is described as ‘the gathering of young people from all over the world with the Pope.’ The event takes place every two, three or four years as an international gathering in a city chosen by the Pope.

In preparation for the event, Lisbon is constructing a roofed stage adjacent to the Vasco Da Gama bridge. The site is positioned northeast of the city center, see Figure 34. It encompasses a total area of 380 449,59 m², equivalent to approximately 38 hectares. The site stretches approximately 770 m in length and 603 m in width. The site is surrounded by public streets on its northern, western, and southern sides, facilitating access for both vehicles and pedestrians. To the east of the site, the Tagus river flows, providing a scenic backdrop. Towards the north of the site, you'll find the Trancão river, which eventually merges with the Tagus river. An aerial photograph of the site can be found in Figure 35. (Lisboa Ocidental SRU, 2022)

The stage with the roof is located south on the worksite. The stage and roof were designed to be a temporary solution and will be most likely removed after the WYD event. Apart from the stage, a military bridge over the Trancão river will also be build. This bridge will be constructed in two platforms to overcome the 60 m gap between the banks of the river. Both the stage and the bridge will use the ductile driven piles in their foundation solution. Only the micropiles of the stage with the roof will be analyzed in this thesis.

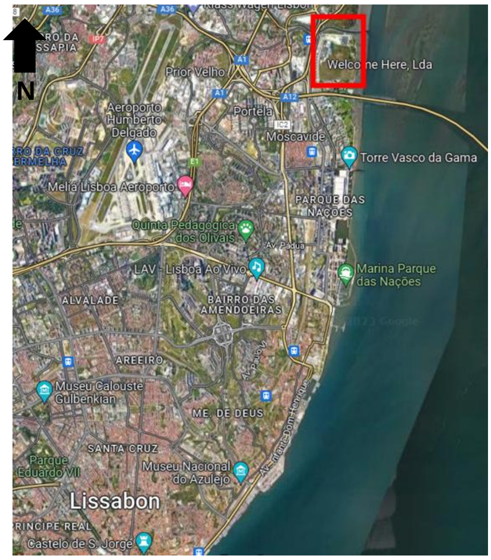

Figure 34: Location of the site in relation to the centre of Lisbon

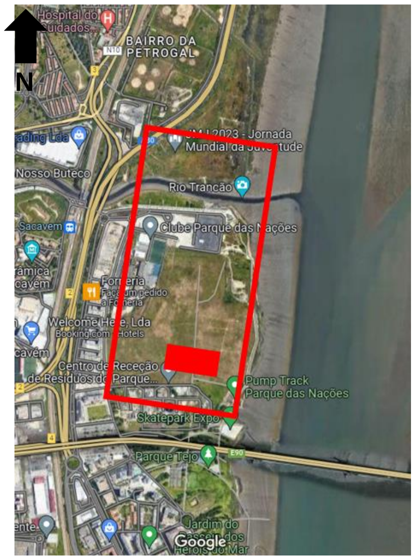

Figure 35: Indication of the site on an aerial photograph

Prior to the construction of the World Youth Day infrastructure, the site served as the sanitary landfill of Beirolas. However, this landfill is currently undergoing a rehabilitation process to transform it into the intermunicipal park known as Tagus-Trancão. In order to optimize visibility, the stage is being built on the highest point of the site. However, due to the natural relief of the terrain and certain restrictions on soil traffic, there are limitations to the frontal visibility of the altar. To address this challenge, the stage is being elevated 9 meters above the ground level, thus enhancing visibility for the audience. A visualisation of the upcoming stage can be found in Figure 36. (Lisboa Ocidental SRU, 2022) (André, M. R., 2022)

In addition to the stage, a wooden cyclopedestrian bridge is built to cross the Trancão river connecting of the municipalities of Lisbon and Loures. This wooden bridge will later, become part of a wooden pathway trough the riverside park. A photomontage of this future bridge can be found in Figure 37. (Lisboa Ocidental SRU, 2022) (André, M. R., 2022)

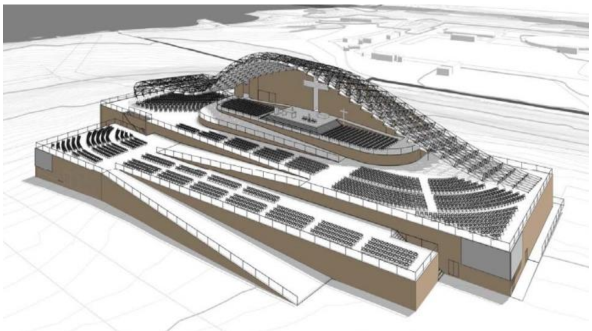

Figure 36: Visualisation of upcoming stage for WYD (Lisboa Ocidental SRU, 2022)

Figure 37: Photomontage of upcoming cyclopedestrian bridge over the Trancão river (Lisboa Ocidental SRU, 2022)

The work of the completion of the intermunicipal park Tagus-Trancão that will first be used as the location of the World Youth Day, is under the responsibility of SRU, the Lisbon municipal works company. At the end of April 2022 they signed a ‘design and built’ contract with the company Oliveiras S.A. who will design and execute the rehabilitation of the landfill. (Lisboa Ocidental SRU, 2022)

3.2 Local geological and geotechnical conditions

The site area, situated on the right bank of the Tagus river, is characterized by its low and flat topography. Within the area where the stage is being constructed, there was a sanitary landfill that housed solid urban waste and contaminated soil, which had been deposited there during the 1990s. The thickness of this layer varies across the site, with a depth of around 22 meter under the upcoming stage. (Lisboa Ocidental SRU, 2022)

Beneath the deposit of contaminated soil and urban waste, there exists a layer of heterogeneous landfill consisting of a mixture of silty-clay materials, sand, and rubble. This artificial layer was deposited at the site during the 1980s and has an average thickness of approximately 4-5 meters. As one approaches the river, the thickness of this layer gradually decreases until it eventually disappears in the tidal zone. (Lisboa Ocidental SRU, 2022)

Below the artificial landfill layer, there exists an alluvial formation consisting of compressible soil. This layer maintains a relatively consistent thickness in the north-south direction, but its thickness increases from 2 to 25 meters from east to west. The compressible muddy-soil layer possesses weak mechanical properties and exhibits low permeability. It acted as a natural barrier, preventing the downward migration of contaminants. Since the sanitary landfill has been on top of this alluvial layer for over 20 years, consolidation has already taken place. Underneath this clay-like soil layer, there is a Miocene age formation comprising layers of sandstones, calcareous materials, and varying degrees of marly soil. This Is a very stable layer with high bearing capacity. (Lisboa Ocidental SRU, 2022)

The waste that was deposited on the sanitary landfill exceeded the originally planned duration, leading to overexploitation and subsequent failure of the leachate and biogas drainage systems. Over the years, efforts have been made to decontaminate the area. This process involved extracting the accumulated leachates and biogas, applying a waterproofing HDPE-geomembrane to prevent further contamination, and smoothing the slopes of the embankment to ensure stability. These measures were implemented to mitigate the environmental impact and restore the site to a safer and more stable condition. (Lisboa Ocidental SRU, 2022)

The military bridge will be installed over the Trancão River, where the alluvial materials present traditionally exhibit weak geotechnical behavior with N_{spt} values of less than 3 blows per 30 cm. These materials are found at depths between 1 and 3 m and have varying thicknesses of 23 m on the north bank and 30 m on the south bank. Under the layer of alluvial materials, the Miocene formation is present. (Lisboa Ocidental SRU, 2022)

Figure 38 shows an extract from the geological map of Portugal showing the site area. The construction area is colored in white on the map, which map indicates ‘Holocene: alluvium and/or sanitary landfill’.

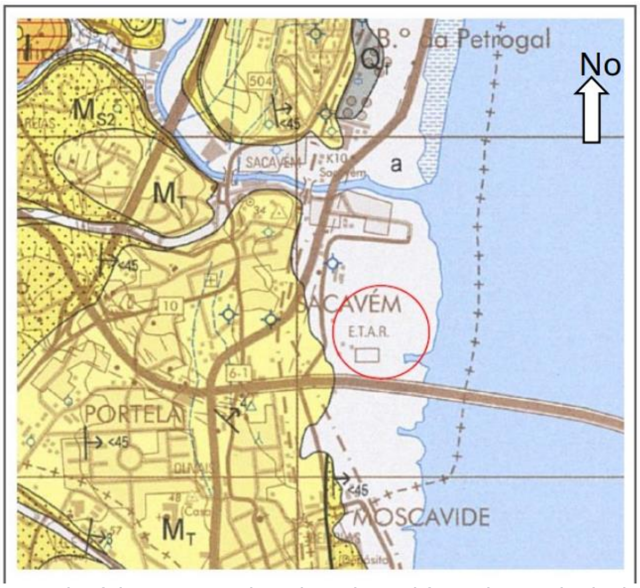

Figure 38: Geological framework of the construction site adapted from the geological map of Portugal (Folha de Loures 34B, scale of 1:50,000 - National Laboratory of Energy and Geology)

Two vertical penetration tests with depths of 29.5 (S1) and 37.5 (S2) metres were carried out at the site. The tests identified the presence of three strata as described in Table 11.

Table 11: Results of the two soundings carried out at the site

Stratum type	Characteristics	Depth [m]
Landfill deposits	Various landfill (urban waste materials, organic materials, textiles, masonry blocks,…)	0,0 - 22,0 (S1) 0,0 - 22,0 (S2)
Alluvium	Clay-mud alluvium	22,0 - 28,0 (S1) 22,0 - 34,0 (S2)
Miocene	Friable calcarenite	28,0 - 29,5 (S1) 34,0 - 37,5 (S2)

3.3 Preparatory works

In preparation for the stage construction, the site will undergo a soil supplementation process to achieve the desired height levels. This involves adding soil in some areas while partially removing higher ground in others. The objective is to create slopes with a slope angle of less than 6%, ensuring practicality and accessibility throughout the site. By carefully adjusting the ground levels, the stage will have excellent visibility from all areas, allowing for an enhanced viewing experience for the audience. (Lisboa Ocidental SRU, 2022)

To establish the paths within the landfill area, the designated areas will be cleared by removing an average thickness of 20 cm of material. The network of paths and surface drainage areas will be constructed in accordance with the implementation plan, following the specified transversal and longitudinal profiles. Special attention will be given to preserving the existing tree vegetation along the Tagus River, with efforts made to maintain it as much as possible during the construction process. This ensures the preservation of the natural landscape and contributes to the overall environmental sustainability of the site. (Lisboa Ocidental SRU, 2022)

As mentioned earlier, a HDPE-geomembrane was formerly installed to contain the waste and contaminated soil. It is important that at any time a layer of at least 1 m of soil is covering the screen. This must guarantee the integrity of it during all works executed. (Lisboa Ocidental SRU, 2022)

After the majority of the ground works, a preload test in the zone of the stage was carried out. The execution of a preload embankment minimizes settlements during the construction of the stage, which may compromise the functionality and security of the built structures. The implementation of the preload was done by placing soil, with at least the same weight as the future stage, to the south of the site where the stage will be installed. Before executing this, a finite element model was created to verify the stability. The stresses transmitted to the ground from the preload need to be at least the same, but preferably higher, than the stresses transmitted from the stage construction. But the stresses of the preload can also not be so high that it exceeds the load capacity of the land. Through the finite elements model, the settlement was also checked. (Lisboa Ocidental SRU, 2022)

The preload landfill will be carried out mainly with borrowed land. The need for borrowed land was estimated at 160 000 m^3. All the additive ground will be and analyzed and submitted to the on-site inspection for prior approval. The landfill will be carried out in overlapping layers of about 30 cm and will be spread with bulldozers type Caterpillar D6 and compacted with 16/18 t cylinders. The preload will have a height around 3,20 m with slopes of inclination 3(h)/2(v). The preferred material is sand silt with a density of approximately 20kN/m^3. (Lisboa Ocidental SRU, 2022)(Braz. I. et al., 2003)

. The preload landfill stayed for a total of 169 days. During this period, the settlements are measured. The measuring takes places trough deep settlement marks to be placed at the level of the existing ground surface. The maximum measured settlement at the site was 25 cm. This is shown in the graph of Figure 39, which shows the settlements over time in area A016. This area is shown in Figure 40. (Braz. I. et al., 2003)

Figure 39: Graph of settlements over time in area A016 (Braz. I. et al., 2003)

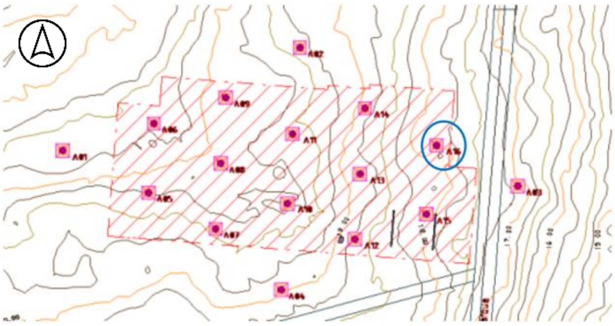

Figure 40: Location of the instrumentation mark of area A016 in the preload landfill (Braz. I. et al., 2003)

After the 169 days, the preload soil was removed again. The removal will cause the soil to spring back a little after the obtained settlement. This rebound will fall away again when the construction of the stage is complete.

After the preload was executed, a reinforcing geomembrane from HDPE 1,5 mm and a protective geotextile was sewn to the existing geomembrane under the execution area of the stage. On top of the reinforcing geomembrane and protective geotextile, a layer of sand with a thickness of approximately 0.15 meters is placed as a protective covering. This layer of sand acts as an additional safeguard, providing an extra buffer between the construction materials and the geomembrane. Figure 41 shows a site overview that shows the black geomembrane being installed at the execution area of the stage. (Lisboa Ocidental SRU, 2022)

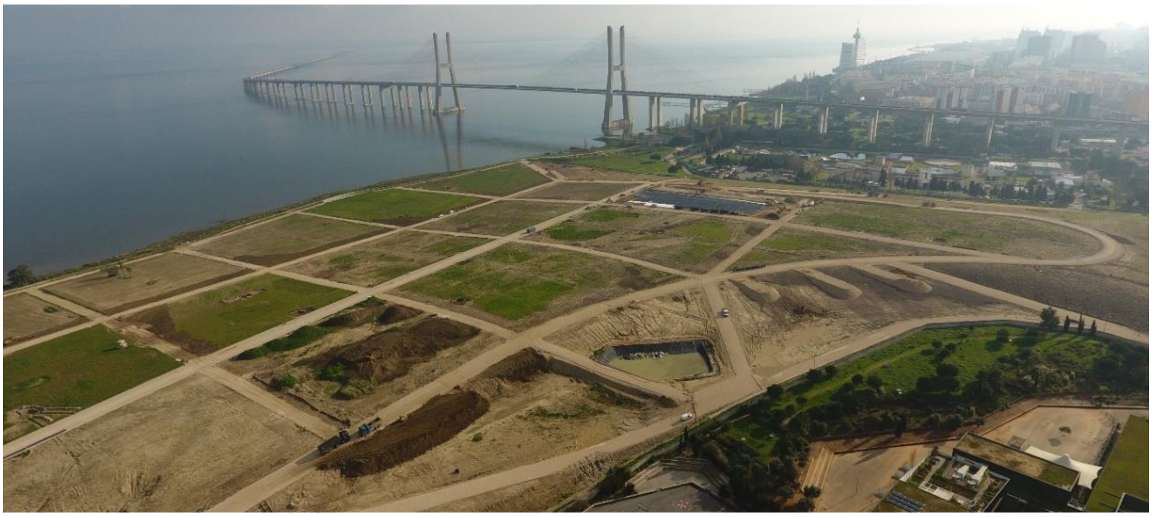

Figure 41: Site overview with the geomembrane being installed at the execution area of the stage

3.4 Adopted foundations solutions

The fact that the site was a former landfill site is the biggest challenge. The behavior of landfills can be quite unpredictable. The waste of the landfill was sealed at the top by a HDPE-geomembrane, so the foundation solution has to ensure that this geomembrane stays as intact as possible. A solution where soil is removed from the ground is also not wanted. This results in the use of less intrusive solutions. Other challenges were the tight schedule and temporary loads, for instance bored pile machines.

Because of the challenges above, the foundation solutions are limited. The adopted solution consists of the preload landfill, as explained before, followed by the installation of ductile driven piles as the foundation for the stage and its roof. The stage itself is supported by pre-cast concrete slabs with strength C35/45 and eight ductile driven piles. The roof of the stage is fully supported by one hundred ductile driven piles. Figure 42 shows a 3D model of the foundations of the stage and roof.

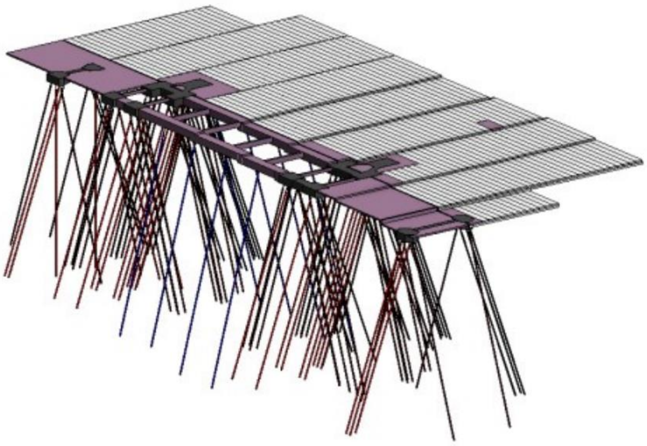

Figure 42: 3D model of the stage and roof foundations (Braz. I. et al., 2023)

The ductile iron driven piles are implemented at this site as a foundation for the roof and under the stage where some containers will be implemented. The piles are from the company TRM and their type is 170 – 7,5 mm with an inside diameter of 155 mm. The ductile piles are installed as end-bearing piles using no external grout. The reason for this is to puncture the geomembrane not more than necessary so it stays as intact as possible. Using the wet method with grout to install the piles would involve too great a risk of contamination of the subsoil and groundwater levels, as well as the injection of micro-concrete into the landfill. The ductile piles are driven dry in the ground using a high-frequency hydraulic hammer, as explained in section 1.4. The used hammer was a MB 2200 from the company Atlas Copco and had a dynamic impact energy of around 2600 kN. The driving is stopped when the refusal criteria is reached, which is around 1 - 1,8 m into the Miocene stratum.

The foundation of a roof is not only heavily loaded in compression but also in tension. The ductile driven piles can absorb the compression but not the tension. They are not externally grouted, not driven deep into the hard rock and the jointing system cannot resist large tensile stresses. The solution for this is to screw a steel self-drilling steel micropile inside the ductile pile and deep into the hard Miocene rock layers. Because the steel bars must go past the ductile piles, the TRM piles are not sealed with their usual pile shoe but with a cement mortar plug. This way the self-drilling bars can go through it. The hollow threaded self-drilling bars have type RR64 H1000. Which means an outer nominal diameter of 64 mm and an ultimate nominal load of 1000 kN. They are connected with couplers and have a drill bit with diameter 130 mm at the end. They are drilled with grout to the desired depth, around 10 m into the Miocene stratum, using a surface hammer. The Miocene stratum soil that mixes with the grout during the drilling operation is not contaminated because the ductile piles are installed first to form a 'protective casing'. With the sealing of the self-drilling micropile in the competent layer, a significant increase in the tensile capacity is achieved. Subsequently, the interior of the ductile iron pile is filled with concrete of type C35/45. This bonds the ductile iron pile and the interior self-drilling steel micropile together.

For the ductile piles of the stage, the installation of a steel bar was not necessary since these piles are not loaded on tension. As reinforcement three ribbed steel bars with a diameter of 32 mm were installed in the ductile pile. Lastly these piles were also filled with concrete of type C35/45.

The installation of the ductile driven piles and the inner steel self-driven pile can be found in Figures 43 and 44. Figure 45 shows the installed piles with steel bars.

Figure 43: Installation of the ductile driven piles at the site

Figure 44: Installaton of the steel self-drilling bars at the site

Figure 45: Installed ductile piles with the steel bars

The structure of the stage itself must ensure that the loads will be distributed as evenly as possible. Therefore, the solution of precast concrete slabs with a minimum of 30 cm thickness and hollow cores was used. Due to the magnitude of the loads on certain alignments, it was necessary to recommend a foundation solution concreted in situ with greater thicknesses in certain areas. In Figure 46, the zones identified in blue and red are in situ beams. The blue zone has a beam section of 1,65x0,45m^2 and the red zone has a beam section of 1,65x1,20m^2. The red zone as shows the area where containers will be installed. Therefore, this is also the area where the ductile piles of the stage will be installed. Figure 47 shows an aerial photograph of the prefabricated hollow core slabs on prefabricated peripheral beams.

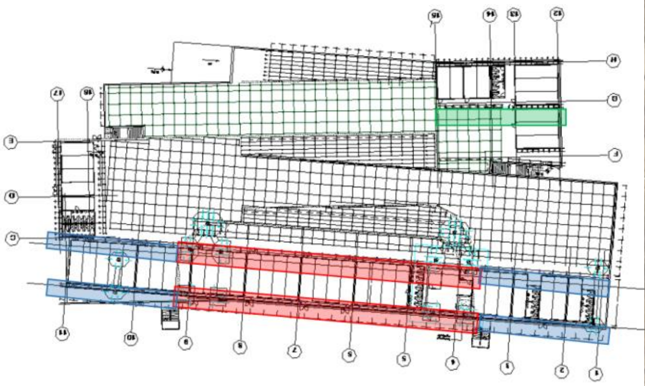

Figure 46: Floor plan of the main stage structure (Braz. I. et al., 2023)

Figure 47: Aerial photograph of the stage foundation – prefabricated hollow core slabs (Braz. I. et al., 2023)

Another reason why some of the concrete slabs have to be fabricated in situ, is because they need to cover the top of the micropiles that will be used as the foundation of the roof.

3.5 Full scale load tests

Load tests were performed on the ductile driven piles to analyze the behavior of these foundation elements. Given the characteristics of the terrain associated with the work carried out, it was recommended to validate the design assumptions and make a possible optimization of the solution.

A full scale load test makes it possible to analyze the impact of dead and live loads on the structural integrity and stability of a structure. With the plan to build a new construction, a full-scale load test can show that a foundation will perform as designed and intended. If the structure does not exceed the calculated maximum deflection and rebounds sufficiently after the load is removed, the structure has passed the load test. To perform a load test, the structure is shored and a tank or other loading devices are installed. Equipment is installed to measure the deformation of the structure during testing. (Exo Inc., 2022) (*Full-scale Load Testing Services*, 2023)

On the ductile driven piles, two full scale load tests were carried out, a compression and a tensile test. The internal measuring equipment was applied to the test piles by strain gauges inserted using a rod with a diameter of 16 mm. A datalogger was used to read the data from the installed equipment. (Geosol, 2023)

3.5.1 Compression load test

The compression load test was carried out with a reaction structure that consists of a reinforced concrete massif with dimensions of 2,5 m x 2,5m and a height of 1 m. The structure can be seen in Figure 48. The tested ductile driven pile had a length of 34,30 m, again reaching the Miocene substrate. No inner steel bar was added since the pile was only loaded by compression. Not adding the steel micropile also minimizes the capacity resistant to buckling, which ensures a better evaluation of ultimate limit state of the pile. The inside of the ductile pile was filled with C25/30 concrete. The structural capacity of this composite pile can be found in the Table 12. (Geosol, 2023)

Table 12: Characteristics and load capacity of the pile

Ductile Pile 170 mm		
	Section [mm²]	3829
	Sacrifical loss of cross section [mm]	0
	Section for calculation [mm²]	3829
	Yield strength [Mpa]	320
Ri,d Pile [kN]		**1225**
Concrete C25/30		
	Section [mm²]	18869
	Cylinder compressive strength (28 days) [Mpa]	25
Ri,d Concrete [kN]		**314**
∑ Ri,d		**1539**

To know the intended load for the compression preload test, the load bearing capacity of the pile is calculated. The calculations of the design resistance $R_{i,d}$ are executed using formulas (12), (13) and (14).

$$R_{i,d} = \frac{R_{sk}}{\gamma_{Ma}} + \frac{R_{ck}}{\gamma_c}$$

$$R_{i,d} = \frac{A_{DP} * f_{t0,2k}}{1,0} + \frac{A_c * f_{ck}}{1,5}$$

$$R_{i,d} = \frac{3829\ mm^2 * 320 * 10^{-3} kN/mm^2}{1,0} + \frac{18869\ mm^2 * 25 * 10^{-3} kN/mm^2}{1,5}$$

$$R_{i,d} = 1125\ kN + 314\ kN$$

$$R_{i,d} = 1539\ kN$$

Table 13 shows the characteristics of the ductile pile and the inner concrete to calculate the flexural stiffness of each component.

Table 13: Characteristics of the ductile pile and inner concrete for the compression test

Equivalent Cross-section ductile pile non-grouted					
	Concrete C25/30			**Ductile Pile 170 x 7,5 mm**	
E_c	25000	[N/mm²]	E_{DP}	170000	[N/mm²]
$f_{c,k}$	25	[N/mm²]	$f_{y,k}$	320	[N/mm²]
γ_c	1,5	(EC3)	γ_{M0}	1	(EC3)
	Concrete			**Pile tube**	
dc	155	[mm]	$D_{DP,ext}$	170	[mm]
			$D_{DP,int}$	155	[mm]
			$t_{sacrificial}$	7,5	[mm]
A_c	18869	[mm²]	A_{DP}	3829	[mm²]
I_c	28333269,4	[mm⁴]	I_{DP}	12665006	[mm⁴]
EI_c	**708,3**	**[kNm²]**	**EI_{DP}**	**2153,1**	**[kNm²]**
EI = 2861,4 kNm²					

The area moments of inertia were calculated as followed:

$$I_c = \frac{\pi * D^4}{64} = \frac{\pi * 155^4}{64} = 28\,333\,269\ mm^4$$

$$I_{DP} = \frac{\pi * D_{tube,ex}{}^4}{64} - \frac{\pi * D_{tube,int}{}^4}{64} = \frac{\pi * (D_{tube,ex}{}^4 - D_{tube,int}{}^4)}{64} = \frac{\pi * (170^4 - 155^4)}{64} = 12\,665\,006\ mm^2$$

The flexural rigidity EI is calculated by multiplying the area moment of inertia by the young's modules.

$$EI_c = E_c * I_c = (25\,000 * 28\,333\,269) * 10^{-9}\ kNm^2 = 708{,}3\ kNm^2$$

$$EI_{DP} = E_{DP} * I_{DP} = (170\,000 * 12\,665\,006) * 10^{-9}\ kNm^2 = 2153{,}1\ kNm^2$$

The total flexural rigidity is calculated by taken the sum of the flexural rigidities of both materials.

$$EI = E_{DP} + I_{DP} = 708{,}3\ kNm^2 + 2153{,}1\ kNm^2 = 2861{,}4\ kNm^2$$

Since the grout and ductile pile work together, it is not entirely correct to take the sum of both resistance capacities and flexural rigidities. This will lead to an underestimation of the load capacity of the pile. Based on the principle of linear behavior of Hooke's Law, Navier Bernoulli's Law and the perfect "interlock" grout/ductile pile, it is admissible to consider the principle of the mixed section where calculations are based on the principle of an equivalent cross section. (Geosol, 2023)

Table 14: Characteristics and load capacity of the equivalent ductile pile

Equivalent Cross-section						
	$W_{el,eq}$	211160,7723	[mm³]	D	170	[mm]
	$W_{pl,eq}$	287191,6767	[mm³]	$E_{con/DP}$	0,147	
				$A_{con\ as\ DP}$	2774,9	[mm²]
	EA_{eq}	965413	[kN]	$A_{c\ as\ DP/\gamma c}$	1849,902	[mm²]
	I_{eq}	17948666	[mm⁴]	$A_{total,eq}$	5678,9	[mm²]
				$d_{int,eq}$	147,2	[mm]
				t_{eq}	11,4	[mm]
		Equivalent cross-section - composite cross-section				
Nsd		**EI_{eq}**	**Npl,k**	**Mpl,k**	**Mel,k**	**α**
[kN]		**[kNm²]**	**[kN]**	**[kNm]**	**[kNm]**	**[-]**
1723		**3051,3**	**1817,2**	**91,9**	**67,6**	**1,36**

The values from Table 14 were calculated as seen below. The values below can differ a little bit from the ones in Table 14 since the table from excel calculates with the unrounded values.

$$E_{c/DP} = \frac{E_c}{E_{DP}} = \frac{25\,000\ N/mm^2}{170\,000\ N/mm^2} = 0{,}147$$

$$A_{con\ as\ DP} = A_c * E_{c/DP} = 18\,869\ mm^2 * 0{,}147 = 2274{,}9\ mm^2$$

$$A_{c\ as\ DP/\gamma_c} = \frac{A_{con\ as\ DP}}{\gamma_c} = \frac{2274{,}9\ mm^2}{1{,}5} = 1849{,}9\ mm^2$$

$$A_{total,eq} = A_{DP} + A_{c\ as\ DP/\gamma_c} = 3828{,}8\ mm^2 + 1849{,}9\ mm^2 = 5678{,}7\ mm^2$$

$$A = \frac{\pi * (D^2 - d^2)}{4} \Leftrightarrow d_{int,eq} = \sqrt{D^2 - \frac{4 * A_{total,eq}}{\pi}} = \sqrt{170^2\ mm^2 - \frac{4 * 5678{,}7\ mm^2}{\pi}} = 147{,}2\ mm$$

$$t_{eq} = \frac{D - d_{int,eq}}{2} = \frac{170\ mm - 147{,}2\ mm}{2} = 11{,}4\ mm$$

$$W_{el,eq} = \frac{\pi * (D^4 - {d_{int,eq}}^4)}{32 * D} = \frac{\pi * (170^4 mm^4 - 147{,}2^4 mm^4)}{32 * 170\ mm} = 211\,154{,}9\ mm^3$$

$$W_{pl,eq} = \frac{D^3 - {d_{int,eq}}^3}{6} = \frac{170^3 mm^3 - 147{,}2^3 mm^3}{6} = 287\,183{,}1\ mm^3$$

$$EA_{eq} = E_{DP} * A_{total,eq} = 170\,000\ MPa * 5678{,}7\ mm^2 = 965\,379\,000\ N = 965\,379\ kN$$

$$I_{eq} = \frac{\pi * (D^4 - {d_{int,eq}}^4)}{64} = \frac{\pi * (170^4 mm^4 - 147{,}2^4 mm^4)}{64} = 17\,951\,979\ mm^4$$

$$EI_{eq} = E_{DP} * I_{eq} = 170\,000\ MPa * 17\,951\,979\ mm^4 = 3\,051\,836\,430\,000\ Nmm^2 = 3051{,}8\ kNm^2$$

$$\boldsymbol{N_{pl,k} = A_{total,eq} * f_{yk} = 5678{,}7\ mm^2 * 320\ MPa = 1\,817\,184\ N = 1817{,}2\ kN}$$

$$M_{pl,k} = W_{pl,eq} * f_{yk} = 287\,183{,}1\ mm^3 * 320\ MPa = 91\,898\,592\ Nmm = 91{,}9\ kNm$$

$$M_{el,k} = W_{el,eq} * f_{yk} = 211\,154{,}9\ mm^3 * 320\ MPa = 67\,569\,568\ Nmm = 67{,}6\ kNm$$

$$\alpha = \frac{W_{pl,eq}}{W_{el,eq}} = \frac{287\,183{,}1\ mm^3}{211\,154{,}9\ mm^3} = 1{,}36$$

After calculating the design axial load and resistance moment of the compression pile, the elastic shortening of the pile under the compression test was estimated in the load test report using the intended compression load with a rounded-up value of 1820 kN. The excel calculations can be found in Table 15. (Geosol, 2023)

Table 15: Estimation of pile head displacement under compression test

Estimation of Pile head displacement							
Compression - elastic shortening							
	Pile length	34	[m]				
	$N_{pl,k}$ (copmpression)	1820	[kN]				
	E_{DP}	170000	[N/mm²]				
	A_{DP}	3829	[mm²]				
	E_c	25000	[N/mm²]		EA_{DP}	650930	[kN]
	A_c	18869	[mm²]		EA_c	471725	[kN]
					EA_{sum}	1122655	[kN]
			ε	0,001621	[-]		
				0,162116	[%]		
			Δl	55	[mm]		
		incial dicplacement			2	[mm]	
		max elastic shortening			**57**	**[mm]**	

For each component, the concrete and the ductile pile, their E-modulus and cross-section are being multiplied. Subsequently both results, EA_{DP} and EA_c, are being added up to calculate the sum EA_{sum}.

Then the strain was calculated using the formula below, where β is 1 for non-grouted piles.

$$\varepsilon = \beta * \frac{N_{pl,k}}{EA_{sum}} = 1 * \frac{1820\ kN}{1\ 122\ 655\ kN} = 0{,}001621 = 0{,}16\ \%$$

The elastic shortening is calculated as followed:

$$\Delta l = \varepsilon * l = 0{,}001621 * 34\ 000\ mm = 55\ mm$$

Taking into account an initial displacement by the soil reaction mobilization, the total pile head displacement is calculated as 57 mm. The real displacement will be measured during the test.

The intended load for the compression test was calculated to be 1820 kN. However, an instability issue was encountered with the micropile header mass when the load exceeded 1400 kN, despite careful alignment of the jack with the micropile axis. This instability caused horizontal displacement of the massif. Despite this displacement, there was a consistent increase in load capacity observed throughout the test. The load capacity progressively increased from approximately 300 kN to 1723 kN. The test involved four load cycles on the pile, with each cycle reaching a maximum load of 599 kN, 984 kN, 1285 kN, and finally 1723 kN (Geosol, 2023)

The horizontal displacement can be seen in Figure 49. Figure 50 gives the graph of the deformation on the horizontal axis with the accompanying compression head loads on the vertical axis.

Figure 48: Reaction structure of the compression load test

Figure 49: Horizontal displacement of the massif when the compression load exceeds 1400 kN

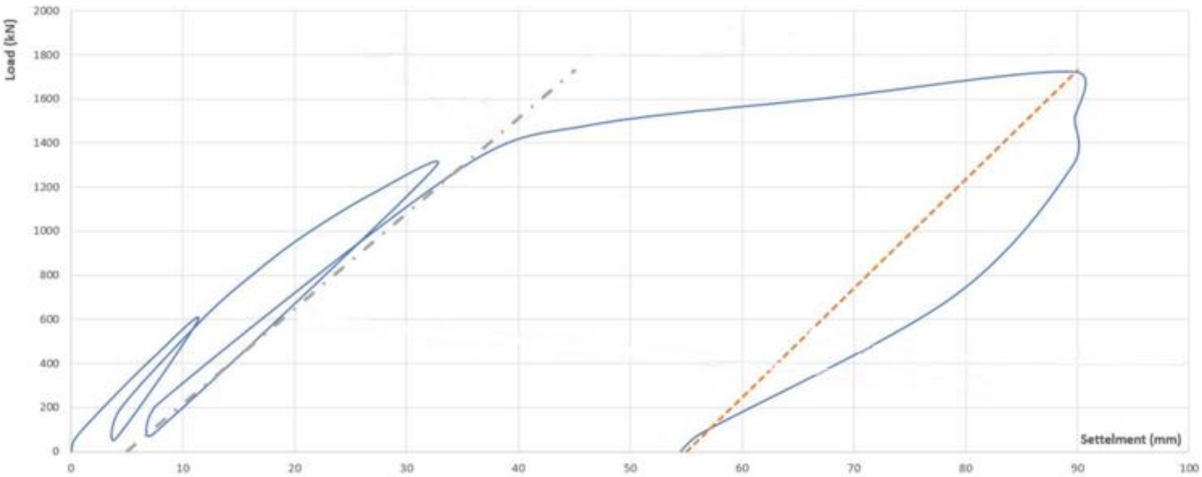

Figure 50: Graph of the deformation of the pile with the accompanying compression loads (Geosol, 2023)

Figure 50 shows the load cycles of 599 kN, 1285 kN and 1723 kN. it can be clearly seen that in the first two cycles, the pile is mostly elastically deformed. Namely, when the load is removed again here, the deformation roughly returns to its original state. Elastic deformation is deformation of a material when load is applied and that is fully reversed when the load is removed again. In the second load cycle, the compressive shortening starts around 4 mm, goes up to 33 mm and goes back to around 7 mm after the load is removed. The third load cycle looks a little weird on the graph because of the displacement of the massif. Therefore, it is not possible to conclude correct values about the deformation from this last load cycle.

Figure 51 shows the result of the strain gauge for the four load cycles that were carried out at the compression load test.

For the compression test, a set of strain gauges were installed at a depth of 2,5 m, 11 m, 20 m, 23 m, 28 m and 33 m. Because of the bending of the graph lines, the conclusion that the alluvial layer is located at 23 m depth can be drawn. This is compatible with the information from previous surveys carried out at the site. (Geosol, 2023)

The graph shows consistency of results in the four load cycles with strain tracings mostly parallel to each other. The top of the graph shows the maximum load applied in the load cycle at the top of the pile. Moving down the graph, it can be observed that the load on the pile decreases. This is because the pile distributes the load to the surrounding ground, resulting in a gradual reduction in load. The graph also indicates a significant load transmission capacity to the ground, particularly within the depth range of 2,5 m to 11 m. In this range, a firm response is observed, indicating effective load distribution and transmission to the surrounding soil. Between the depths of 11 m and 20 m, the load transmission to the embankment appears to be negligible. However, another strong load transmission response is evident between 20 meters and 23 meters depth.

Taking a look at the subjected load of 1723 kN, shows that the residual force on the miocene layer is around 550 kN.

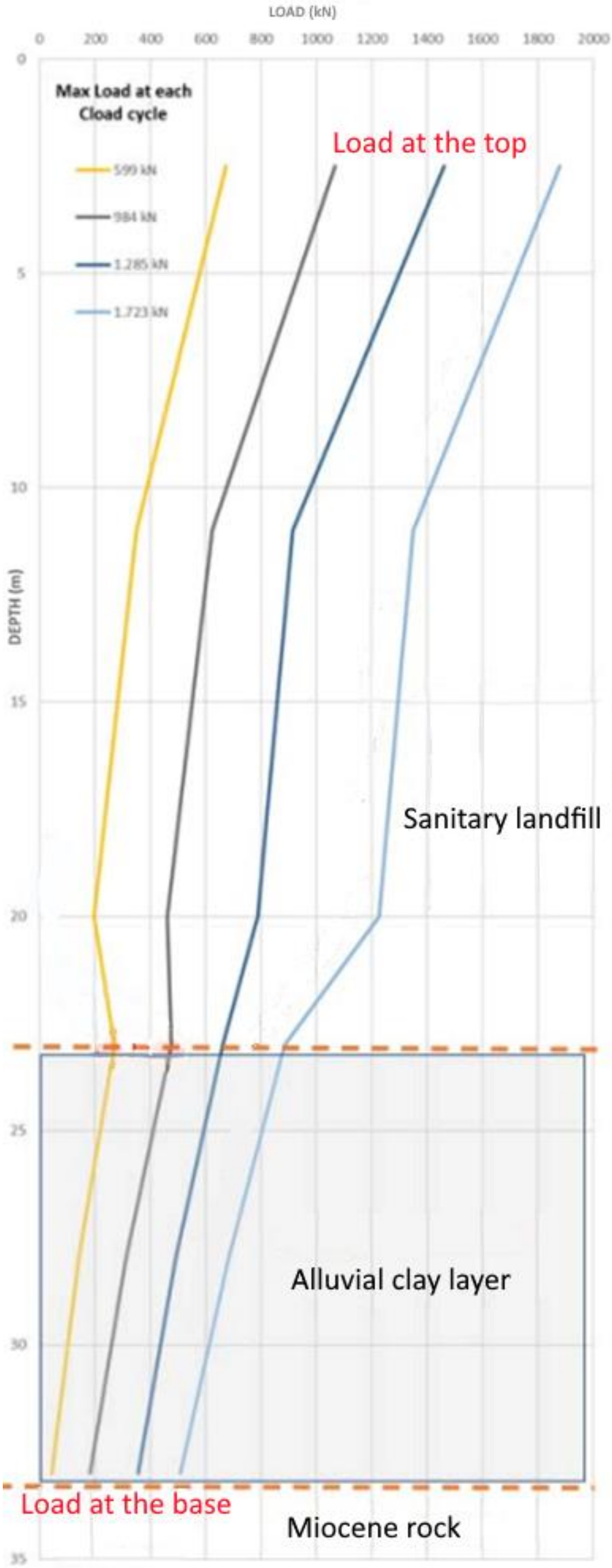

Figure 51: Strain gauges graph for the compression load test (Geosol, 2023)

3.5.2 Tensile load test

The tensile load test was carried out with a similar structure as the compression load test. As seen in Figure 52, a reinforced concrete massif with dimensions of 2,5 m x 2,5m and a height of 1 m was used. The tested ductile driven pile had a length of 30,45 m, again reaching the Miocene substrate. This time the inner self-drilling steel pipe was added. The bar was 41,50 m long while approximately 10 m in the Miocene. As designed, the interior of the piles were completely filled to ground surface with C25/30 concrete. (Geosol, 2023)

Figure 52: Reaction structure of the tensile load test (Geosol, 2023)

The tensile load test was executed with an inner bar of type RR108 H2400 instead of the designed bar RR64 H1000 for the foundation solution. The reason for this change in bars is that the outer diameter of 64 mm with inner diameter of 42 mm is too small. The insertion of the internal instrumentation is impossible since the strain gauges can be up to 35 mm thick and a 5 mm cable has to be inserted with a 16 mm rod. The bar used RR108 H2400 which has an outer diameter of 108mm and an inner diameter of 82.5mm which solves the problem. The missing bit of the bar stays the designed 130 mm. (Geosol, 2023)

The tensile load test was carried out with four load cycles with a maximum load of 922 kN. A fifth cycle was performed up to 1598 kN to test the resistant capacity of the seal in the Miocene layer. Even after reaching the load of 1598 kN, failure was not verified. Figure 53 gives the graph of the deformation on the horizontal axis with the accompanying tensile head loads on the vertical axis. (Geosol, 2023)

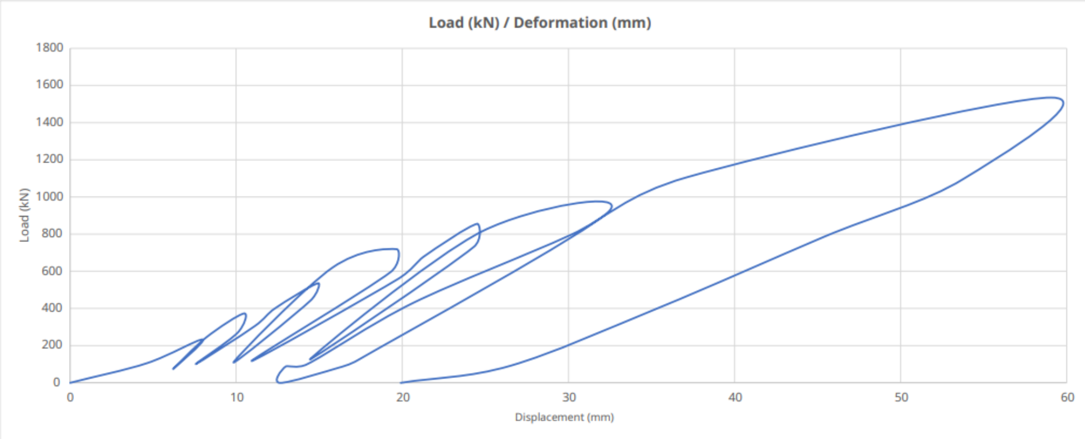

Figure 53: Graph of the deformation of the pile with the accompanying tensile loads (Geosol, 2023)

During the tension test, a deformation of 33 mm was measured for a load of 922 kN. After removing the load, the deformation reduced to 13 mm, indicating elastic recovery. In the fifth load cycle, a maximum deformation of 59 mm with a residual plastic deformation of 20 mm was recorded.

Figure 54 shows the result of the strain gauge for four load cycles that were carried out at the tensile load test. The measured tensile loads at the top of the piles for each cycle are 106 kN, 373 kN, 536 kN and 855 kN. (Geosol, 2023)

For the tensile test, a set of strain gauges were installed at a depth of 2,5 m, 10 m, 20 m, 26 m, 30 m and 38,5 m. The last one was placed at the depth of the transition between the alluvial layer and the Miocene rock. Because of the light bending of the graph lines at 20 m, the conclusion that the alluvial layer is located around this depth. This is compatible with the information from previous surveys carried out at the site, which indicates 22-23 m. (Geosol, 2023)

The graph shows consistency of results in the four load cycles with pressure tracings often parallel to each other. Similar to the compression test graph, going down shows that the load on the pile decreases since the pile distributes the load to the surrounding ground. For the first three load cycles, it can be observed that approximately 50% of load is transmitted to the sanitary landfill. At the deepest strain gauge, no load is registered. This means that the last 2,5 m of the pile is unloaded and theoretically unnecessary. It is important to note that the sanitary landfill is very heterogeneous and may contain hollow gaps that do not absorb any force. Therefore, a sealing depth of 10 m in the Miocene layer for the steel bar is still opted, of which 30% is reserve for safety reasons. (Geosol, 2023)

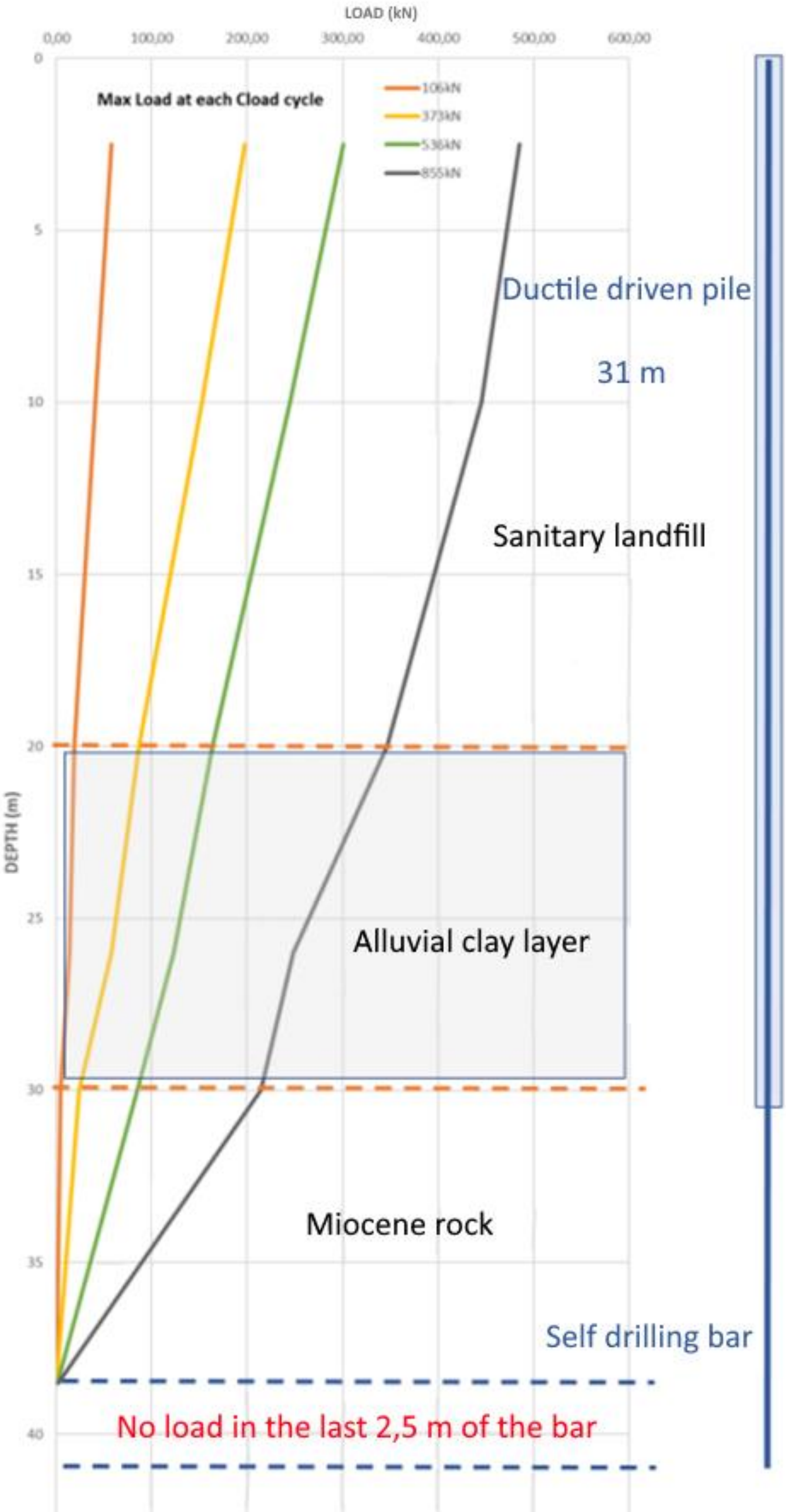

Figure 54: Strain gauges graph for the tensile load test (Geosol, 2023)

3.6 Foundations design

3.6.1 Design loads

3.6.1.1 Design loads of the stage roof foundation piles

To design the foundations of the stage and roof, it must be known what forces will act on them. The given loads of the roof at the nodes can be found in Table 16 with the accompanying Figure 55.

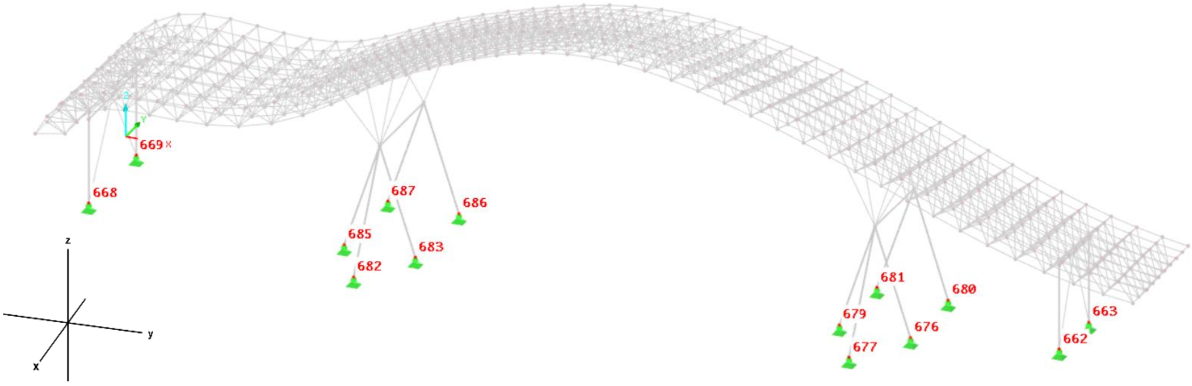

Figure 55: Node numbers of the roof

Table 16: Given loads of the stage roof foundation for the accompanying nodes

Node No.		Support Forces [kN]		
		$P_{X'}$	$P_{Y'}$	$P_{Z'}$
662	Max	7.13	198.64	719.71
	Min	-5.80	-160.10	-453.37
663	Max	7.06	197.42	499.05
	Min	-5.56	-156.89	-709.63
668	Max	0.23	195.04	1549.05
	Min	-0.51	-90.40	-873.94
669	Max	0.22	195.86	600.11
	Min	-0.48	-80.11	-675.41
676	Max	725.82	0.68	2185.26
	Min	-730.15	0.00	-2185.18
677	Max	0.14	1469.28	2539.25
	Min	-0.20	-613.70	-1072.37
679	Max	201.20	0.70	598.87
	Min	-253.41	0.00	-765.72
680	Max	687.06	0.21	1206.85
	Min	-388.43	-0.05	-2148.92
681	Max	188.01	0.21	535.41
	Min	-169.94	0.00	-496.37
682	Max	0.08	1589.84	2748.17
	Min	-0.09	-776.02	-1353.56
683	Max	422.96	0.66	1071.32
	Min	-358.57	0.00	-1277.20
685	Max	607.70	0.66	1818.06
	Min	-728.69	0.00	-2193.92
686	Max	319.59	0.21	548.31
	Min	-182.88	0.00	-977.21
687	Max	376.58	0.23	1110.11
	Min	-697.60	0.00	-2071.47

In each case, the maximum compressive force in Table 16 is shown as a positive value and the maximum tensile force as a negative value. Each load should be divided by the number of poles over which the load will be distributed. The number of piles per node can be found in the drawing of the foundations in annex 7, with the green numbers responding to the figure and table above. The figures from annex 7 also show that the piles are aimed to be installed following the x or y-direction. Therefore, only F_x or F_y, the one with the biggest value, will be considered. Tables 17 and 18 show the maximum horizontal and vertical load on each pile.

Table 17: Vertical characteristic loads per pile from the roof

Node number	Max. $F_{V,compr}$ [kN]	Max. $F_{V,tens}$ [kN]	Number of piles	Max. vertical compression load per pile [kN]	Max. vertical tension load per pile [kN]
668	1549,05	873,94	5	309,81	174,79
669	600,11	675,41	5	120,02	135,08
662	719,71	453,37	5	143,94	90,67
663	499,05	709,63	5	99,81	141,93
686	548,31	977,21	6	91,39	162,87
687	1110,11	2071,47	6	185,02	345,25
680	1206,85	2148,92	6	201,14	358,15
681	535,41	496,37	6	89,24	82,73
682	2748,17	1353,56	12	229,01	112,80
683	1071,32	1277,20	8	133,92	159,65
685	1818,06	2193,92	8	227,26	274,24
677	2539,25	1072,37	12	211,60	89,36
676	2185,26	2185,18	8	273,16	273,15
679	598,87	765,72	8	74,86	95,72

Table 18: Horizontal characteristic loads per pile from the roof

Node number	Max. $F_{H,compr}$ [kN]	Max. $F_{H,tens}$ [kN]	Number of piles	Max. horizontal compression load per pile [kN]	Max. horizontal tension load per pile [kN]
668	195,04	90,40	5	39,01	18,08
669	195,86	80,11	5	39,17	16,02
662	198,64	160,10	5	39,73	32,02
663	197,42	156,89	5	39,48	31,38
686	319,59	182,88	6	53,27	30,48
687	376,58	697,60	6	62,76	116,27
680	687,06	388,43	6	114,51	64,74
681	188,01	169,94	6	31,34	28,32
682	1589,84	776,02	12	132,49	64,67
683	422,96	358,57	8	52,87	44,82
685	607,70	728,69	8	75,96	91,09
677	1469,28	613,70	12	122,44	51,14
676	725,82	730,15	8	90,73	91,27
679	201,20	253,41	8	25,15	31,68

To get the design loads of each pile, the axial load needs to be calculated. For this, the inclination of 15° at which the piles were installed must be taken into account. Figure 56 illustrates the vertical and horizontal load acting on the pile. The formula next to the figure shows the used formula to calculate the projected axial load. Lastly this characteristic axial load is multiplied by a partial safety factor to get the design axial load. Table 19 shows the values of the partial factors according to Eurocode 0. If the loads are permanent or variable is unknown. Therefore, the value 1,40, a value between 1,35 and 1,50, is chosen as the partial factor.

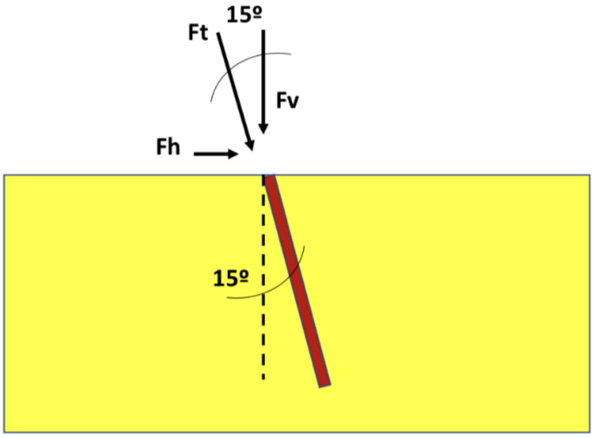

$$\mathbf{F}_{\mathbf{axial}} = \frac{\mathbf{F}_V}{\mathbf{cos\ 15°}} + \frac{\mathbf{F}_H}{\mathbf{sin\ 15°}}$$

Figure 56: Projection of the horizontal and vertical load to calculate the axial load on the pile

Table 19: Partial factors on action loads

Action load		Partial factor symbol	Partial factor value
Permanent	Unfavorable	γ_G	1,35
	Favorable		1,0
Variable	Unfavorable	γ_Q	1,5
	Favorable		0

Using the formula from Figure 56, the maximum axial loads on a pile are calculated. To get the maximum values of the loads, a vertical compression load is combined with a horizontal compression load and a vertical tension load is combined with a horizontal tension load. The calculated characteristic and design axial loads can be found in Table 20.

Table 20: Axial loads per pile of the stage

Max. char. axial compression load per pile [kN]	Max. char. axial tension load per pile [kN]	Max. design axial compression load per pile [kN]	Max. design axial tension load per pile [kN]
471,45	250,81	660,04	351,13
275,60	201,75	385,85	282,45
302,52	217,59	423,52	304,62
255,89	268,17	358,24	375,44
300,41	286,38	420,57	400,93
434,04	806,64	607,66	1129,30
650,67	620,92	910,94	869,28

213,45	195,08	298,83	273,11
748,98	366,63	1048,57	513,29
342,91	338,46	480,08	473,84
528,77	635,84	740,28	890,18
692,14	290,11	969,00	406,16
633,34	635,42	886,67	889,59
174,67	221,48	244,54	310,07

Table 20 above shows that for pressure, the heaviest design load on a ductile driven pile for the stage is 1049 kN. For tension the maximum value is 1129 kN. Both loads will be compared to the calculated load bearing capacity of the used pile type.

3.6.1.2 Design loads of the stage foundation piles

At the level of the containers, the concrete slabs will not be continuous and ductile piles will also be driven into the ground to absorb the necessary forces. Figure 57 shows the location of these micropiles in blue. The position of the piles corresponds to the alignments with the letters J and H. These alignments refer to the characteristic loads acting on them, which can be found in Table 21. The alignments J and H both represent the load of the wall at this location that will go up to the roof.

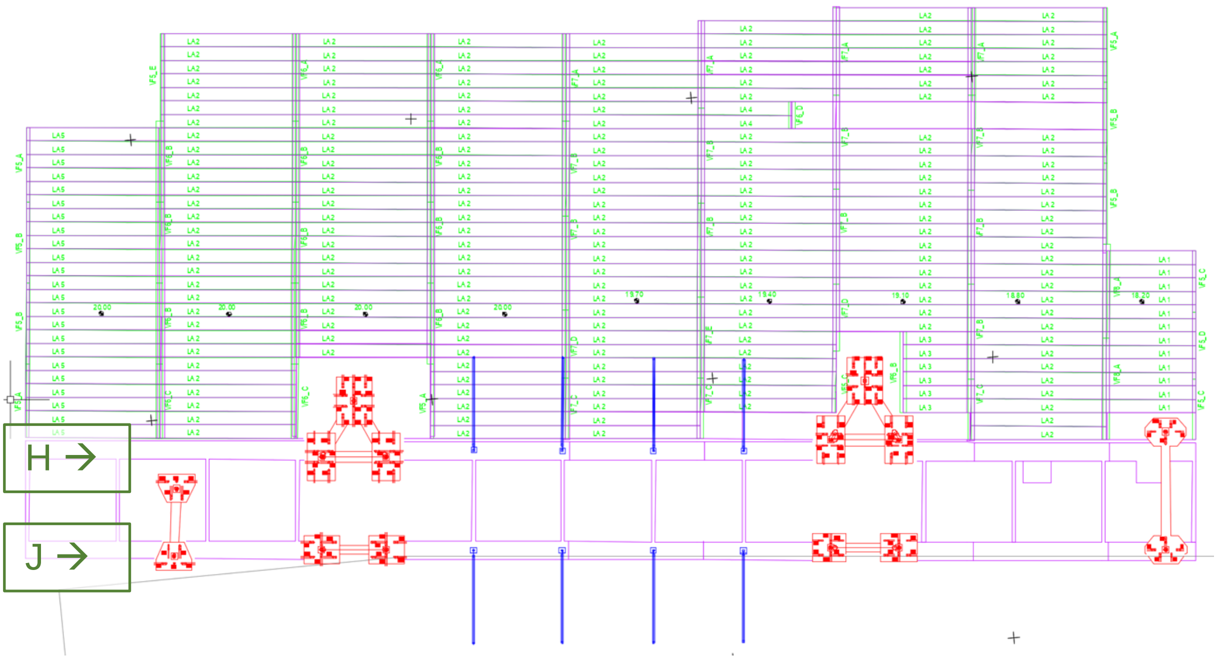

Figure 57: Drawing of the stage with micropiles under the stage in blue

Table 21: Characteristic loads of the alignments H and J

Alignment	Type of load	Symbol of load	Value of the load [kN/m]
H	Permanent load (vertical)	G_k	35
	Variable load (vertical)	Q_k	29
	Vertical load caused by wind on the wall	$W_{k,\mathrm{v}}$	30
	Horizontal load caused by the wind on the wall	$W_{k,\mathrm{h}}$	43

J	Permanent load (vertical)	G_k	40
	Variable load (vertical)	Q_k	29
	Vertical load caused by wind on the wall	$W_{k,\mathrm{v}}$	30
	Horizontal load caused by the wind on the wall	$W_{k,h}$	43

To get the total vertical loads of the micropiles, the characteristic loads of the table above are multiplied by the corresponding partial factor, then added together and lastly multiplied by the length in between the piles. According to Eurocode 0, the partial factors from Table 19 can be considered on the action loads.

With a distance of 8,14 m between the micropiles under the stage, their design load is calculated as follow:

$$F_{d,\mathrm{v},H\,stage\,pile} = \left(\gamma_G * G_k + \gamma_Q * Q_k + \gamma_Q * W_{k,v}\right) * 8{,}14\,m$$
$$= (1{,}35 * 35\,kN/m + 1{,}50 * 29\,kN/m + 1{,}35 * 30\,kN/m) * 8{,}14\,m = 1105{,}01\,kN$$

$$F_{d,\mathrm{v},,J\,stage\,pile} = \left(\gamma_G * G_k + \gamma_Q * Q_k + \gamma_Q * W_{k,v}\right) * 8{,}14\,m$$
$$= (1{,}35 * 40\,kN/m + 1{,}50 * 29\,kN/m + 1{,}35 * 30\,kN/m) * 8{,}14\,m = 1159{,}23\,kN$$

The full horizontal load cannot be taken into account since the passive forces that will be mobilized due to the fact that the beams are buried need to be subtracted. This passive load was calculated considering the height of the beam, the weight of the soil and the passive lateral pressure coefficient K_p with an internal friction angle ϕ of 30°. This coefficient is defined as the ratio of the horizontal to vertical stress.

$$F_{h,passive} = h * \rho_{soil} * K_p * \frac{h}{2}$$

$$F_{h,passive} = 1{,}3\,m * 19\frac{kN}{m^3} * 1{,}73 * \frac{1{,}3\,m}{2}$$

$$F_{h,passive} = 27{,}78\,kN/m$$

The passive load is not multiplied by a partial factor since this load will be distracted and therefore alleviate the solution. The total design horizontal load per meter is calculated as followed:

$$F_\mathrm{h} = 1{,}5 * 43\,\frac{kN}{m} - 27{,}78\frac{kN}{m} = 36{,}72\,kN/m$$

Analogous to the vertical forces, this force is multiplied by the distance between the piles to obtain the horizontal design load.

$$F_{d,\mathrm{h},H/J\,stage\,pile} = F_\mathrm{h} * 8{,}14\,m = 36{,}72\,\mathrm{kN/m} * 8{,}14\,m = 298{,}90\,kN$$

Since the piles of the stage also have the inclination of 15°, the formula from Figure 56 is used to calculate the design axial load for alignment H and J.

$$F_{\text{d,H stage pile}} = \frac{F_{d,\text{v},H\ stage\ pile}}{\cos 15°} + \frac{F_{d,\text{h},H/J\ stage\ pile}}{\sin 15°} = \frac{1105{,}01\ \text{kN}}{\cos 15°} + \frac{298{,}90\ \text{kN}}{\sin 15°} = 2298{,}85\ kN$$

$$F_{\text{d,J stage pile}} = \frac{F_{d,\text{v},J\ stage\ pile}}{\cos 15°} + \frac{F_{d,\text{h},H/J\ stage\ pile}}{\sin 15°} = \frac{1159{,}95\ \text{kN}}{\cos 15°} + \frac{298{,}90\ \text{kN}}{\sin 15°} = 2355{,}73\ kN$$

Since the same piles for alignment H and J will be used, the biggest value of 2356 kN will be compared with the load bearing capacity.

Additionally, it was checked if the piles would experience tension due to wind action. It is necessary to verify if the vertical component of the load is sufficient if the horizontal component of the load would cause tension instead of compression. For this verification was the axial load of a pile calculated with the horizontal load being a negative value.

$$F_{\text{d,J stage pile}} = \frac{F_{d,\text{v},J\ stage\ pile}}{\cos 15°} - \frac{F_{d,\text{h},H/J\ stage\ pile}}{\sin 15°} = \frac{1159{,}95\ \text{kN}}{\cos 15°} - \frac{298{,}90\ \text{kN}}{\sin 15°} = 46{,}01\ kN$$

$$F_{\text{d,H stage pile}} = \frac{F_{d,\text{v},H\ stage\ pile}}{\cos 15°} - \frac{F_{d,\text{h},H/J\ stage\ pile}}{\sin 15°} = \frac{1105{,}01\ \text{kN}}{\cos 15°} - \frac{298{,}90\ \text{kN}}{\sin 15°} = -10{,}87\ kN$$

When the calculated value is positive, it may be assumed that these piles will not experience tension. Alignment H gives a small negative value which may indicate tension. The whole stage was modeled in a finite element program to check the loads on the piles. This resulted in the smallest axial load value on a stage pile to be a positive (compression load of 2 kN). Therefore, it was assumed that all micropiles for the stage are loaded only on compression and not on tension. This is the reason why the piles of the stage didn't need a self-drilling steel bar drilled into the Miocene layer.

As a summary, the three rounded up design values to compare with the load bearing capacity of the piles can be found in Table 22.

Table 22: Design loads on the micropiles

Design value of the most heavily pressure-loaded micropile of the roof	1049 kN
Design value of the most heavily tension-loaded micropile of the roof	1129 kN
Design value a micropile of the stage (compression)	2356 kN

3.6.2 Structural load bearing capacity

3.6.2.1 Structural load bearing capacity of the stage roof foundation piles

The piles for the stage roof foundation consist of a ductile driven pile with an outside diameter of 170 mm and a wall thickness of 7,5 mm. Inside this pile there is a self-drilled steel bar with an outer diameter of 64 mm. The piles are filled with concrete with strength C35/45. Based on this information, the structural load bearing capacity is calculated. Table 23 gives the results.

Table 23: Structural load bearing capacity of the piles of the roof

Ductile pile	
Outer diameter (mm)	170
Wall thickness (mm)	7,5
Inner diameter (mm)	155
Section (mm2)	3829
sacrificial loss of cross section (mm)	1,8
Section for calculation (mm2)	2878
yield strength (MPa)	320
γM	1,0
Ri,d Pile (kN)	**921**
Concrete	
Section (mm2)	18869
characteristic cylinder compressive strength (MPa)	35
nc (scaling factor)	0,5637
γM	1,5
Ri,d Concrete C35/45 (kN)	**688**
Σ R,id with C35/45 (kN)	**1609**
Reinforcement	
Self-drilling (mm)	64
Section for calculation (mm2)	1471
yield strength (MPa)	550
γM	1,0
Ri,d steel bar	**809**
Σ R,id total (kN)	**2418**

For the ductile pile the section was calculated as follow:

$$A_{DP} = \frac{\pi * (D^2 - d^2)}{4} = \frac{\pi * (170^2\ mm^2 - 155^2\ mm^2)}{4} = 3829\ \ mm^2$$

For the design of the piles, a sacrificial loss of 1,8 mm was taken into account. This gives a new section that is further used in the calculation.

$$A_{DP\ with\ loss} = \frac{\pi * (D^2 - d^2)}{4} = \frac{\pi * ((170 - 2 * 1{,}8)^2\ mm^2 - 155^2\ mm^2)}{4} = 2878\ \ mm^2$$

The design resistance of the ductile driven piles is calculated using the following formula:

$$R_{i,d\ Pile} = \frac{R_{i,k\ Pile}}{\gamma_M} = \frac{A_{DP\ with\ loss}\ *\ f_y}{\gamma_M} = \frac{2878\ \ mm^2 * 320\ N/mm^2}{1{,}0} = 921\ kN$$

For the concrete the calculations go as follow:

$$A_c = \frac{\pi * d^2}{4} = \frac{\pi * 155^2\ mm^2}{4} = 18869\ \ mm^2$$

A scaling factor is calculated to consider the pressure exerted by the steel pipe as a result of radial expansion caused by the axial load on the pile. The expansion of the concrete is blocked by the ductile iron pile. A simplifed formula is given by Yan-Gang Zhao (2009).

$$\eta_c = 1{,}8 * \frac{t}{D} * \frac{f_y}{f_c} = 1{,}8 * \frac{7{,}5\ mm - 1{,}8\ mm}{170\ mm - 2 * 1{,}8\ mm} * \frac{320\ MPa}{35\ MPa} = 0{,}5637$$

The design resistance of the ductile driven piles is calculated using the following formula:

$$R_{i,d\ concrete} = \frac{R_{i,k\ Pile}}{\gamma_M} = \frac{A_c * f_y * (1 + \eta_c)}{\gamma_M} = \frac{18869\ mm^2 * 35\ \mathrm{N}/mm^2 * (1 + 0{,}5637)}{1{,}5} = 688\ kN$$

To calculate the design resistance of the ductile pile with the filling concrete together, both values are added up.

$$R_{i,d\ Pile\ with\ concrete} = R_{i,d\ Pile} + R_{i,d\ concrete} = 921\ kN + 688\ kN = 1609\ kN$$

This design resistance has a larger value than the design compression load of 1049 kN on the piles for the roof. This shows that these piles for the roof were designed to be strong enough regarding the compression. The steel bar was not considered yet since this bar was only added for the tension loads. Therefore, the concrete section was calculated as a full circle, as if there was no reinforcement. In execution the steel bar is present, which will only increase the carrying capacity.

The design resistance of the self-drilling steel bar is calculated in the same way as the design resistance of the ductile pile.

$$R_{i,d\ steel\ bar} = \frac{R_{i,k\ steel\ bar}}{\gamma_M} = \frac{\mathrm{A} * f_y}{\gamma_M} = \frac{1471\ mm^2 * 550\ N/mm^2}{1{,}0} = 809\ kN$$

The calculated design resistance of the steel bar is a lot lower than the design tension load of 1129 kN on the piles of the stage roof. If it is assumed that the ductile iron pile can also absorb tensile forces, the structural load bearing capacity is increased by 921 kN making the total design resistance 1730 kN. This value is well above the design load of 1129 kN.

3.6.2.2 Structural load bearing capacity of the stage foundation piles

The piles for the stage consist of a ductile driven pile with an outside diameter of 170 mm and a wall thickness of 7,5 mm. Inside this pile there are three reinforcement steel bars with an outer diameter of 32 mm. The piles are filled with concrete with strength C35/45. Based on this information, the structural load bearing capacity is calculated. Table 24 gives the results.

Table 24: Structural load bearing capacity of the piles for the stage

Ductile pile	
Outer diameter (mm)	170
Wall thickness (mm)	7,5
Inner diameter (mm)	155
Section (mm2)	3829
sacrificial loss of cross section (mm)	1,8
Section for calculation (mm2)	2878
yield strength (MPa)	320
γM	1,0
Ri,d Pile (kN)	**921**
Concrete	
Section (mm2)	16456
characteristic cylinder compressive strength (MPa)	35
nc (scaling factor)	0,5637
γM	1,5
Ri,d Concrete C35/45 (kN)	**600**
Σ R,id with C35/45 (kN)	**1521**
Reinforcement	
Self-drilling (mm)	3*32
Section for calculation (mm2)	2413
yield strength (MPa)	435
γM	1,0
Ri,d steel bar	**1050**
Σ R,id total (kN)	**2571**

The design resistance of the ductile pile and the concrete are calculated in the exact same way as for the piles for the roof. Since the same type of ductile micropile was used, the design resistance value of the pile is the same. The value of the design resistance of concrete is different because the cross-section of the reinforcement is subtracted from the concrete cross-section. Therefore, it is important to also consider the design resistance of the reinforcement when comparing it with the design loads. The total design resistance of the piles for the stage is calculated as follow:

$$A_{reinforcement} = \frac{\pi * 3 * 32^2\, mm^2}{4} = 2413\, mm^2$$

$$A'_c = A_c - A_{reinforcement} = 18869\ mm^2 - 2413\, mm^2 = 16456\, mm^2$$

$$R_{i,d\ concrete} = \frac{R_{i,k\ Pile}}{\gamma_M} = \frac{A'_c * f_y * (1+\eta_c)}{\gamma_M} = \frac{16456\, mm^2 * 35\ \mathrm{N}/mm^2 * (1+0{,}5637)}{1{,}5} = 600\, kN$$

$$R_{i,d\ reinforcement} = \frac{R_{i,k\ Pile}}{\gamma_M} = \frac{A_{reinforcement} * f_y}{\gamma_M} = \frac{2413\ mm^2 * 435\, N/mm^2}{1{,}0} = 1050\, kN$$

$$R_{i,d\ total} = R_{i,d\ Pile} + R_{i,d\ concrete} + R_{i,d\ reinforcement} = 921\, kN + 600\, kN + 1050\, kN = 2571\, kN$$

This design resistance has a larger value than the design load of 2356 kN on the piles for the stage. This shows that these piles for the stage were designed to be strong enough.

3.6.3 Geotechnical load bearing capacity

3.6.3.1 Shaft resistance

The geotechnical load bearing capacity of the piles is mainly verified trough the performed load tests. The shaft resistance unit can be found through the strain gauges graph, using the following formula:

$$q_s = \frac{\Delta F}{L * P}$$

With:

ΔF = The value of the load distributed from the pile to the ground through the shaft resistance

L = The length over which the load was distributed to the soil

P = The perimeter of the pile = $\pi * 0{,}170\ m$ = 0,534 m

The strain gauges graphs, found in Figures 51 and 54 don't have the correct load values on their x-asis that correspond with the load cycle value. With the use of the rescaling program 'Web plot digitizer', a new x-axis was designed.

For the tension graph, the new axis is based on the value 0 at the origin and the value 855 kN at the end of the black line. The load cycle of 855 kN was chosen since the load is closest to the tension design load of the piles. For every segment of the gragh, the corresponding loads were gathered from 'Web plot digitizer'. These values can be found in Table 25.

Table 25: Load values from the strain gauge chart of the tension test (Web plot digitizer)

Strain gauge chart – tensile test	
x-values - Load [kN]	y-values – depth [m]
855	2,5
786	10
612	20
438	26
381	30
0	38,5

These load values lead to the calculated shaft resistance units that can be found in Table 26.

Table 26: Calculated shaft resistance units out the strain gauge graph from the tension load test

Tension (black load cycle 855 kN)					
		ΔF	ΔL	P	q_s
Sanitary landfill	P_1	69	7,5	0,5341	17,23
	P_2	174	10	0,5341	32,58
Alluvial layer	P_1	174	6	0,5341	54,30
	P_2	57	4	0,5341	26,68
Miocene		381	8,5	0,5341	83,93

For tension, it is important that almost all of the load can be distributed to the Miocene and the alluvial layer. These are trustworthy layers because the Miocene is a very homogenous hard rock layer and the alluvial has been consolidated because of the weight of the sanitary landfill over many years. The sanitary landfill is very untrustworthy since the sanitary landfill is very heterogenous which causes very different values of the shaft resistance unit within the same layer.

Knowing that the steel bar is installed 10 m deep in the Miocene, the total shaft resistance that this steel bar has in the Miocene can be calculated as follow:

$$Q_{s,Miocene} = q_{s,Miocene} * A_{shaft,Miocene} = 83{,}93\ \frac{kN}{m^2} * 10\ m * \pi * 0{,}170\ m = 448\ kN$$

Since the load tension load test of 1598 kN confirmed that the no failing of the sealing in the Miocene was registered, it can be assumed that all the tension loads on the piles of the roof will be able to be carried over to the soil through shaft resistance and that the shaft resistance in the calculation above is not correct.

For the compression graph, the new axis is based on the value 0 at the origin and the value 1285 kN at the end of the dark blue line. The load cycle of 1285 kN was chosen since a load over 1400 kN gives the deformation of the massif, which can lead to incorrect test values. For every segment of the gragh, the corresponding loads were gathered from ‘Web plot digitizer’. These values can be found in Table 27.

Table 27: Load values from the strain gauge chart of the tension test (Web plot digitizer)

Strain gauge chart – compression test	
x-values - Load [kN]	y-values - depth [m]
1292	2,5
810	11
691	20
587	23
438	28
319	33

These load values lead to the calculated shaft resistance units that can be found in Table 28.

Table 28: Calculated shaft resistance units out the strain gauge graph from the compression load test

Compression (dark blue load cycle 1285 kN)					
		ΔF	ΔL	P	q_s
Sanitary landfill	P_1	482	8,5	0,5341	106,18
	P_2	119	9	0,5341	24,76
	P_3	104	3	0,5341	64,91
Alluvial layer	P_1	149	5	0,5341	55,80
	P_2	119	5	0,5341	44,56
Miocene		/	/	/	/

From the 1285 kN compression that was applied to the pile, a total load of 973 kN was distributed to the surrounding soil through shaft resistance. This can vary a lot from pile to pile since the sanitary landfill is a very heterogenous layer which causes very different values of the shaft resistance unit within the same layer.

3.6.3.2 End-bearing resistance

The compression piles mainly operate in the soil through their end-bearing resistance. As mentioned above, there is also a compression load carried to the surrounding ground through the shaft resistance of the pile but with the unpredictable character of the sanitary landfill, it is safe to count on the end-bearing resistance.

It is assumed that the pile design load can be transferred to the soil via end-bearing when the pile is driven to refusal in the ground. The refusal criteria of dropping maximum 30 mm in 1 minute was reached in the Miocene layer, meaning that the end bearing capacity is sufficient for the pressure piles.

3.6.4 Buckling potential analysis

Professor Stefan Vogt from the Technical University of Munich has done a lot of research and studies in the field of buckling of (micro)piles in soil. He suggests that in a simplistic approach to assessing the critical load of buckling, a landfill with average age greater than 25 years, can be analysed as undrained cohesive soil. This is the case for the site in question. (Geosol, 2023)

A SPT-test that was carried out at the site gives SPT-values between 15-30 strokes, which corresponds to a hard cohesive with an undrained shear strength c_u between 100 and 200 kPa. Figure 58 of a table gives an overview of the different soil parameters. (Geosol, 2023)

Kind of probe	Soil density/ CONSISTENCY	LRS 5 (DPL-5)	LRS 10 (DPL)	SRS 15 (DPH)	SPT	CPT	$D = \frac{n_{max} - n_0}{n_{max} - n_{min}}$	$I_D = D \cdot \frac{1 - n_{min}}{1 - n}$	q_u	c_u	$I_C = \frac{W_L - W}{W_L - W_P}$
		n/10cm	n/10cm	n/10cm	n/30cm	q_s = kN/m²			kN/m²	kN/m²	
non-cohesive soils	very soft				1 - 4	0 - 2.500	0 - 0,15	0 - 0,15			
	soft	3 - 8	0 - 4	2 - 3	4 - 10	2.500 - 5.000	0,15 - 0,30	0,15 - 0,35			
	soft to medium dense					5.000 - 10.000	0,25 - 0,35	0,35 - 0,65			
	medium dense	8 - 25	4 - 10	4 - 10	10 - 30	10.000 - 15.000	0,30 - 0,50	0,65 - 0,85			
	dense	25 - 40	10 - 25	10 - 25	30 - 50	> 15.000	0,50 - 0,75	> 0,85			
	very dense	> 40	> 25				> 0,75				
cohesive soils	very soft	Attention: measurements are not significant due to 1. skin friction 2. pore water pressure			< 2	400	not clear	not clear	< 25	12,5	0 - 0,50
	soft				2 - 4	400 - 800			25 - 50	12,5 - 25	0,50 - 0,75
	medium soft				4 - 8	800 - 1.600			50 - 100	25 - 50	0,75 - 1,0
	firm				8 -15	1.600 - 3.000			100 - 200	50 - 100	1,0 -
	stiff				15 - 30	3.000 - 6.000			200 - 400	100 - 200	
	very stiff/hard				> 30	> 6.000			> 400	> 200	

Figure 58: Non-cohesive and cohesive soil parameters (Geosol, 2023)

It was concluded that a buckling analysis for the piles at the site were unnecessary. The analysis of buckling is not needed for non-cohesive soils because the lateral support by the embedding is sufficient. Eurocode states that in soils with an undrained shear strength (c_u) of lower than 10 kPa, the buckling of piles needs to be investigated. Since the undrained shear strength significantly is higher at the site, a buckling analysis was not carried out.

4. Optimized solution

4.1 Optimized solution of the roof compression foundation piles

The maximum compression design load on these piles is 1049 kN and compression resistance of the pile is 1609 kN. This gives a room for optimization of the piles with a possible loss of up to about 550 kN on the structural load bearing capacity.

Optimization of the piles can be said to occur when the total ductile pile section is smaller. Taking into consideration a corrosion loss of 1,8 mm on the piles, the cross-section of the six different pile types was calculated. Table 29 shows the results.

Table 29: Optimalization of the compression piles of the roof

	Ductile pile 118 mm			Ductile pile 170 mm		
Outer diameter with loss of 1,8 mm	Ø	114,4	[mm]	Ø	166,4	[mm]
	Thickness [mm]			Thickness [mm]		
Wall thickness	7,5	9	10,6	**7,5**	9	10,6
Thickness with loss of 1,8 mm	5,7	7,2	8,8	**5,7**	7,2	8,8
Section steel [mm²]	1946	2425	2919	**2878**	3601	4357
Section concrete [mm²]	8332	7854	7359	**18869**	18146	17390
η_c for C25/30	1,1480	1,4501	1,7723	0,7892	0,9969	1,2185
η_c for C30/37	0,9566	1,2084	1,4769	0,6577	0,8308	1,0154
η_c for C35/45	0,8200	1,0358	1,2659	**0,5637**	0,7121	0,8703
Ri,d for C25/30	298	321	340	**563**	604	643
Ri,d for C30/37	326	347	365	626	664	701
Ri,d for C35/45	354	373	389	688	725	759
Ri,d Pile	623	776	934	**921**	1152	1394
Ri,d Pile and concrete C25/30	921	1097	1274	1484	1756	2037
Ri,d Pile and concrete C30/37	949	1123	1299	1546	1817	2095
Ri,d Pile and concrete C35/40	977	1149	1323	**1609**	1877	2153

The only two piles with a smaller ductile iron pile section than the original 170 – 7,5 mm, are 118 – 7,5 mm and 118 – 9 mm. To check If these pile types are a good optimalization for the site, the structural load bearing capacity must be checked. The values of these design resistances can be found at the bottom of Table 29. This shows that pile type 118-7,5 mm has a smaller design resistance than the compression design load of 1049 kN. Pile type 118-9 mm has a design resistance of 1149 kN, which is higher than the design load, therefore this pile could be used to optimize the foundation solution for the roof.

Table 29 also shows the calculations for different types of concrete and the use of a different thickness-to-diameter ratio. This was done to calculate the different confinement efficiencies, which is scaling factor of the concrete η_c, for each pile and concrete type. Getting the scaling factor of the concrete η_c as high as possible, should improve the structural load bearing capacity following the formula. Unfortunately, the calculations determine that the decrease in concrete strength outweighs any potential advantages associated with increasing the coefficient of confinement for the concrete core (η_c). If the cost of concrete C30/37 and C25/30 are cheaper, they can be considered to fill the inside of the ductile piles, since considering these concrete strengths still gives a total design resistance that is higher than the the design load of 1049 kN.

To summarize, Table 30 shows the comparison of the cross section and total volume of ductile iron pile for the adapted and optimized solution. For this comparison the thickness loss due to corrosion was not considered. To calculate the volume, an average pile length of 30 m was used. It can be concluded that the optimized solution safes 0,0224 m^3 ductile iron per pile. Since there are one hundred micropiles used for the foundation of the roof, a total of 2,24 m^3 of ductile iron can be saved. When taking into account the mass density of 7050 kg/m^3 for ductile iron, a mass of 158 kg per pile can be saved. For the hundred piles, this is a total of 15 800 kg.

Table 30: Comparison of adapted and optimized solution

Ductile iron driven pile	Adopted solution 170 – 7,5 mm	Optimized soluation 118 – 9 mm
Cross section [mm^2]	3829	3082
Volume [m^3]	0,1149	0,0925
Mass [kg]	810	652

4.2 Optimized solution of the stage roof tension foundation piles

An optimalization for the tension piles of the roof that could be considered is to install the self-drilling steel bar only 8,5 m into the Miocene layer instead of 11 m. The reason for this consideration is that the tension load test showed that at the depth of 38,5 m, 8,5 m into the Miocene, no load was registered on the pile. This means that the last 2,5 m of steel bar was not mobilized in the steel test and could be considered unnecessary. This is not a safe optimization when considering the heterogeneity of the sanitary landfill. To ensure that if the soil above the sealing length does not have the necessary resistance to take up any load, the load can still be mobilized at the Miocene layer.

4.3 Optimized solution of the stage foundation piles

Following the optimalization of the compression piles of the roof, the only ductile pile types with a smaller section than the currant and therefor will be checked for their design resistance are type 118 – 7,5 mm and type 118 – 9 mm. The calculations of the structural load bearing capacities of these piles can be found in Table 31.

Table 31: Optimalization of the piles of the stage

Ductile pile		
Outer diameter (mm)	118	118
Wall thickness (mm)	7,5	9
Inner diameter (mm)	103	100
Section (mm2)	2604	3082
sacrificial loss of cross section (mm)	1,8	1,8
Section for calculation (mm2)	1946	2425
yield strength (MPa)	320	320
γM	1,0	1,0
Ri,d Pile (kN)	**623**	**776**
Concrete		
Section (mm2)	5920	5441
characteristic cylinder compressive strength (MPa)	35	35
nc (scaling factor)	0,8200	1,0358
γM	1,5	1,5
Ri,d Concrete C35/45 (kN)	**251**	**258**
Σ R,id with C35/45 (kN)	**874**	**1034**
Reinforcement		
Self-drilling (mm)	3*32	3*32
Section for calculation (mm2)	2413	2413
yield strength (MPa)	435	435
γM	1,0	1,0
Ri,d steel bar	**1050**	**1050**
Σ R,id total (kN)	**1924**	**2084**

The total design resistances of both piles, 1924 kN and 2084 kN, are both smaller than the design load of 2356 kN on the piles. These piles cannot be used for an optimized solution. The compression foundation piles of the stage cannot be optimized.

5. Final remarks

This thesis analyzed the use of ductile driven piles in general and also looked at the use of them as a special foundations solution at the World Youth Day site.

Looking at the different components of the ductile piles, it can be concluded that there are three different types of pile pipes, four different types of driving shoes and three different types of piles heads. Next, the difference between regular cast iron and ductile cast iron was discussed. The process of manufacturing the piles was also explained. It was also clarified that when installing the piles, it’s either as an end-bearing or skin-friction pile. When skin-friction is necessary for the piles, external grout should be used. Lastly it can be concluded that the production process with especially the cupola furnace has the biggest environmental impact, when analyzing the life cycle of the piles.

The site for the WYD event, is located northeast in relation to central Lisbon, next to the Vasco Da Gama bridge on the right bank of the Tagus. The site is situated on a sanitary landfill. This landfill causes a very unpredictable ground with the risk of contamination. Therefor the foundation options very limited. The chosen solution consists of first a preload landfill for 169 days. The stage is founded on concrete slabs with eight end-bearing ductile driven piles. For the roof, the foundation exists of a hundred ductile piles in combination with a self-drilling steel bar grouted in the Miocene rock layer to resist tensile stresses.

To analyze the implemented foundations solutions, the load tests were investigated. The calculations that were done in the load test report were explained. The graphs of the deformations showed what load cycles gave which elastic and which plastic deformations. The strain gauges graphs were also looked into. These concluded how much load was distributed to the ground at what depth. The compression piles had still a lot of load left at their toe since they are end-bearing piles while for the tension piles, no load was registered even 2,5 m above the toe of the pile. Next, the design loads were calculated and checked if they were smaller than the calculated design resistances. This was the case for all the piles. Lastly, it was checked if the piles could be optimized. The conclusion is that for the piles of the roof a ductile pile with smaller diameter could be used. It can be concluded that the optimized solution safes 158 kg ductile iron. The ductile iron driven piles of the stage could not be optimized. For future developments it is important to analyze the foundations solutions behavior during and after the World Youth Day.

References

About Us (n.d.). TRM. https://trm.at/en/piling-systems.

About SimaPro - SimaPro. (2022, October 13). SimaPro. https://simapro.com/about/.

André, M. R. (2022). Jornada Mundial da Juventude: o que vai mudar na frente ribeirinha equal o ponto de situação. *Lisboa Para Pessoas*. https://lisboaparapessoas.pt/en/2022/07/31/jornada-mundial-da-juventude-trancao-tejo-lisboa-loures/ (In Portuguese).

ANP-Systems GmbH FPG Piles Full displacement pressurized grouted Piles. (n.d.).

Bauer. (2019). *PGF Pile System.*

BRAZ, I.; PINTO, A; SILVA, N; SIMOES, C; GOMES, T; CAXIAS, C (2003). *Soluções de fundações nemo bras localizadas perto do rio trancão, em Lisboa.* XVII Portuguese National Congress, Evora University (In Portuguese).

David. (2023). Ductile Iron. *Reliance Foundry Co. Ltd*. https://www.reliance-foundry.com/blog/ductile-iron#:~:text=Ductile%20iron%E2%80%94also%20referred%20to,twisted%2C%20or%20deformed%20without%20fracturing.

DeLavaud process - Bhamwiki. (n.d.). https://www.bhamwiki.com/w/DeLavaud_process.

Dey, A. K. (2023, January 24). What is Ductile Iron? | Types, Properties, and Applications of Ductile Iron (With PDF). *What is Piping*. https://whatispiping.com/ductile-iron/.

Ductile Iron Pipe Research Association. (n.d.). DIPRA. https://dipra.org/.

Exo Inc. (2022, January 12). *Full-Scale Load Testing Services | Exo*. Exo. https://exoinc.com/full-scale-load-testing.

Full-Scale Load Testing Services | ECS. (2023, June 6). ECSLimited. https://www.ecslimited.com/services/facilities-consulting/full-scale-load-testing/#:~:text=Full%2Dscale%20load%20testing%20allows%20you%20to%20evaluate%20the%20impact,under%20load%20due%20to%20gravity.

Geosol. (2023). *Ensaio de compressão em microestaca dúctil cravada - ensaio de tracção em microestaca dúctil vravada com autoperfurante interior* (In Portuguese).

Iqbal, S., & Iqbal, S. (2017, November 25). Difference between End Bearing Piles and Skin Friction Piles. - Iamcivilengineer. *Iamcivilengineer - Civil Engineering Website*. https://www.iamcivilengineer.com/2017/11/difference-between-end-bearing-piles-and-skin-friction-piles.html.

Kinematics, G. (2020, November 16). Ductile Iron and Ductile Iron Casting. *General Kinematics*. https://www.generalkinematics.com/blog/ductile-iron-casting/#:~:text=The%20difference%20between%20traditional%20cast,iron%20or%20nodular%20cast%20iron.

Lisboa Ocidental SRU. (2022). *Projeto de modelacao do terreno* – memoria descriptiva e justificativa. (In Portuguese).

Machinery, S. (2021, July 29). *Friction Piles: What is it,When & Where to Use[6 FAQs]*. Shuanglong Machinery. https://www.machinesl.com/what-is-friction-piles/#:~:text=End%20load%2Dbearing%20piles%20resist,skin%20friction%20on%20their%20surface.

Nagel I Pfahl Zertifiziert, A. I. (n.d.). *ANP-Systems GmbH Ductile Iron Piles-sounds and vibrations*. http://www.anp-systems.at.

NBN EN 1990. (2002). *Eurocode 0 - Bases of structural design.* NBN Standard.

NBN EN 1993. (2015). *Eurocode 3 - Design of steel structures.* NBN Standard.

NBN EN 1994. (2005). *Eurocode 4 – Design of composite steel and concrete structures.* NBN Standard.

NBN EN 1997. (2005). *Eurocode 7 – Geotechnical design*. NBN Standard.

Obra Beirolas JMJ | Lisboa Ocidental SRU. (n.d.). Lisboa Ocidental SRU. https://www.lisboaocidentalsru.pt/beirolas-jmj (In Portuguese).

OIB – Austrian Institute of Construction Engineering. (2017). *European Technical Assesment.*

Poulos, H. G., Davis, E. H. (1980). *Pile foundation analysis and design.*

Rohre GmbH, T. (n.d.). *General technical approval Z-34.*

Roughness Parameters - Rubert & Co Ltd. (2019, November 29). Rubert & Co Ltd. http://www.rubert.co.uk/faqs/roughness-parameters/#:~:text=The%20Mean%20Roughness%20Depth%20(Rz,Rz%20are%20micrometres%20or%20microinches.

Solos das Petrolíferas / Aterro Sanitário de Beirolas. (n.d.). http://www.portaldasnacoes.pt/item/solos-das-petroliferas-aterro-sanitario-de-beirolas/ (In Portuguese).

Steel pipe piles Finnish National Road Administration (FinnRA) Bridge Engineering. (2000).

Steinlechner, E. (n.d.). *DUCTILE IRON PILES-The TRM Piling System-Data sheet*.

The EPD | *EPD International*. (n.d.). https://www.environdec.com/all-about-epds/the-epd.

Tiroler Rohre: Ductile Iron Piles. (n.d.). https://trm.at/en/piling-systems.

Tiroler Rohre. (n.d.). *About Us*. http://www.trm.at.

Tiroler Rohre. (n.d.). *External load-bearing capacity of TRM ductile driven piles*. http://www.trm.at.

TRM Piling Systems. (n.d.). http://www.trm.at.

TRM Piling Systems Fast. Simple. Safe. (n.d.). http://www.trm.atwww.trm.at.

TRM PILING SYSTEMS Tiroler Rohre GmbH. (2022). http://www.bau-epd.at.

Vogt, N., Vogt, S., & Kellner, C. (2009). Buckling of slender piles in soft soils. *Bautechnik*, *86* (SUPPL. 1), 98-112.

What is it - WYD Lisbon 2023. (n.d.). JMJ 2023. https://www.lisboa2023.org/en/what-is-it.

Annexes

Annex 1: Pile head plates for TRM piling system

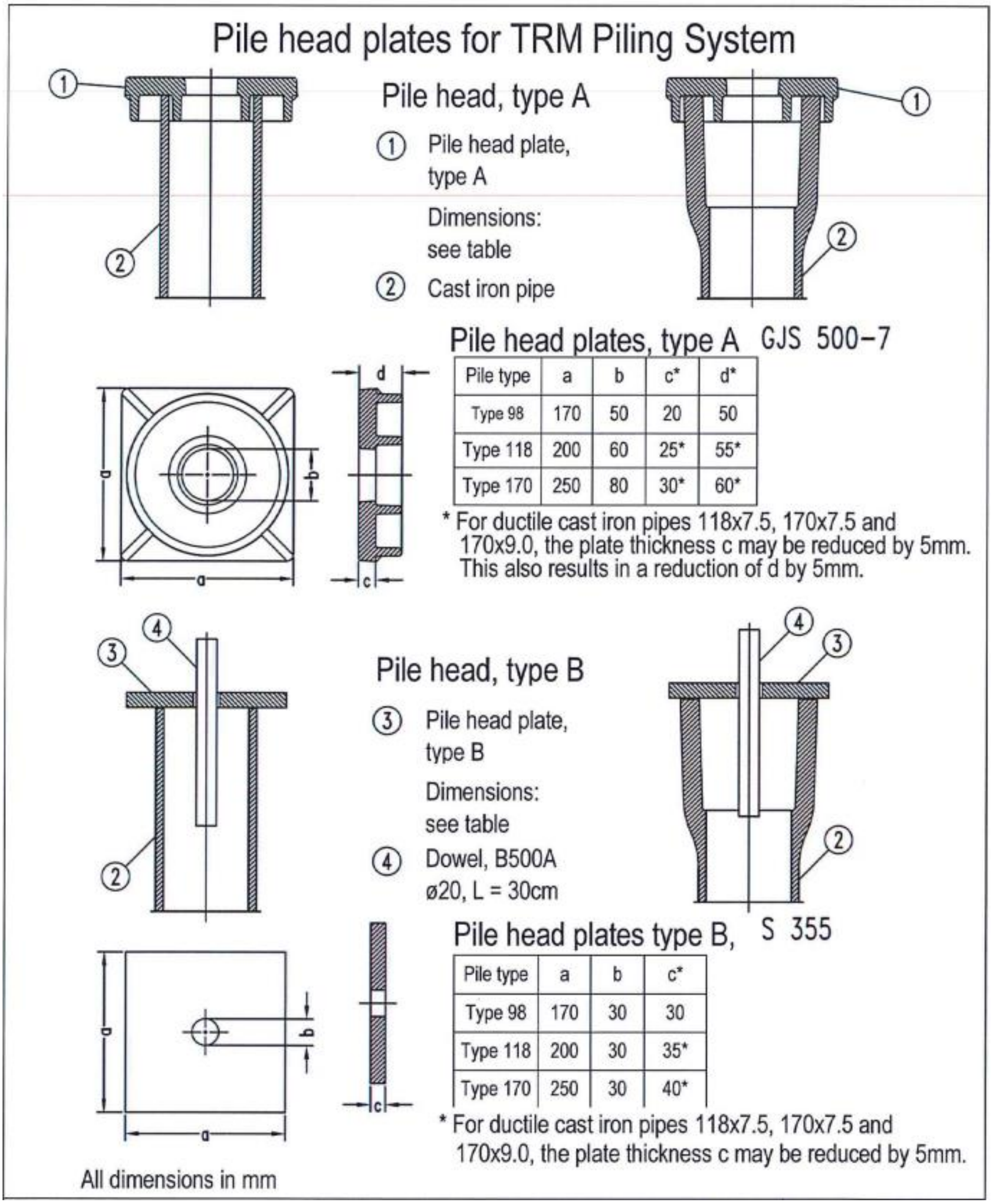

Pile head plates, type A GJS 500-7

Pile type	a	b	c*	d*
Type 98	170	50	20	50
Type 118	200	60	25*	55*
Type 170	250	80	30*	60*

* For ductile cast iron pipes 118x7.5, 170x7.5 and 170x9.0, the plate thickness c may be reduced by 5mm. This also results in a reduction of d by 5mm.

Pile head plates type B, S 355

Pile type	a	b	c*
Type 98	170	30	30
Type 118	200	30	35*
Type 170	250	30	40*

* For ductile cast iron pipes 118x7.5, 170x7.5 and 170x9.0, the plate thickness c may be reduced by 5mm.

All dimensions in mm

Pile head plates for TRM Piling System, GJS 500-7

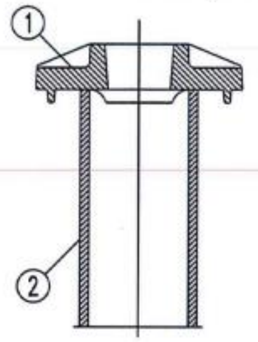

Pile head, type C

① Pile head plate, type C

Dimensions: see table

② Cast iron pipe

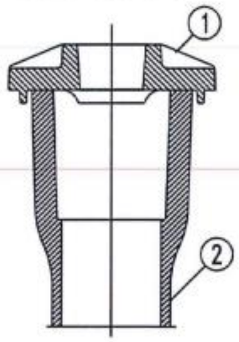

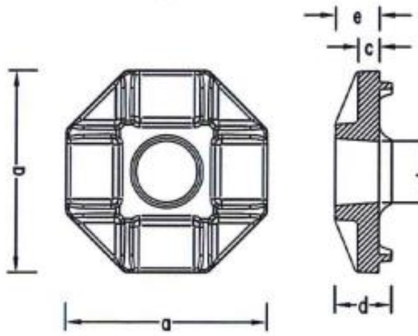

Pile head plates, type C GJS 500−7

Head plate, type C	a	b	c	d	e
Octagon 220 1)	220	67	23	62	48
Octagon 275 2)	275	67	25	70	50
Octagon 330 2)	330	67	27.5	70	55

1) Suitable for pile type 118

2) Suitable for pile types 118 and 170

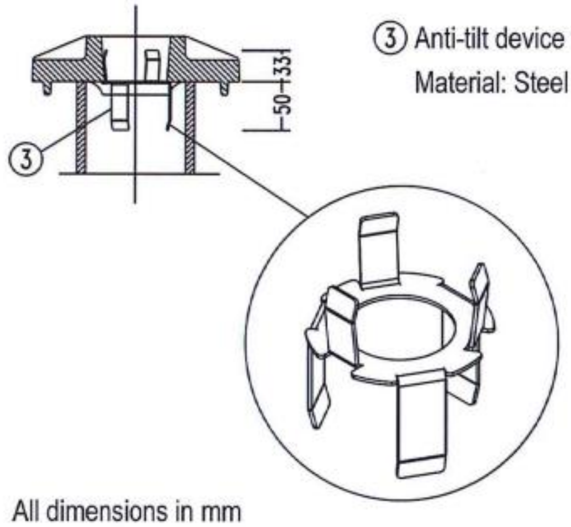

③ Anti-tilt device for compression pile, pile type 118
Material: Steel DC01 (1.0330)

All dimensions in mm

Annex 2: Illustration of a tensile or alternating load pile

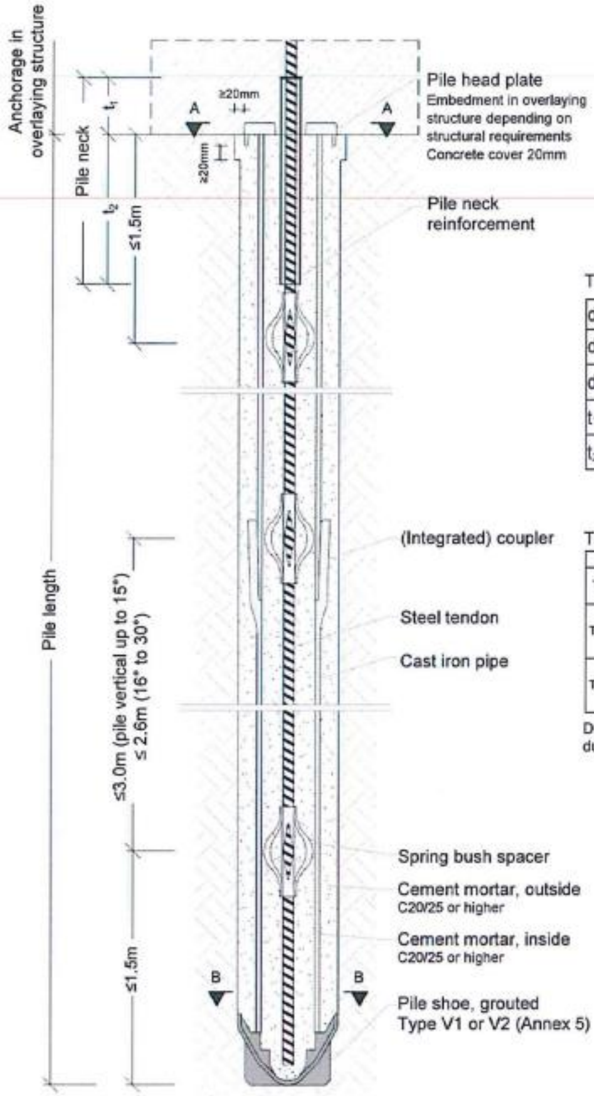

Anchoring of steel tendon

1. End anchorage/plate anchorage in accordance with decision Z -1.5-76, Z-1.5-149 or Z-1.5-174
2. Anchoring by bonding in accordance with decision for threaded rebar B500B

Pile neck reinforcement – steel tendon

Ribbed plastic pipe with inner diameter Ø d_{Ri} and outer diameter Ø d_{Ra} in accordance with Table 1

Table 1: Ribbed plastic pipe

d steel tendon [mm]	20	25	28	32	40	50
d_{Ri} [mm]	≥35	≥39	≥41	≥46	≥55	≥66
d_{Ra}[mm]	≤50	≤50	≤50	≤56	≤65	≤79
t_1 [mm]	150	150	150	150	200	200
t_2 [mm]	600	600	600	600	600	600

Table 2: Spring bush spacers

d steel tendon [mm]		20	25	28	32	40	50
Type 98	d x s (minD/maxD) [mm]	32 x 2 (80/125)	32 x 2 (80/125)	32 x 2 (80/125)	–	–	–
Type 118		32 x 2 (80/125)	32 x 2 (80/125)	32 x 2 (80/125)	40 x 3 (100/190)	50 x 3 (100/210)	–
Type 170		40 x 3 (100/190)	40 x 3 (100/190)	40 x 3 (100/190)	40 x 3 (100/190)	50 x 3 (100/210)	63 x 3 (125/220)

D is to be adapted to the inner pipe diameter of the ductile iron pipe by compressing the spring bush spacers

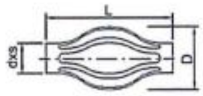

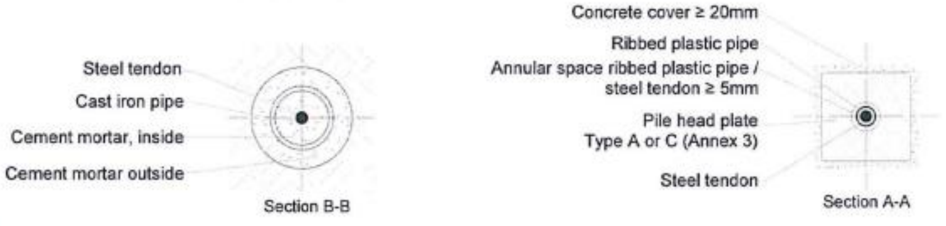

Annex 3: Design values of the cross-sectional load-bearing capacity of ductile iron piles

Internal load bearing capacity of the piles without cement mortar filling

Type	Nominal wall thick-ness	Assessment method	Safety coefficient γ_{M0}	Internal load bearing ca-pacity design value N_{Sd} [kN]
98	6,0	Calculation according to EAD, clause 2.2.1	1,0	555
	7,5		1,0	682
118	7,5		1,0	833
	9,0		1,0	986
	10,6		1,0	1144
170	7,5		1,0	1225
	9,0		1,0	1457
	10,6		1,0	1699
	13,0		1,0	2052

Note: The load bearing capacity is calculated for the cross section. Buckling is not taken into account.

Internal load bearing capacity of the piles with cement mortar filling

Ductile cast iron pipe TRM-Pfahl-Duktil [mm]	Without shaft-grouting, with subsequent cement mortar backfill				With shaft-grouting, pile inclination ≤ 5° out of the vertical***	
	Service life ≤ 50 years*		Service life ≤ 100 years**			
	C20/25	C25/30	C20/25	C25/30	C20/25	C25/30
Ø 98 x 6.0	450 kN	469 kN	406 kN	426 kN	582 kN	601 kN
Ø 98 x 7.5	560 kN	578 kN	517 kN	535 kN	692 kN	710 kN
Ø 118 x 7.5	709 kN	737 kN	656 kN	684 kN	869 kN	896 kN
Ø 118 x 9.0	842 kN	868 kN	789 kN	815 kN	1,001 kN	1,027 kN
Ø 118 x 10.6	979 kN	1,003 kN	927 kN	951 kN	1,139 kN	1,163 kN
Ø 170 x 7.5	1,134 kN	1,197 kN	1,058 kN	1,121 kN	1,365 kN	1,428 kN
Ø 170 x 9.0	1,335 kN	1,396 kN	1,259 kN	1,320 kN	1,566 kN	1,627 kN
Ø 170 x 10.6	1,545 kN	1,603 kN	1,469 kN	1,527 kN	1,776 kN	1,834 kN
Ø 170 x 13.0	1,851 kN	1,906 kN	1,775 kN	1,830 kN	2,082 kN	2,137 kN

Reduced internal load bearing capacity due to corrosion for unfilled piles in different soils through the years

Table 3.2: Reduced internal load bearing capacity [kN] for TRM-pile-pipes in undisturbed natural soils (sand, silt, clay, schist, etc.)

Type	Nominal wall thickness	5 years		25 years		50 years		75 years		100 years	
		Loss of thickness	Reduced internal load bearing capacity	Loss of thickness	Reduced internal load bearing capacity	Loss of thickness	Reduced internal load bearing capacity	Loss of thickness	Reduced internal load bearing capacity	Loss of thickness	Reduced internal load bearing capacity
98	6,0		555		525		496		467		438
	7,5		682		653		624		594		566
118	7,5		833		798		762		727		692
	9,0		986		951		915		880		845
	10,6	0,00 mm	1144	0,30 mm	1109	0,60 mm	1074	0,90 mm	1039	1,20 mm	1004
170	7,5		1225		1174		1123		1072		1022
	9,0		1457		1406		1355		1304		1253
	10,6		1699		1647		1596		1546		1495
	13,0		2052		2001		1950		1899		1848

Table 3.3: Reduced internal load bearing capacity [kN] for TRM-pile-pipes in polluted natural soils and industrial sites

Type	Nominal wall thickness	5 years		25 years		50 years		75 years		100 years	
		Loss of thickness	Reduced internal load bearing capacity	Loss of thickness	Reduced internal load bearing capacity	Loss of thickness	Reduced internal load bearing capacity	Loss of thickness	Reduced internal load bearing capacity	Loss of thickness	Reduced internal load bearing capacity
98	6,0		540		482		409		338		268
	7,5		668		609		537		466		396
118	7,5		815		745		657		571		486
	9,0		968		898		811		724		639
	10,6	0,15 mm	1127	0,75 mm	1056	1,50 mm	969	2,25 mm	883	3,00 mm	798
170	7,5		1200		1098		971		846		722
	9,0		1431		1329		1203		1077		953
	10,6		1673		1571		1445		1319		1195
	13,0		2026		1924		1798		1672		1548

Note: The load bearing capacity is calculated for the cross section. Buckling is not taken into account.

Table 3.4: Reduced internal load bearing capacity [kN] for TRM-pile-pipes in aggressive natural soils (swamp, marsh, peat,...)

Type	Nominal wall thickness	5 years		25 years		50 years		75 years		100 years	
		Loss of thickness	Reduced internal load bearing capacity	Loss of thickness	Reduced internal load bearing capacity	Loss of thickness	Reduced internal load bearing capacity	Loss of thickness	Reduced internal load bearing capacity	Loss of thickness	Reduced internal load bearing capacity
98	6,0		535		457		386		315		- 1)
	7,5		663		585		513		442		373
118	7,5		809		716		629		543		458
	9,0		963		869		782		696		611
	10,6	0,20 mm	1121	1,00 mm	1027	1,75 mm	940	2,50 mm	854	3,25 mm	770
170	7,5		1191		1055		929		804		680
	9,0		1423		1287		1161		1036		912
	10,6		1664		1529		1403		1278		1154
	13,0		2018		1882		1756		1631		1507

Table 3.5: Reduced internal load bearing capacity [kN] for TRM-pile-pipes in non-compacted and non-aggressive fills (clay, schist, sand, silt,...)

Type	Nominal wall thickness	5 years		25 years		50 years		75 years		100 years	
		Loss of thickness	Reduced internal load bearing capacity	Loss of thickness	Reduced internal load bearing capacity	Loss of thickness	Reduced internal load bearing capacity	Loss of thickness	Reduced internal load bearing capacity	Loss of thickness	Reduced internal load bearing capacity
98	6,0		537		486		438		390		343
	7,5		665		614		566		518		470
118	7,5		812		751		692		634		577
	9,0		965		904		845		787		730
	10,6	0,18 mm	1123	0,70 mm	1062	1,20 mm	1004	1,70 mm	946	2,20 mm	888
170	7,5		1194		1106		1022		938		854
	9,0		1426		1338		1253		1169		1086
	10,6		1668		1579		1495		1411		1327
	13,0		2021		1933		1848		1764		1681

1) According to the manufacturer residual wall thickness of the pile pipes of < 3 mm are not used for design.
Note: The load bearing capacity is calculated for the cross section. Buckling is not taken into account.

Table 3.6: Reduced internal load bearing capacity [kN] for TRM-pile-pipes in non-compacted and aggressive fills (ashes, slag,...)

Type	Nominal wall thickness	5 years		25 years		50 years		75 years		100 years	
		Loss of thickness	Reduced internal load bearing capacity	Loss of thickness	Reduced internal load bearing capacity	Loss of thickness	Reduced internal load bearing capacity	Loss of thickness	Reduced internal load bearing capacity	Loss of thickness	Reduced internal load bearing capacity
98	6,0	0,50 mm	506	2,00 mm	362	3,25 mm	-[1]	4,50 mm	-[1]	5,75 mm	-[1]
	7,5		633		489		373		259		-[1]
118	7,5		774		600		458		320		-[1]
	9,0		927		753		611		473		337
	10,6		1085		911		770		631		496
170	7,5		1140		887		680		477		-[1]
	9,0		1371		1119		912		708		507
	10,6		1613		1361		1154		950		749
	13,0		1967		1714		1507		1303		1102

Reduced internal load bearing capacity due to corrosion for unfilled piles and filled piles with a planned service life of 100 years

Type (outer diameter)		mm	98		118			170			
Nominal wall thickness		mm	6.0	7.5	7.5	9.0	10.6	7.5	9.0	10.6	13.0
Wall thickness loss due to corrosion 0.60 mm											
Cross-sectional load-bearing capacity[1]	Pile	kN	496	624	762	915	1,074	1,123	1,355	1,596	1,950
	Pile + C20/25	kN	574	696	873	1,020	1,172	1,375	1,596	1,828	2,167
	Pile + C25/30	kN	593	714	901	1,046	1,196	1,438	1,657	1,886	2,221
Wall thickness loss due to corrosion 0.90 mm											
Cross-sectional load-bearing capacity	Pile	kN	467	594	727	880	1,039	1,072	1,304	1,546	1,899
	Pile + C20/25	kN	545	667	838	985	1,137	1,324	1,546	1,777	2,116
	Pile + C25/30	kN	564	685	866	1,011	1,161	1,387	1,606	1,835	2,170
Wall thickness loss due to corrosion 1.00 mm											
Cross-sectional load-bearing capacity	Pile	kN	457	585	716	869	1,027	1,055	1,287	1,529	1,882
	Pile + C20/25	kN	535	657	827	973	1,125	1,307	1,529	1,761	2,099
	Pile + C25/30	kN	554	675	854	999	1,150	1,370	1,589	1,819	2,153
Wall thickness loss due to corrosion 1.20 mm											
Cross-sectional load-bearing capacity[1]	Pile	kN	438	566	692	845	1,004	1,022	1,253	1,495	1,848
	Pile + C20/25	kN	516	638	803	950	1,102	1,273	1,495	1,727	2,065
	Pile + C25/30	kN	535	656	831	976	1,126	1,336	1,555	1,785	2,120
Wall thickness loss due to corrosion 1.75 mm											
Cross-sectional load-bearing capacity[1]	Pile	kN	386	513	629	782	940	929	1,161	1,403	1,756
	Pile + C20/25	kN	463	585	740	886	1,038	1,181	1,403	1,634	1,973
	Pile + C25/30	kN	482	603	768	913	1,063	1,244	1,463	1,692	2,027
Wall thickness loss due to corrosion 2.00 mm											
Cross-sectional load-bearing capacity	Pile	kN	[2]	489	600	753	911	887	1,119	1,361	1,714
	Pile + C20/25	kN	[2]	561	711	858	1,009	1,139	1,361	1,593	1,931
	Pile + C25/30	kN	[2]	580	739	884	1,034	1,202	1,421	1,651	1,985
Wall thickness loss due to corrosion 2.50 mm											
Cross-sectional load-bearing capacity	Pile	kN	[2]	442	543	696	854	804	1,036	1,278	1,631
	Pile + C20/25	kN	[2]	514	654	801	952	1,056	1,278	1,510	1,848
	Pile + C25/30	kN	[2]	533	682	827	977	1,119	1,338	1,567	1,902
Wall thickness loss due to corrosion 3.25 mm											
Cross-sectional load-bearing capacity	Pile	kN	[2]	373	458	611	770	680	912	1,154	1,507
	Pile + C20/25	kN	[2]	445	569	716	868	932	1,154	1,386	1,724
	Pile + C25/30	kN	[2]	463	597	742	892	995	1,214	1,444	1,778

Annex 4: Wall thickness loss of the piles due to corrosion

Applied load value of the cross-sectional load-bearing capacity of piles without/with synchronous grouting under compressive stress without wall thickness loss due to corrosion (in accordance with ÖNORM B 2567, Table 5)											
Type (outer diameter)		mm	98		118			170			
Nominal wall thickness		mm	6.0	7.5	7.5	9.0	10.6	7.5	9.0	10.6	13.0
Cross-sectional load-bearing capacity [1)]	Pile	kN	555	682	833	986	1,144	1,225	1,457	1,699	2,052
	Pile + C20/25	kN	632	754	944	1,091	1,243	1,477	1,699	1,930	2,269
	Pile + C25/30	kN	652	773	972	1,117	1,267	1,540	1,759	1,988	2,323
Load value of the cross-sectional load-bearing capacity of piles without synchronous grouting under compressive stress for a planned service life of up to 100 years in accordance with the soil-dependent thickness loss table as shown in Chapter 7.3.1 including the allowable limit values as shown in Chapter 7.2											
Type (outer diameter)		mm	98		118			170			
Nominal wall thickness		mm	6.0	7.5	7.5	9.0	10.6	7.5	9.0	10.6	13.0
Wall thickness loss due to corrosion 0.60 mm											
Cross-sectional load-bearing capacity [1)]	Pile	kN	496	624	762	915	1,074	1,123	1,355	1,596	1,950
	Pile + C20/25	kN	574	696	873	1,020	1,172	1,375	1,596	1,828	2,167
	Pile + C25/30	kN	593	714	901	1,046	1,196	1,438	1,657	1,886	2,221
Wall thickness loss due to corrosion 0.90 mm											
Cross-sectional load-bearing capacity	Pile	kN	467	594	727	880	1,039	1,072	1,304	1,546	1,899
	Pile + C20/25	kN	545	667	838	985	1,137	1,324	1,546	1,777	2,116
	Pile + C25/30	kN	564	685	866	1,011	1,161	1,387	1,606	1,835	2,170
Wall thickness loss due to corrosion 1.00 mm											
Cross-sectional load-bearing capacity	Pile	kN	457	585	716	869	1,027	1,055	1,287	1,529	1,882
	Pile + C20/25	kN	535	657	827	973	1,125	1,307	1,529	1,761	2,099
	Pile + C25/30	kN	554	675	854	999	1,150	1,370	1,589	1,819	2,153
Wall thickness loss due to corrosion 1.20 mm											
Cross-sectional load-bearing capacity [1)]	Pile	kN	438	566	692	845	1,004	1,022	1,253	1,495	1,848
	Pile + C20/25	kN	516	638	803	950	1,102	1,273	1,495	1,727	2,065
	Pile + C25/30	kN	535	656	831	976	1,126	1,336	1,555	1,785	2,120
Wall thickness loss due to corrosion 1.75 mm											
Cross-sectional load-bearing capacity [1)]	Pile	kN	386	513	629	782	940	929	1,161	1,403	1,756
	Pile + C20/25	kN	463	585	740	886	1,038	1,181	1,403	1,634	1,973
	Pile + C25/30	kN	482	603	768	913	1,063	1,244	1,463	1,692	2,027
Wall thickness loss due to corrosion 2.00 mm											
Cross-sectional load-bearing capacity	Pile	kN	[2)]	489	600	753	911	887	1,119	1,361	1,714
	Pile + C20/25	kN	[2)]	561	711	858	1,009	1,139	1,361	1,593	1,931
	Pile + C25/30	kN	[2)]	580	739	884	1,034	1,202	1,421	1,651	1,985
Wall thickness loss due to corrosion 2.50 mm											
Cross-sectional load-bearing capacity	Pile	kN	[2)]	442	543	696	854	804	1,036	1,278	1,631
	Pile + C20/25	kN	[2)]	514	654	801	952	1,056	1,278	1,510	1,848
	Pile + C25/30	kN	[2)]	533	682	827	977	1,119	1,338	1,567	1,902
Wall thickness loss due to corrosion 3.25 mm											
Cross-sectional load-bearing capacity	Pile	kN	[2)]	373	458	611	770	680	912	1,154	1,507
	Pile + C20/25	kN	[2)]	445	569	716	868	932	1,154	1,386	1,724
	Pile + C25/30	kN	[2)]	463	597	742	892	995	1,214	1,444	1,778

Annex 5: Environmental impact analysis

To draw conclusions about the environmental impact, the EPD of the TRM Piling System is studied. EPD stands for 'Environmental Product Declaration'. This document is an ISO type III environmental declaration according to the international standard ISO 14025. ISO type I documents are third-party independent eco-labels. These labels are typically used by manufactures to communicate the environmental aspects of their products in a highly simplified way. The ISO type II is a self-declared eco-label. EPD, ISO type III, differentiates itself by being the only instrument to give the full picture of the environmental performance of the product in a life cycle perspective. In contrary to the eco-labels, EPD gives not only the good but also the bad aspects of the environmental performance of the product. (The EPD | EPD International, n.d.)

The EPD report is based on a life cycle assessment (LCA). This LCA is typically executed by the software 'SimaPro'. This software collects, analyzes and monitors the sustainability performance data of products and services. The life cycle assesment takes into account the entire value chain, from material sourcing to manufactured product, the utilization phase and end of life. In this way, the environmental impact over the entire life cycle is evaluated. The valuation takes place by a third-party to obtain an objective report. All registered EPD's are publicly and free available to download. This way it is easy to compare the environmental impact results of products within the same group. (The EPD | EPD International, n.d.), (About SimaPro - SimaPro, 2022)

At the end of their use as a foundation, the piles can either be left in the ground if they don't hinder other foundation work or they can be removed and recycled. The piles are very rarely disposed as waste. It is technically and economically feasible to remove and recycle the ductile driven piles. Therefore the EPD takes the 100% removal of the piles in to account. However, this scenario should be examined and adjusted according to the particular case. (*TRM PILING SYSTEMS Tiroler Rohre GmbH*, 2022)

To perform the LCA, a unit of 1 meter of pile is considered. This meter focusses exclusively on the ductile iron pipe. The pile shoe, pile cap, concrete filling and external grouting are not taken into account. The following table gives the mass of one meter pile according to the pile type. (*TRM PILING SYSTEMS Tiroler Rohre GmbH*, 2022)

Pile type	Longitudinally related mass [kg/m]
98 x 6,0	14,40
98 x 7,5	17,20
118 x 7,5	21,00
118 x 9,0	24,42
118 x 10,6	27,96
170 x 7,5	33,80
170 x 9,0	37,14
170 x 10,6	42,54
170 x 13,0	50,42

All the stages of life of the ductile iron piles are being examined. The included stages can be found in the table below. With these stages a process flow chart can be created for the ductile iron piles. This chart can found in the figure below.

Product stage	A1	Raw material supply
	A2	Transport
	A3	Manufacturing
Construction stage	A4	Transport
	A5	Construction/installation
Use stage	B1	Use
	B2	Maintenance
	B3	Repair
	B4	Replacement
	B5	Refurbishment
	B6	Operational energy use
	B7	Operational water use
End-of-life stage	C1	Demolition
	C2	Transport
	C3	Waste processing
	C4	Disposal
Benefits and loads	D	Reuse, recovery, recycling potential

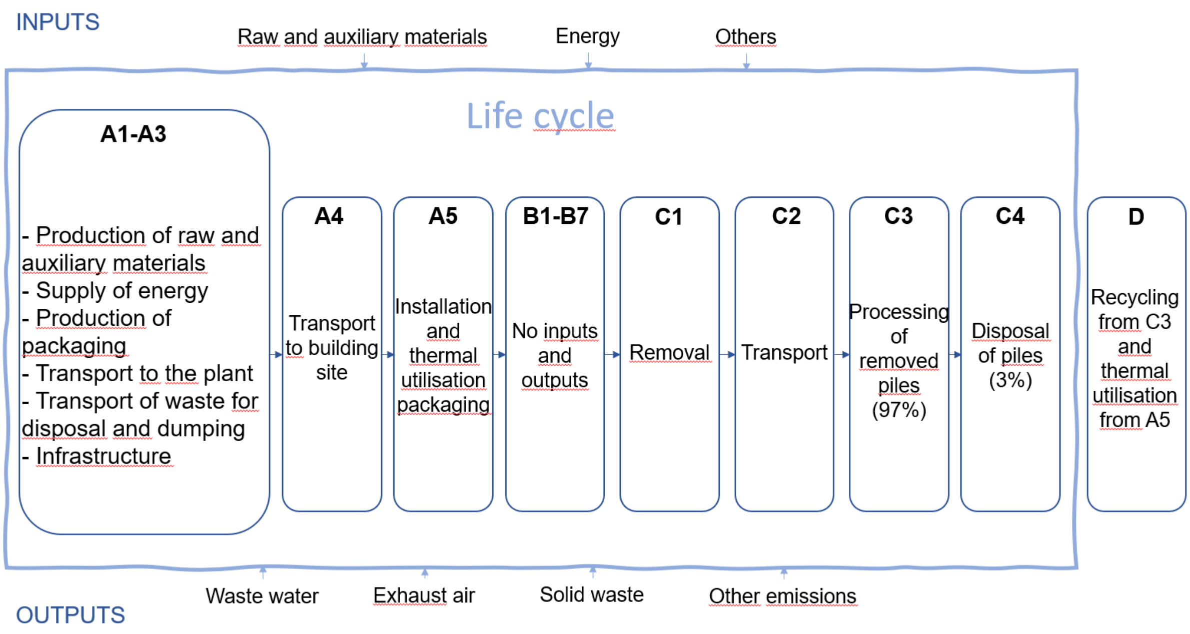

The producer of the ductile iron piles has to calculate the quantity of materials used, the energy required, the waste material generated with the method of disposal, the transport distances and the necessary infrastructure for production. All these data is generated according to the annual average production in 2020 and submitted in the SimaPro program. Ecoinvent 3.8 from 2021 with the system model cut-off by classification was used as the background database. (*TRM PILING SYSTEMS Tiroler Rohre GmbH*, 2022)

The total number of non-significant processes is assumed to be less than 5% of the impact categories. This category includes admixtures with a material flow of less than 1%. Some examples of these materials are lubricating oils, additives for cooling circuits, hydraulic fluid and marking ink. Internal transports in the company were also not taken into account due to the short distances. The production of the by-products slag and coke can be ignored as well since the sale of them as district heating contributes less than 1% of the operational income. The heat treatment applied to the piles vary minimally in energy expenditure in relation to the pile types. Therefore no distinction is made between pile types when analyzing heat treatment. (*TRM PILING SYSTEMS Tiroler Rohre GmbH*, 2022)

For stages A1-A4 the required information is provided by the producer of the piles. The table below regarding stage A1 gives an overview of the distances over which the piles are transported. With these distances the average fuel consumption is taken into account. This is 25,3 L diesel per 100 km or 9 000 heavy oil per 100 km. Other parameters that are taken into account are vehicle type according to Commision Directive 2007/37/EC, the average transport mass, the average capacity utilization, the average gross density of the transported products and the volume capacity utilization factor.

Country	Allocation	Truck [km]	Ship [km]
Austria	41,2%	303	
Switzerland	9,3%	297	
Germany	34,0%	327	
Italy	2,8%	204	
Spain	0,7%	1 955	
France	8,3%	949	
England	0,1%	1 452	
Czech Republic	0,5%	539	
Luxembourg	0,2%	658	
USA	1,8%	3 810	6 500
South Africa	1,1%	16 350	12 700

Regarding stage A5 of the life cycle, the energy demand for the installation of the piles is calculated. Assuming a hydraulic excavator with and engine power of 150 kW and 300 m of installed pile a day (8 hours), the energy demand is 4 kWh or 14,4 MJ per meter of pile. Taken into account a diesel requirement of 0,125 kg per kWh, the installing of the piles requires 0,5 kg per meter of pile. This is 0,595 liter diesel per meter of pile assuming 0,84 kg/L diesel. Lastly the stacked wood and PET binding tapes for transportation are also considered. A 100 km away, they are thermally recycled in a waste incinerator.

In the use stage B1-B7 is ignored since there are no relevant activities with material or energy flow that take place. For the end-of-life stage C1-C4 the LCA looks at a removal of all piles. This may vary in practice. The same energy flow of 14,4 MJ per meter pile and 0,595 liter diesel per meter is taken into account. For transportation a recycling company of a 100 km away is considered. The same parameters from stage A4 such as the required fuel of 25,3 liter diesel per 100 km are used. For the life cycle analyses it is assumed that 97% of the piles are recycled and 3% is disposed. For both proceedings the mass per meter of pile type is taken into account.

For the last stage D it is stated that the scrap input to produce one meter of pile is higher than the mass of pile that is recycled per meter. As a result, there is a small negative net flow according to the pile type which is displayed in the table below.

Pile type	Mass per meter of pile [kg/m]	Total pile mass for recycling [kg/m]	Scrap input per meter of pile [kg/m]	D from C3 Net flow
98/6	14,4	13,97	14,227	-0,259
98/7,5	17,2	16,68	16,994	-0,310
118/7,5	21	20,37	20,748	-0,378
118/9	24,42	23,69	24,127	-0,440
118/10,6	27,96	27,12	27,624	-0,503
170/7,5	33,8	32,79	33,394	-0,608
170/9	37,14	36,03	36,694	-0,669
170/10,6	42,54	41,26	42,030	-0,766
170/13	50,42	48,91	49,815	-0,908

The recycled energy and heat from the recycling process of the stacked wood and PET binding tapes from the transportation in A5 is also calculated in stage D. For this computation the lower heat values from the ecoinvent data sets for thermal utilization is used. The assumption that the energy recovery is split into 1/3 for electricity (with 17% efficiency) and 2/3 heat (with 75% efficiency) is made. The values for this can be found in annex 5.

A couple conclusions can be drawn from the analysis. The production of piles (A1-A3) is the main contributor to the most impact categories. Transport (A4) to the building site and installation (A5)/removal (C1) of piles are identified as the next most influential processes. Recycling in C3, particularly the recycling plant infrastructure, is the main contributor to the parameter ADP minerals and metals (abiotic depletion potential). Waste disposal in C4 has a corresponding influence on NHWD (non-hazardous waste disposed).

The definitions of raw materials and auxiliary substances like cokes, ferrosilicon and silicon carbide, are not easily applicable to the production of the piles, so there is no splitting of A1-A3 in the interpretation. A1-A3 are dominant modules for most investigated indicators in the entire life cycle of the piles. The influence of individual processes in A1-A3 is identical for all pile types.

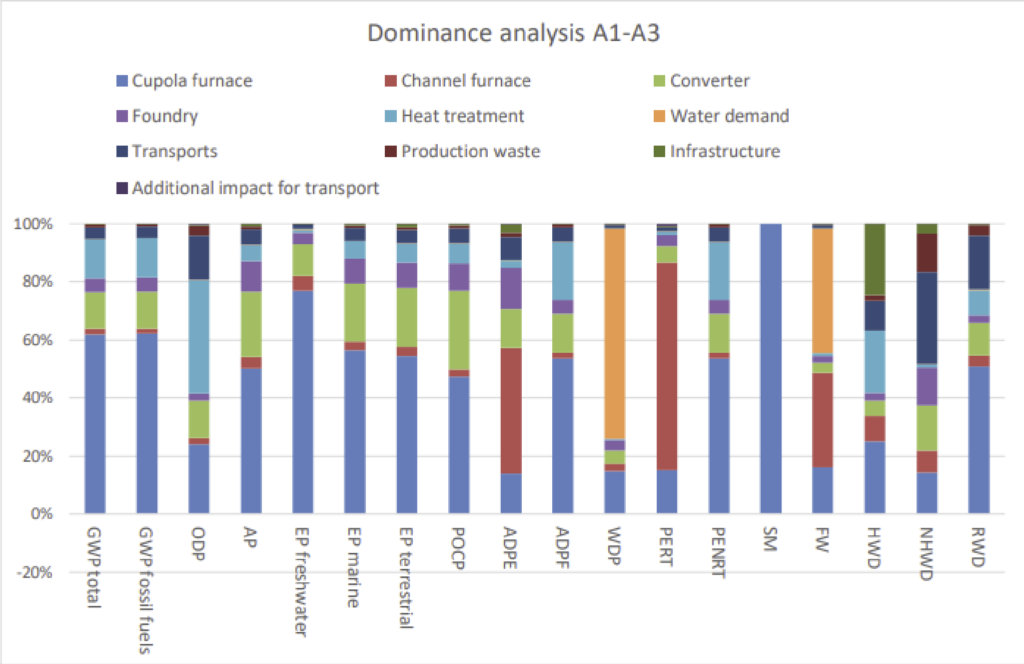

The figure shows that the cupola furnace process (production of the cast iron) has the greatest influence on the majority of indicators, with foundry coke combustion and production being the main driving factors (due the emission of carbon dioxide and methane). The SiC pellets used in the cupola furnace also have an influence. However, the exact impact of the SiC pellets is subject to fluctuation potential due to uncertainties in the modelling or estimation of their production. Water demand strongly influences the indicators WDP (water deprivation potential) and FW (use of fresh water). The processes in the channel furnace have a strong influence on the indicators ADP minerals and metals, PERT (total use of renewable primary energy resources), and FW due to the power required by the channel furnace.

The heat treatment process in the annealing furnace results in different energy expenditures for each pile type due to their varying throughputs. A sensitivity analysis shows that extreme values for some pile types result in ODP (depletion of the stratospheric ozone layer) values that are up to 11.3% different from the mean value, while other indicators differ by less than 1.8%. However, the manufacturer only provides average throughput values, and the actual throughputs fluctuate, so heat treatment was not split by pile type to avoid complexity.

The study used ecoinvent data sets for modelling the life cycle inventory models. Some of these data sets were more than 10 years old. The results for A1-A3 of the new EPD for the piles show a reduction in GWP (global warming potential), ODP, and ADP fossil fuels compared to the EPD in 2017. The reduction in GWP is actually higher than reported because the old results did not take the carbon in SiC into account. All reductions are mainly due to the reduction of foundry coke used in the cupola furnace. The increase in PERT compared to 2017, which is due to the inclusion of TIWAG electricity supplied and the share of renewable energies contained in it.

Annex 6: Recycled energy from A5 in the LCA

Pile type 98/6	Output	Heating value, lower	Electricity benefit	Heat benefit
	[kg/m]	[MJ/kg]	[MJ/m]	[MJ/m]
Waste incineration (stacked wood)	5.66E-03	13.99	4.49E-03	3.96E-02
Waste incineration (PET)	2.02E-04	22.95	2.62E-04	2.31E-03
D from A5			**4.75E-03**	**4.19E-02**

Pile type 98/7.5	Output	Heating value, lower	Electricity benefit	Heat benefit
	[kg/m]	[MJ/kg]	[MJ/m]	[MJ/m]
Waste incineration (stacked wood)	6.76E-03	13.99	5.36E-03	4.73E-02
Waste incineration (PET)	2.41E-04	22.95	3.13E-04	2.76E-03
D from A5			**5.67E-03**	**5.01E-02**

Pile type 118/7.5	Output	Heating value, lower	Electricity benefit	Heat benefit
	[kg/m]	[MJ/kg]	[MJ/m]	[MJ/m]
Waste incineration (stacked wood)	8.26E-03	13.99	6.54E-03	5.77E-02
Waste incineration (PET)	2.94E-04	22.95	3.82E-04	3.37E-03
D from A5			**6.93E-03**	**6.11E-02**

Pile type 118/9	Output	Heating value, lower	Electricity benefit	Heat benefit
	[kg/m]	[MJ/kg]	[MJ/m]	[MJ/m]
Waste incineration (stacked wood)	9.60E-03	13.99	7.61E-03	6.72E-02
Waste incineration (PET)	3.42E-04	22.95	4.45E-04	3.92E-03
D from A5			**8.06E-03**	**7.11E-02**

Pile type 118/10.6	Output	Heating value, lower	Electricity benefit	Heat benefit
	[kg/m]	[MJ/kg]	[MJ/m]	[MJ/m]
Waste incineration (stacked wood)	1.10E-02	13.99	8.71E-03	7.69E-02
Waste incineration (PET)	3.91E-04	22.95	5.09E-04	4.49E-03

Pile type 170/7.5	Output	Heating value, lower	Electricity benefit	Heat benefit
	[kg/m]	[MJ/kg]	[MJ/m]	[MJ/m]
Waste incineration (stacked wood)	1.33E-02	13.99	1.05E-02	9.29E-02
Waste incineration (PET)	4.73E-04	22.95	6.15E-04	5.43E-03
D from A5			**1.11E-02**	**9.84E-02**

Pile type 170/9	Output	Heating value, lower	Electricity benefit	Heat benefit
	[kg/m]	[MJ/kg]	[MJ/m]	[MJ/m]
Waste incineration (stacked wood)	1.46E-02	13.99	1.16E-02	1.02E-01
Waste incineration (PET)	5.20E-04	22.95	6.76E-04	5.97E-03
D from A5			**1.23E-02**	**1.08E-01**

Pile type 170/10.6	Output	Heating value, lower	Electricity benefit	Heat benefit
	[kg/m]	[MJ/kg]	[MJ/m]	[MJ/m]
Waste incineration (stacked wood)	1.67E-02	13.99	1.33E-02	1.17E-01
Waste incineration (PET)	1.73E-03	22.95	2.25E-03	1.99E-02
D from A5			**1.55E-02**	**1.37E-01**

Pile type 170/13	Output	Heating value, lower	Electricity benefit	Heat benefit
	[kg/m]	[MJ/kg]	[MJ/m]	[MJ/m]
Waste incineration (stacked wood)	1.98E-02	13.99	1.57E-02	1.39E-01
Waste incineration (PET)	7.06E-04	22.95	9.18E-04	8.10E-03
D from A5			**1.66E-02**	**1.47E-01**

Annex 7: Number of foundation piles for the roof per node